BRUNEL UNIVERSITY

Ultrasonic Guided Wave Testing of Pipelines using a Broadband Excitation

by

Keith Thornicroft

A thesis submitted in partial fulfillment for the
degree of Doctor of Philosophy

in the

College of Engineering, Design and Physical Sciences
Division of Mechanical Engineering

May 2015

3 year embargo from the date of publication

Declaration of Authorship

I, KEITH THORNICROFT, declare that this thesis titled, *'Ultrasonic Guided Wave Testing of Pipelines using a Broadband Excitation'* and the work presented in it are my own. I confirm that:

- This work was done wholly or mainly while in candidature for a research degree at this University.
- Where any part of this thesis has previously been submitted for a degree or any other qualification at this University or any other institution, this has been clearly stated.
- Where I have consulted the published work of others, this is always clearly attributed.
- Where I have quoted from the work of others, the source is always given. With the exception of such quotations, this thesis is entirely my own work.
- I have acknowledged all main sources of help.
- Where the thesis is based on work done by myself jointly with others, I have made clear exactly what was done by others and what I have contributed myself.

Signed: _____

Date: _____

"We search for the truth, we could die upon the tooth, but the thrill of just the chase is worth the pain."

Ronnie James Dio

BRUNEL UNIVERSITY

Division of Mechanical Engineering

Abstract

Doctor of Philosophy

by Keith Thornicroft

Guided Wave Testing (GWT) is a relatively new development in non-destructive testing. Conventional Ultrasonic Testing (UT) methods are operated at high frequencies (MHz) and are capable of detecting very small (down to micrometre-scale) flaws within a range of millimetres from a transducer. GWT, however, is carried out at lower frequencies (kHz) and is capable of highlighting the position of volumetric structural detail and discontinuities, such as gross corrosion at a minimum of 9% of the cross-sectional area, tens of metres from a test location. Conventional ultrasonic testing relies on the transmission of bulk waves whereas GWT employs so-called *ultrasonic guided waves* (UGW). To simplify UGW inspections, several tests are conducted sequentially at a range of different excitation frequencies. The frequency bandwidth of each of these tests needs to be controlled to avoid complexities caused by the frequency dependent nature of the propagation of guided waves. This gives rise to the current GWT inspection procedure, where a number of different *narrowband* tests are conducted at several distinct frequencies. It is also found that different test circumstances (such as pipe coating or defect type) are inspected more easily with certain excitation frequencies than with others - and the optimum frequency can not always be predicted ahead of time. Thus, where time allows it is often beneficial to carry out a *frequency sweep*, whereby a large range of excitation frequencies are incrementally generated - for example, from 20 to 80kHz in 1kHz steps. This research proposes a novel approach to the existing pipeline inspection procedure by utilising the information contained within a broadband response. The overarching proposition given by this research is that the current collection procedure be entirely rewritten. This thesis will present ideas related to every area of the inspection procedure beginning with the tuning of excitation signals and concluding with recommendations on how tooling and excitation configuration can be modified to further optimise the technique for broadband excitation.

Acknowledgements

I would like to take this opportunity to thank my project supervisor Dr. Cristinel Mares for recognising the promise in me during my MSc, for his endless patience and constructive discussions on the topic. I would also like to extend my gratitude to my industrial supervisor Peter Mudge for his generation of ideas and inspiration on the topic at hand. Particular thanks goes out to Dr. Phil Catton and Dr. Alex Haig for their advice and direction on programming, signal processing and surviving my PhD. A massive Teletest tech. support thanks goes out to Alan Lank and Nick Farrant who are fountains of knowledge on the subject of guided wave testing of pipelines and have helped me no end.

I thank also my research colleagues old and new: Bhavin, Hugo, Matt, Vichaar, Devashish, Yousef, Abbas, Kenny, Kena, Nacho, Billy, Sina and Shehan for maintaining an uplifted spirit in our department at TWI despite various pressures.

I would like to thank my family for bearing with me during a busy and stressful time. I owe a lot to you all. Much love.

...and last but definitely not least I would like to thank my partner Hazel for her unparalleled devotion, moral support and for helping me to forget the stresses and strains of writing this thesis.

Contents

Declaration of Authorship i

Abstract iii

Acknowledgements iv

List of Figures viii

List of Tables xii

Abbreviations xiii

1 Introduction 1
- 1.1 Thesis Outline . . . 1
- 1.2 Introduction . . . 1
- 1.3 Guided Wave Testing . . . 1
- 1.4 Potential Areas for Improvement in the GWT Technique . . . 3
- 1.5 Aims and Objectives . . . 5
- 1.6 Contributions to Knowledge . . . 6

2 Introduction to the Guided Wave Inspection of Pipes 9
- 2.1 Introduction . . . 9
- 2.2 Wave propagation in unbounded media . . . 10
- 2.3 Surface waves . . . 11
  - 2.3.1 Rayleigh waves . . . 11
  - 2.3.2 Love waves . . . 12
- 2.4 Guided waves in plates . . . 13
  - 2.4.1 Lamb waves . . . 13
  - 2.4.2 Waves in a dispersive medium . . . 15
- 2.5 Guided waves in hollow cylinders . . . 16
  - 2.5.1 Wavemode nomenclature for hollow cylinders . . . 17
  - 2.5.2 Guided wave testing of pipelines . . . 18
  - 2.5.3 Interpretation of results . . . 21
- 2.6 Summary . . . 22

3 Literature Review **23**
3.1 Introduction . . . 23
3.2 Theoretical development of guided wave propagation within Pipes . . . 23
3.3 Transition from Theory to a Valid Pipeline Inspection Technique . . . 25
3.3.1 Transducer Development . . . 26
3.3.2 Commercial GWT Tool Development . . . 28
3.4 Output Normalisation and Control of GWT Tools . . . 29
3.5 Applications of Broadband Signals in other Fields . . . 30
3.6 Broadband Excitation of Lamb Waves . . . 32
3.7 Time-Frequency Representations of Lamb Waves . . . 33
3.8 Summary . . . 34

4 Implementation of a Broadband Excitation for Ultrasonic Guided Waves in Hollow Cylinders **36**
4.1 Background . . . 36
4.1.1 Potential benefits of implementing a broadband signal in GWT . . . 37
4.2 Objectives . . . 38
4.3 Methodology . . . 38
4.3.1 Excitation signal generation . . . 38
4.3.2 Laboratory trials . . . 39
4.3.3 Post-processing . . . 39
4.4 Optimisation of a Broadband Excitation Signal . . . 40
4.4.1 Linear Frequency Modulation (LFM) . . . 40
4.4.2 Amplitude Modulation via a Suitable Window Function . . . 42
4.5 Experimental Validation . . . 49
4.5.1 Experimental set up . . . 49
4.5.2 Initial results . . . 51
4.6 Post-Processing . . . 55
4.6.1 Filtering using FFT Convolution . . . 55
4.6.2 Adapting FFT Convolution for Broadband Excitation . . . 57
4.6.3 Proposed FFT Phase Manipulation . . . 60
4.7 Results . . . 63
4.8 Conclusions . . . 64

5 The Application of a Broadband Excitation to a Commercial Guided Wave Inspection System **78**
5.1 Background . . . 78
5.2 Objectives . . . 79
5.3 Methodology . . . 79
5.3.1 Unidirectional propagation of an LFM chirp . . . 79
5.3.2 Laboratory trials . . . 80
5.3.3 Post-processing . . . 80
5.4 Unidirectional Propagation of Guided Wave Signals in a Pipeline . . . 81
5.4.1 Using the dispersion curves to model wave propagation . . . 82
5.5 The two ring torsional propagation routine . . . 87
5.6 The three ring torsional propagation routine . . . 92
5.6.1 Three ring torsional using a 30mm ring spacing . . . 93

5.6.2 Three ring torsional using a 45mm ring spacing 95
5.7 The three ring longitudinal propagation routine 97
5.7.1 Three ring longitudinal using a 30mm ring spacing 98
5.8 Experimental Set Up 101
5.9 Discussion of Results 103
5.10 Conclusions 104

6 Field Validation of Broadband Excitation for a Guided Wave Inspection Technique 116
6.1 Background 116
6.2 Objectives 117
6.3 Methodology 117
6.3.1 Software implementation 117
6.3.2 Data collection 118
6.3.3 Data analysis 118
6.4 Gathering of Broadband GWT Field Data 119
6.4.1 Test schedule 119
6.5 Pre-processing GWT signals 120
6.5.1 Minimising initial signal crosstalk (XT) 120
6.5.2 Enveloping the signal 121
6.6 Discussion of Results 122
6.7 Conclusions 135

7 Conclusions and Further Work 136
7.1 Thesis Review 136
7.2 Brief summary of the main contributions 138
7.3 Further Work 140
7.3.1 Using a non-linear FM to correct a biased transfer function in an ultrasonic guided wave system 140
7.3.2 Adapting transducer ring spacing to provide a wider range of test frequencies 143

References 145

List of Figures

1.1 The Teletest Focus$^+$ GWT system showing the key components; the transducer array, the pulser/receiver and the PC controller. 2

2.1 A graphical representation of the displacement pattern of a Rayleigh wave 12
2.2 A graphical representation of the displacement pattern of a Love wave . . 13
2.3 A graphical representation of the displacement pattern of Lamb waves . . 14
2.4 An example of the distortion of a 3 cycle, 30kHz pulse when propagated in a dispersive medium. The upper axes show that propagation of a non-dispersive wavemode results in no pulse distortion whereas the lower axes show that when there is a frequency dependence to the phase and group velocities, the pulse spreads out and does not retain its original shape. . . 15
2.5 A Finite Element Analysis (FEA) representation of the $F(5,1)$ wavemode 17
2.6 A Finite Element Analysis (FEA) representation of the $L(0,2)$ wavemode 18
2.7 A Finite Element Analysis (FEA) representation of the $T(0,1)$ wavemode 19
2.8 A narrowband 10 cycle, Hann windowed pulse with the associated frequency response. 20
2.9 An example of a typical GWT A-Scan. 21

3.1 The phase velocity dispersion curves for an 8inch schedule 40 steel pipe . 30

4.1 An LFM chirp signal swept between 20 kHz and 100 kHz with a pulse length of 500μs. 42
4.2 A demonstration of the effect low frequency chirps have on the symmetry of the Fresnel ripples. All of the LFM chirp signals plotted here have the following parameters kept constant: pulse length = 300μs, $\alpha = 0$ and sample frequency = 10MHz. 43
4.3 The effect of varying the Tukey ratio (α) between 0 and 1 on the frequency spectrum. $f_1 = 20$ kHz, $f_2 = 100$ kHz and $B = 80$ kHz. Both unwrapped phase (centre axes) and magnitude (lower axes) are presented. 45
4.4 The effect of a varying LFM chirp pulse length on the frequency spectrum (phase and magnitude). Here the *unwrapped* phase is presented in order to give an idea of the accumulative effect across the spectrum. The input parameters are:
$\alpha = 0.2$, $f_1 = 20$ kHz and $f_2 = 100$ kHz 46
4.5 A frequency domain comparison of three 10 cycle, Hann-windowed pulses used in GWT (20 kHz, 60 kHz and 100 kHz) with two LFM chirp pulses; one with no Tukey window and the other with a 20% Tukey ratio applied 48
4.6 Experimental set up 50

4.7 LFM chirp distance domain responses for the sum of the octants from the 8 inch schedule 40 pipe derived from the time domain using the theoretical group velocity for $T(0,1)$. For each test the pulse length (τ) was varied to be the following: 50μs, 100μs, 200μs, 300μs, 400μs and 500μs. The bandwidth used here was 5 kHz - 115 kHz. 51
4.8 This is the frequency response of the chirp pipe-end reflection. The excitation bandwidth was 5 kHz - 115 kHz 53
4.9 This is the frequency response of the chirp pipe-end reflection in dB. The excitation bandwidth was 5 kHz - 115 kHz 54
4.10 The normalised spectrum of an example narrowband GWT signal at 60kHz. The filter kernel is shown in blue, the ideal Tx spectrum in red, the raw Rx spectrum in black and the result of the FFT convolution in green 58
4.11 The magnitude and phase spectrum of two example transmission signals used as templates in the FFT phase manipulation process. The red trace is the narrowband signal, in this case it is a Hann-windowed, 10 cycle pulse with a centre frequency (f_s) of 60kHz. The blue trace represents the spectrum of a broadband LFM chirp. (τ = 300μs and a Tukey ratio of $\alpha = 0.2$) 61
4.12 A Comparison of the narrowband test at 20 kHz, 5 cycles and the emulated narrowband result filtered down from a 300μs (α= 0.2, f_1=5 kHz and f_2 = 115 kHz) 66
4.13 A Comparison of the narrowband test at 60 kHz, 5 cycles and the emulated narrowband result filtered down from a 300μs (α= 0.2, f_1=5 kHz and f_2 = 115 kHz) 67
4.14 A Comparison of the narrowband test at 100 kHz, 5 cycles and the emulated narrowband result filtered down from a 300μs (α= 0.2, f_1=5 kHz and f_2 = 115 kHz) 68
4.15 A Comparison of the narrowband test at 20 kHz, 10 cycles and the emulated narrowband result filtered down from a 300μs (α= 0.2, f_1=5 kHz and f_2 = 115 kHz) 69
4.16 A Comparison of the narrowband test at 60 kHz, 10 cycles and the emulated narrowband result filtered down from a 300μs (α= 0.2, f_1=5 kHz and f_2 = 115 kHz) 70
4.17 A Comparison of the narrowband test at 100 kHz, 10 cycles and the emulated narrowband result filtered down from a 300μs (α= 0.2, f_1=5 kHz and f_2 = 115 kHz) 71
4.18 A Comparison of the narrowband test at 20 kHz, 15 cycles and the emulated narrowband result filtered down from a 300μs (α= 0.2, f_1=5 kHz and f_2 = 115 kHz) 72
4.19 A Comparison of the narrowband test at 60 kHz, 15 cycles and the emulated narrowband result filtered down from a 300μs (α= 0.2, f_1=5 kHz and f_2 = 115 kHz) 73
4.20 A Comparison of the narrowband test at 100 kHz, 15 cycles and the emulated narrowband result filtered down from a 300μs (α= 0.2, f_1=5 kHz and f_2 = 115 kHz) 74
4.21 A Comparison of the narrowband test at 20 kHz, 20 cycles and the emulated narrowband result filtered down from a 300μs (α= 0.2, f_1=5 kHz and f_2 = 115 kHz) 75

4.22 A Comparison of the narrowband test at 60 kHz, 20 cycles and the emulated narrowband result filtered down from a 300μs (α= 0.2, f_1=5 kHz and f_2 = 115 kHz) 76
4.23 A Comparison of the narrowband test at 100 kHz, 20 cycles and the emulated narrowband result filtered down from a 300μs (α= 0.2, f_1=5 kHz and f_2 = 115 kHz) 77

5.1 The fundamental axisymmetric wavemodes transmitted during an ultrasonic inspection using guided waves 82
5.2 Propagation of a 10 cycle Hann windowed pulse at 50kHz and an LFM chirp (α= 0.2, f_1=5 kHz and f_2 = 115 kHz). The phase velocities used here were extracted from the $T(0,1)$ dispersion curve 84
5.3 Propagation of a 10 cycle Hann windowed pulse at 50kHz and an LFM chirp (α= 0.2, f_1=5 kHz and f_2 = 115 kHz). The phase velocities used here were extracted from the $L(0,2)$ dispersion curve 85
5.4 Propagation of a 10 cycle Hann windowed pulse at 50kHz and an LFM chirp (α= 0.2, f_1=5 kHz and f_2 = 115 kHz). The phase velocities used here were extracted from the $L(0,1)$ dispersion curve 86
5.5 A simplified schematic showing the axial distribution of the transducers in a two ring tool 87
5.6 Torsional 2 ring 30mm ring spacing input signals, unidirectional signal (forwards) and the resulting suppressed signal (backwards) 88
5.7 Demonstration of how cross-correlation can be used to detect the end of a propagated pulse 89
5.8 Two ring output curves for $T(0,1)$ 91
5.9 A simplified schematic showing the axial distribution of the transducers in a three ring torsional tool 92
5.10 Torsional 3 ring 30mm ring spacing input signals and unidirectional signal (forwards) and the resulting suppressed signal (backwards) 93
5.11 Three ring output curves for $T(0,1)$ at a ring spacing of 30mm 94
5.12 Torsional 3 ring 45mm ring spacing input signals and unidirectional signal (forwards) and the resulting suppressed signal (backwards) 95
5.13 Three ring output curves for $T(0,1)$ at a ring spacing of 45mm 96
5.14 A simplified schematic showing the axial distribution of the transducers in a three ring longitudinal tool 98
5.15 Longitudinal 3 ring 30mm ring spacing input signals and unidirectional signal (forwards) and the resulting suppressed signal (backwards) 99
5.16 Three ring output curves for $L(0,2)$ at a ring spacing of 30mm 100
5.17 An example of a *multi-mode* GWT tool produced by Plant Integrity Ltd.. The lower image shows the orientation of the transducers within the transducer module for torsional and longitudinal excitation 101
5.18 An example of a *torsional* module produced by Plant Integrity Ltd.. . . . 102
5.19 Two ring torsional unidirectional result at 27kHz 106
5.20 Two ring torsional unidirectional result at 81kHz 107
5.21 Three ring torsional unidirectional result at 36kHz (30mm ring spacing) . 108
5.22 Three ring torsional unidirectional result at 72kHz (30mm ring spacing) . 109
5.23 Three ring torsional unidirectional result at 24kHz (45mm ring spacing) . 110
5.24 Three ring torsional unidirectional result at 48kHz (45mm ring spacing) . 111

5.25 Three ring longitudinal unidirectional result at 51kHz (30mm ring spacing) 112
5.26 Three ring longitudinal unidirectional result at 61kHz (30mm ring spacing) 113
5.27 Three ring longitudinal unidirectional result at 65kHz (30mm ring spacing) 114
5.28 Three ring longitudinal unidirectional result at 71kHz (30mm ring spacing) 115

6.1 An example of the removal of the crosstalk from a 50kHz GWT signal (in blue) using a smoothed heaviside step function. The reception of the later signals in the green trace are unaffected 120
6.2 An example of the formation of an envelope of a 50kHz GWT signal (in blue) using the absolute values of the Hilbert transform (in red) 121
6.3 Comparison between narrowband and filtered broadband inspection results. Test ID 106: 64kHz, three ring torsional at 30mm ring spacing . . . 122
6.4 Comparison between narrowband and filtered broadband inspection results. Test ID 106: 64kHz, three ring torsional at 30mm ring spacing . . . 123
6.5 Comparison between narrowband and filtered broadband inspection results. Test ID 47: 72kHz, three ring torsional at 30mm ring spacing . . . 126
6.6 Comparison between narrowband and filtered broadband inspection results. Test ID 83: 48kHz (10 cycles), three ring torsional at 45mm ring spacing 127
6.7 Comparison between narrowband and filtered broadband inspection results. Test ID 124: 48kHz (10 cycles), three ring torsional at 45mm ring spacing 128
6.8 Comparison between narrowband and filtered broadband inspection results. Test ID 788: 36kHz (7 cycles), three ring torsional at 30mm ring spacing 129
6.9 Comparison between narrowband and filtered broadband inspection results. Test ID 59: 48kHz (10 cycles), three ring torsional at 45mm ring spacing 130
6.10 Comparison between narrowband and filtered broadband inspection results. Test ID 72: 36kHz (10 cycles), three ring torsional at 30mm ring spacing 131
6.11 Comparison between narrowband and filtered broadband inspection results. Test ID 89: 72kHz (10 cycles), three ring torsional at 30mm ring spacing 132
6.12 Comparison between narrowband and filtered broadband inspection results. Test ID 98: 72kHz (10 cycles), three ring torsional at 30mm ring spacing 133
6.13 Comparison between narrowband and filtered broadband inspection results. Test ID 127: 48kHz (10 cycles), three ring torsional at 45mm ring spacing 134

7.1 An example of the effect chirp rate bias has on the frequency content of the signal. The bias applied here is 0.2 (the data in green) 141
7.2 Initial promising results which show that in principle the received spectrum can be corrected. The bias here was set to 0.4. 142
7.3 An example of the increase in available bandwidth as a result of changing the ring spacing to 15mm. 143

List of Tables

4.1 Narrowband tests carried out 63
4.2 Broadband tests carried out 63

5.1 Schedule of tests carried out 103

6.1 Schedule of field tests presented 119
6.2 Summary of Test ID 106 measurements 125
6.3 Summary of Test ID 47 measurements 126
6.4 Summary of Test ID 83 measurements 127
6.5 Summary of Test ID 124 measurements 128
6.6 Summary of Test ID 788 measurements 129
6.7 Summary of Test ID 59 measurements 130
6.8 Summary of Test ID 72 measurements 131
6.9 Summary of Test ID 89 measurements 132
6.10 Summary of Test ID 98 measurements 133
6.11 Summary of Test ID 127 measurements 134

Abbreviations

AM	**A**mplitude **M**odulation
ASME	**A**merican **S**ociety of **M**echanical **E**ngineers
BS	**B**ritish **S**tandard
CAD	**C**omputer **A**ided **D**esign
CFRP	**C**arbon **F**ibre **R**einforced **P**lastic
CSA	**C**ross-**S**ectional **A**rea
DAC	**D**istance **A**mplitude **C**orrection
DFT	**D**iscrete **F**ourier **T**ransform
DSP	**D**igital **S**ignal **P**rocessing
EMAT	**E**lectromagnetic **A**coustic **T**ransducer
FEA	**F**inite **E**lement **A**nalysis
FFT	**F**ast **F**ourier **T**ransform
FIR	**F**inite **I**mpulse **R**esponse
FM	**F**requency **M**odulation
GWT	**G**uided **W**ave **T**esting
ID	Identification
LFM	**L**inear **F**requency **M**odulation
LRUT	**L**ong-**R**ange **U**ltrasonic **T**esting
Nd:YAG	**N**eodymium-**d**oped **Y**ttrium **A**luminium **G**arnet
NDE	**N**on-**D**estructive **E**valuation
NDT	**N**on **D**estructive **T**esting
NLFM	**N**on-**L**inear **F**requency **M**odulation
OD	**O**utside **D**iameter
PC	**P**ersonal **C**omputer
PCB	**P**rinted **C**ircuit **B**oard

PHMSA	**P**ipeline and **H**azardous **M**aterials **S**afety **A**dministration
PWVD	**P**seudo **W**igner-**V**ille **D**istribution
Rx	**R**eception
SAW	**S**urface **A**coustic **W**ave
SH	**S**hear **H**orizontal
SHM	**S**tructural **H**ealth **M**onitoring
SNR	**S**ignal to **N**oise **R**atio
TFR	**T**ime-**F**requency **R**epresentation
TWI	**T**he **W**elding **I**nstitute
Tx	**T**ransmission
UGW	**U**ltrasonic **G**uided **W**aves
UT	**U**ltrasonic **T**esting
WT	**W**all **T**hickness
XT	Crosstalk

For Mum & Dad

Chapter 1

Introduction

1.1 Thesis Outline

1.2 Introduction

Non-Destructive Testing (NDT) is a field within engineering with the primary aim of assessing and quantifying the integrity of a component or system without causing damage to the component and in many cases assessment is carried out on components in situ and in service. NDT is a very wide field and encompasses many different techniques each of which utilises a different physical phenomenon to assess damage. Depending upon the inspection criteria required the technique may vary in complexity from a simple hammer tap to generate resonant vibrational modes in a train wheel to the ultrasonic imaging of a turbine blade used within an aircraft engine. The most important attribute NDT offers is the ability to detect flaws and predict the service life of many critical components across all sectors of industry thus reducing the risk of commercial, environmental and human catastrophe via sudden structural failures within these systems.

1.3 Guided Wave Testing

Guided Wave Testing (GWT) utilises so-called Ultrasonic Guided Waves (UGW) for the inspection of large areas and distances of metallic and non-metallic components. The

technique is currently applied commercially in the Non-Destructive Evaluation (NDE) of pipelines and tubular structures.

Transduction takes place via a bracelet of transducers fixed into a modular tool which is wrapped around the circumference of the tubular section under inspection. The transducers are dry-coupled to the outer surface via pneumatic pressure (shown below in Figure 1.1) or, in some cases, spring force.

FIGURE 1.1: The Teletest Focus$^+$ GWT system showing the key components; the transducer array, the pulser/receiver and the PC controller.

The transducers work in a specified sequence to produce an axisymmetric stress wave which propagates away from the tool. A propagation routine specified within the GWT software specifies the order in which each sector of transducers are employed and has the ability to minimise the energy propagating in a selected direction and maximise

(albeit with a frequency dependent cyclic output) energy propagating in the test direction. The wavelength of the UGW produced by the system exceeds the thickness of the material under inspection, due to the high acoustic impedance between sound travelling within the material being tested and the surrounding air, the wave propagation becomes bounded by the so-called wave guide. UGWs propagating along a waveguide are sensitive to relatively sharp changes in cross-section and any changes representing more than 9% Cross-Sectional Area (CSA) will be detected by the process as a reflection from the feature back at the tool. A feature within the test range which is axisymmetric in nature, such as a girth weld or pipe support clip, will generate an axisymmetric response or wave mode. Similarly, localised corrosion or pipe fittings such as T-Pieces section or small branches will cause a non-axisymmetric response which in terms of received signal manifests itself as a non-uniform distribution of signal amplitude around the circumference. Due to the modular design of the transducer array within the tool non-axisymmetric responses (also known as flexural modes) can be detected as the amplitude trace of each circumferential sector within the tool can be measured. The interpretation of the received signal is subject to the principle that an axisymmetric wave mode is generated by the tool and any flexural wave modes (non-axisymmetric responses) received back at the tool must have been the result of wave mode conversion at a localised, non-axisymmetric anomaly present within the test range. The operator carrying out the inspection will base any conclusions on the integrity of the pipeline on this fundamental principle.

1.4 Potential Areas for Improvement in the GWT Technique

Due to the frequency dependent nature of nearly every aspect of this technique it is often beneficial to sweep through and collect data for many frequencies in order to select an optimum frequency or to track a feature which may appear on a time trace at a limited group of test frequencies. This discrete frequency approach leads to problems with the amount of data collected and stored for a GWT test, especially for coated pipelines or for pipelines containing viscous substances such as bitumen where test data can be poor. It is therefore best practice in these circumstances to carry out a dense frequency sweep. This process produces a large amount of data which must be sifted through and is therefore inefficient in terms of time and data storage space. If a routine were to be

introduced to make data collection more efficient in these terms then it would transform the whole inspection process.

The performance of current GWT tool and transducer array is not optimum and there is no robust method of quantifying output. The tool is designed to produce a near pure axisymmetric wave mode, provide a unidirectional test and to absorb local acoustic energy produced during excitation. Using an array of transducers the tool must by definition be segmented. The more number of transducers used in the array the more non-axisymmetric modes are suppressed. It is also important for the array to be balanced in output and in geometry so that the axisymmetric out put of the tool is guaranteed. The generation of non-axisymmetric modes by the tool increases the risk of making false conclusions on the presence of damage within the structure being inspected. In a similar sense the directional performance of the tool is also of paramount importance. The axisymmetric wave mode problem concerns the circumferential distribution and coupling of the array whereas directionality is largely due to the axial position and output of each ring array within the tool. In theory, if the circumferential distribution and coupling is balanced throughout the tool and the outputs of all of the rings are balanced with each other then the GWT would produce a near perfect ring of sound with perfect suppression of signals travelling in the opposite direction to the desired test direction. If a process could be derived and validated to provide results for the actual output of any GWT tool, it would provide a platform upon which the design rules for future GWT tools could be built.

GWT tool calibration is currently carried out using a reference signal from girth welds along the pipe line being inspected. This method is not robust enough for several reasons. The main being that the process assumes that an equal amount of weld metal has been deposited around the circumference during the welding process. The ASME standard which dictates the size of a weld cap is used to give a dB value which represents 20% of the total energy reflected by a flange or pipe end. Subsequent damage thresholds are also calculated using the weld amplitude (-14dB below a 100% reflector). There are some situations whereby there is not a weld present within the inspected length, which makes defining an accurate acceptable level of noise within the scan very difficult. For optimum test conditions the Signal to Noise Ratio (SNR) is typically in the region of 40dB with the actual accepted noise threshold within the Teletest software of 32dB. If the array could be calibrated within the tool it would improve the output significantly.

The fundamental idea behind GWT transmission is to transmit a pure wave mode and receive a mix of axisymmetric and non-axisymmetric wave modes depending on what is present within the tested structure. This can only achieved using an array with a balanced output.

1.5 Aims and Objectives

The overall purpose of NDT is to evaluate the structural health of an engineering asset and reduce the risk of component failure. The NDT industry has a key role in providing safety and assessing the reliability of such systems. Guided Wave Testing (GWT) is among several techniques used in the gas and petro-chemical sectors and has become an important tool in pipeline life assessment. The technique is expanding into other areas such as the rail and renewable energy sectors. The aim of this research is to develop a broadband excitation and data processing procedure using an available GWT inspection system. This was achieved by adopting the following methodology:

- To investigate past and present literature to find potential voids in research or areas for improvement in the specific area of GWT for pipelines.
- To derive and design digital signal processing (DSP) methods to incorporate broadband signals into the current GWT procedure.
- To improve and maximise the efficiency of the GWT process through the application of these routines.
- To recommend a shift in the GWT data collection and data interpretation procedures over to the specifics stated in this thesis.

1.6 Contributions to Knowledge

Validation of a Broadband Technique Using UGWs in Hollow Cylinders via Experimentation

Chapter 4 introduces a novel broadband excitation method for a hollow cylinders. The technique has been derived, trialed and proven to correlate with equivalent narrowband results. One of the limiting factors concerning the generation of guided waves within plates, pipes and other prismatic structures is dispersion. Dispersion is the frequency dependent variation of the phase and group velocity of a given ultrasonic wave mode. Group velocity is derived from phase velocity and each mode has a different relationship between phase velocity and frequency for a given structure. If a mode is excited at a frequency where there is a large variation in phase velocity with respect to frequency then the pulse will spread out and distort thus reducing temporal resolution. This has led to the adoption of a narrowband excitation pulse in the current GWT procedure. However, this research has proven that a broadband excitation signal can be implemented with similar performance. This initial study was carried out for the fundamental torsional mode $T(0,1)$ using a single ring of transducers in order to prove the concept. This is the simplest case not just because the geometry is elementary, but additionally $T(0,1)$, equivalent to the SH0 mode in plates, is non-dispersive. The concepts of the $T(0,1)$ wavemode and other wavemodes are explained in section 2.5. An adaptable FFT filter with phase compensation was developed based upon the required equivalent narrowband response. A comparison has been made between the narrowband and filtered broadband results for the laboratory trials showing good agreement.

Demonstration of Broadband Excitation for GWT of Pipelines using a Unidirectional T(0,1) Wavemode

The novel broadband method established in Chapter 4 is now applied to a multi-ring pipeline inspection array incorporating a non-dispersive propagation routine to achieve directionality for broadband excitation using a GWT tool. The simple single ring $T(0,1)$ case is expanded to incorporate additional transducer rings. The purpose of a multi-ring array is to give the inspection directionality through a propagation algorithm consisting of phase delays and superposition. A directional broadband test has been carried out with comparable results to that of the current narrowband equivalent. The basic 2 ring $T(0,1)$ excitation has been validated across the bandwidth typically used within commercial GWT procedure. In addition a 3 ring torsional variant, which provides additional output has been tested using the proposed broadband excitation method with equivalent results. **(The routines developed in this thesis are now an integral part of the data collection procedure within the Teletest GWT software.)**

Demonstration of Broadband Excitation for GWT of Pipelines using a Unidirectional L(0,2) Wavemode

The proposed broadband method has been modified to accommodate the dispersion characteristics of the $L(0,2)$ wave mode and provide directionality. Using the longitudinal wave mode of choice for the current guided wave inspection procedure, $L(0,2)$, a unidirectional test using a broadband excitation has been developed and validated. Using the $L(0,2)$ phase velocity gained from the analytical software DISPERSE, a phase delay was set up within the excitation signals. The phase delay was incorporated in order to provide a unidirectional $L(0,2)$ wave mode. Results from these tests were validated under controlled laboratory conditions and also using data from site trials.

Publications Arising from this Research

- K. Thornicroft and P. Catton. LRUT using chirp and broadband excitation methods. *The Welding Institute: Core Research Project (Internal Report)*, July 2010.
- K. Thornicroft and P. Catton. Long range ultrasonic testing using a broadband excitation method. *The Welding Institute: Industrial Member Report*, September 2011.
- K. Thornicroft, C. Mares and P. Mudge. Time-frequency analysis of long range ultrasonic signals. *Journal of Physics: Conference Series, Modern Practice in Stress and Vibration Analysis*, Institute of Physics, 382(1), University of Glasgow, 2012.

Chapter 2

Introduction to the Guided Wave Inspection of Pipes

2.1 Introduction

This chapter introduces some of the underlying theory concerning the propagation of Ultrasonic Guided Waves (UGWs). The latter part of the chapter introduces the use of UGWs for the evaluation of pipeline integrity. The most common application of ultrasonic waves within the NDT industry is via the implementation of bulk waves to determine the local condition of a given structure. Standard Ultrasonic Testing (UT) using bulk waves gives excellent spatial resolution and therefore sensitivity. In addition, the results produced via bulk wave transmission are easy to interpret and can be viewed in real time. Unlike the majority of guided wave modes, the velocity of bulk waves (shear and longitudinal) do not depend on excitation frequency. There are two main configurations for a standard UT inspection; *pulse echo* whereby the transmitter and receiver are positioned at the same point and *through transmission* whereby the receiver is positioned at a given distance away from the transmission point. In both configurations time of flight of features appearing on the received time trace and attenuation measurements are made to provide a quantified assessment of the condition of the tested structure. The propagation range of standard UT techniques is limited to hundreds of millimetres and is therefore not considered as an efficient solution for the inspection of large or embedded structures. Due to the comparatively low frequencies and

therefore low attenuation associated with the Guided Wave Testing (GWT) technique, large structures can be efficiently screened for changes in wall thickness resulting from erosion or corrosion. Despite the potential of UGWs for the testing of large structures, the generation and control of transmission and reception of a guided wave test is not an elementary operation. This complexity is driven by the governing equations describing the propagation of UGWs.

2.2 Wave propagation in unbounded media

The nature of wave propagation within an elastic solid depends upon imposed boundary conditions such as geometry, stiffness and density. The concept of bulk waves is applied to wave propagation in an infinite media where as guided waves can only exist where there is a physical boundary within the medium. Both propagation conditions are governed by the same differential equations of motion.

Navier's differential equation of motion for an isotropic elastic medium is as following:

$$\mu\nabla^2 u + (\lambda + \mu)\nabla\nabla \cdot u = \rho\frac{\partial^2 u}{\partial t^2} \tag{2.1}$$

The parameter u is a three dimensional displacement vector, λ and μ are two material constants known as the Lamé constants, ∇ is a three dimensional differential operator and ρ is the material density. Upon expansion, Equation 2.1 provides direct access to x,y and z components and is stated in full in texts on the subject [Graff (1991) and Rose (1999)]. This equation describes the motion of all elastic waves propagating within the material and are therefore termed as the wave equations. These equations are linear but cannot be integrated directly. Using Helmholtz decomposition, Equation 2.1 can be expressed more conveniently in terms of a summed scalar potential, ϕ, (compressional) and the vector field, Φ.

$$u = \nabla\phi + \nabla \times \Phi \tag{2.2}$$

with

$$\nabla \cdot \Phi = 0$$

As a consequence of the decomposition of Equation 2.1, the two unknown potentials, ϕ and Φ, can be solved using two partial differential equations:

$$\frac{\partial^2 \phi}{\partial t^2} = c_l^2 \nabla^2 \phi \tag{2.3}$$

$$\frac{\partial^2 \Phi}{\partial t^2} = c_s^2 \nabla^2 \Phi \tag{2.4}$$

Equation 2.3 governs longitudinal wave velocity c_l and Equation 2.4 governs shear wave velocity c_s within an infinite isotropic medium.

$$c_l = \sqrt{\frac{\lambda + 2\mu}{\rho}} \tag{2.5}$$

$$c_s = \sqrt{\frac{\mu}{\rho}} \tag{2.6}$$

2.3 Surface waves

Surface waves are a family of elastic waves that propagate along a bounding surface of a body or medium. This category of waves, also known as Surface Acoustic Waves (SAWs) are studied in other fields such as oceanography and seismology.

2.3.1 Rayleigh waves

First predicted by Lord Rayleigh [Strutt (1896)], Rayleigh waves are a class of surface acoustic waves that propagate along the surface of elastic solids. Their displacement pattern is an out-of-plane elliptical motion and can be seen overleaf in Figure 2.1. They can be generated by local surface impact or via mode conversion from other elastic waves impinging on a surface from within a body. The surface waves observed during seismic events are intiated in this way. In NDT, these waves are often used to inspect surface flaws and can be generated by using a wedge probe or Electro-Magnetic Acoustic Transducers (EMATs).

The velocity of a Rayleigh wave on the surface of a given elastic medium found using:

$$c_r = \frac{0.87 + 1.12\nu}{1 + \nu} c_s \tag{2.7}$$

Where ν is Poisson's ratio of the medium. The surface displacement of Rayleigh waves decays exponentially with depth below the material surface and only occurs up to approximately a wavelength. This in some sense limits the Rayleigh wave but given enough control, the excitation frequency can be selected to cause displacements at a desired depth.

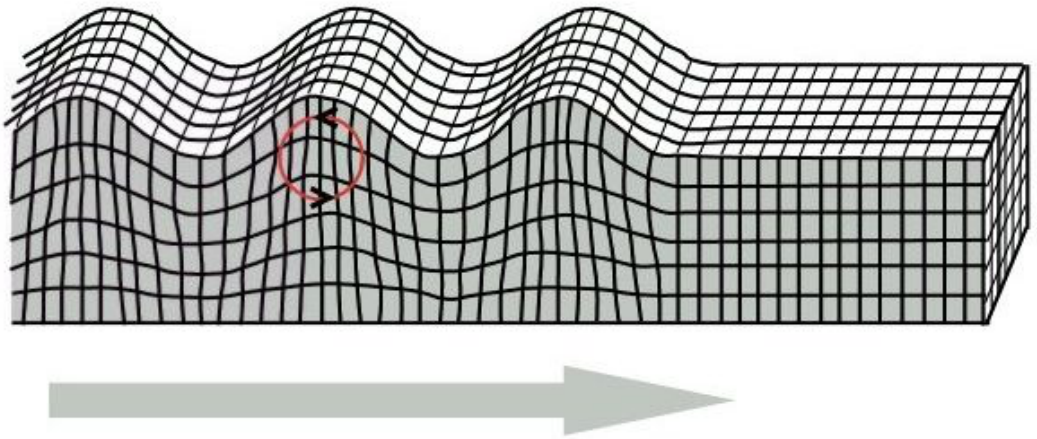

FIGURE 2.1: A graphical representation of the displacement pattern of a Rayleigh wave

2.3.2 Love waves

Like the Rayleigh wave, Love waves [Love (1911)] can exist at the surface of an elastic solid. However, Love waves exhibit a different particle displacement. The in-plane displacement of the particles display a shearing motion which exists again up to a wavelength in material depth. Figure 2.2 displays particle motion and gives a sense of overall propagation of a Love wave. This class of surface also exists during a seismic event.

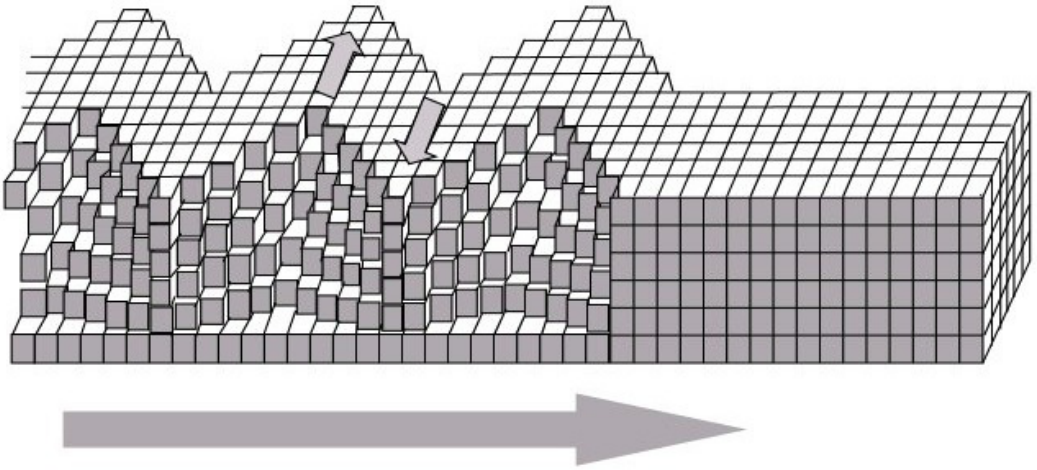

FIGURE 2.2: A graphical representation of the displacement pattern of a Love wave

2.4 Guided waves in plates

Surface waves exist where only one boundary is present and surface displacement orientation is dependent upon the nature of excitation. In plate-like structures a second boundary is present thus creating another class of elastic waves. This class of propagation was first examined by Horace Lamb [Lamb (1917)].

2.4.1 Lamb waves

Lamb discovered that an infinite number of different modes can exist within plates. The displacement pattern for these modes can be classified according to the displacement symmetry. Figure 2.3 shows the through wall displacement pattern for the two fundamental Lamb modes for each classification: 'Asymmetric' (A0) and 'Symmetric' (S0). The line of symmetry here is shown as the dotted centre line of the plate. The particle displacements for Lamb waves are similar to the elliptical motion observed in Rayleigh waves. The propagation characteristics of Lamb waves depend on the excitation frequency as through wall displacement depends upon wavelength. Excitation parameters for this class of wavemode is sometimes expressed in terms of the frequency thickness product. An increase in excitation frequency or thickness results in the presence of more wavemodes. It is beneficial to work towards wavemode purity in order to keep received test data comprehensive and containing a low level of coherent noise. The nomenclature

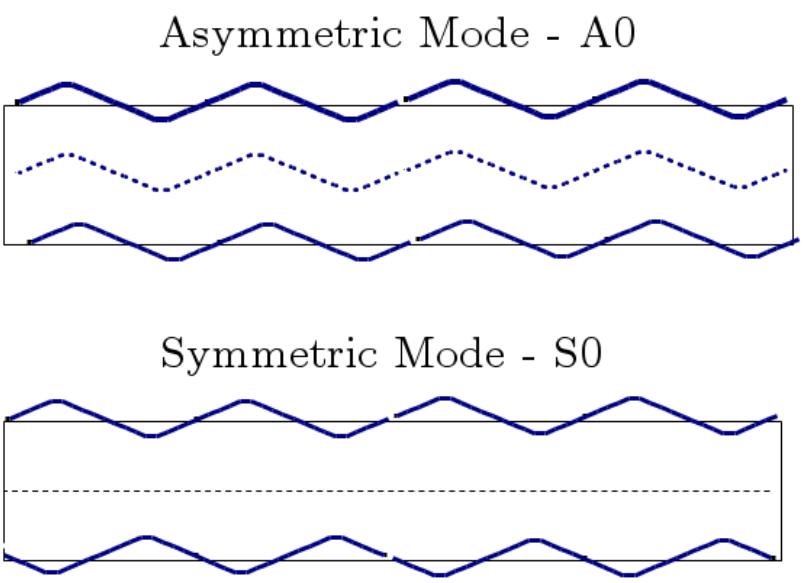

FIGURE 2.3: A graphical representation of the displacement pattern of Lamb waves

for sorting Lamb wave modes is as follows: for the symmetric modes the fundamental mode is S0 and higher order modes increase by n in the form S1, S2, S3,...Sn, for the asymmetric modes this becomes A0, A1, A2, A3,...An.

Lamb waves can be considered as the superposition of longitudinal and shear modes defined by Equations 2.5 and 2.6. By using the wave vectors p and q the characteristic equations describing each class of Lamb wave mode can be developed.

$$p^2 = \left(\frac{\omega}{c_l}\right)^2 - k^2 \tag{2.8}$$

and

$$q^2 = \left(\frac{\omega}{c_s}\right)^2 - k^2 \tag{2.9}$$

Where ω is angular frequency and k is wave number. The characteristic equations then become:

$$\frac{\tan(qh)}{\tan(ph)} = -\frac{4k^2pq}{(q^2-k^2)^2} \tag{2.10}$$

for symmetric modes

$$\frac{\tan(qh)}{\tan(ph)} = -\frac{(q^2-k^2)^2}{4k^2pq} \tag{2.11}$$

for asymmetric modes. Where h represents half of the plate thickness and k is the wavenumber $(2\pi/\lambda)$.

2.4.2 Waves in a dispersive medium

Waves propagating within an elastic medium can be subject to a phenomenon known as *dispersion*. The causes of dispersion are not fully understood but the effect manifests itself as a distortion of the propagating pulse. This distortion is caused by the frequency dependent phase and group velocity of a given wavemode propagating within the medium. A pulse or pulse train contains a number of frequency components within and if propagated in a dispersive medium will possess a range of group and phase velocity values. During propagation through the dispersive medium, this range of velocity values will result in some frequency components overtaking others. The change in phase and group information for the pulse causes distortion. All guided wave modes exhibit this effect (shown in Figure 2.4 below) to a given degree with the two fundamental shear-based modes ($T(0,1)$ and $SH0$) being exceptions to this rule as they do not exhibit frequency dependent velocities during propagation.

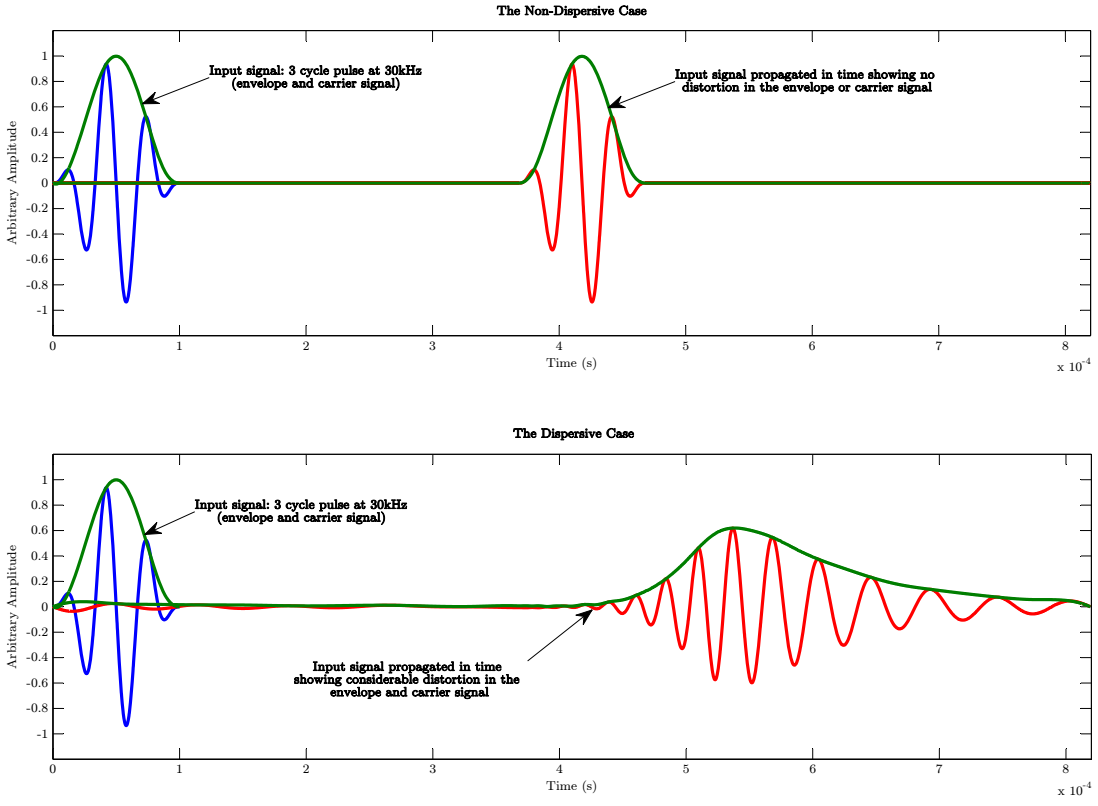

FIGURE 2.4: An example of the distortion of a 3 cycle, 30kHz pulse when propagated in a dispersive medium. The upper axes show that propagation of a non-dispersive wavemode results in no pulse distortion whereas the lower axes show that when there is a frequency dependence to the phase and group velocities, the pulse spreads out and does not retain its original shape.

2.5 Guided waves in hollow cylinders

A pipe can be considered as a plate which has been formed into a cylinder and joined along an axial seam. This means that the axial cross-section of the pipe wall will support a Lamb wave which propagates along the length of the pipe. However, the circumference presents an additional boundary condition hence other wavemodes are possible. Extensive research into the behaviour of the propagation of elastic waves in cylinders has been carried out, notably the research of Gazis, Meitzler and Zemanek [Gazis (1959a), Meitzler (1961) and Zemanek (1972)].

Cylindrical wavemodes are categorised into three main families based upon their displacement patterns:

- **Longitudinal** - This family of modes exhibit similar through-wall displacements to Lamb waves in plates where the $L(0,2)$ wavemode is equivalent to S0 and $L(0,1)$ is equivalent to A0. Within the frequency bandwidth used in GWT the Longitudinal family are dispersive. When transmitting a longitudinal wavemode within a pipe using a circumferential array of transducers it is possible to excite more than one axisymmetric wavemode. In the case of the longitudinal family and at the lower region in the dispersion curves two axisymmetric wavemodes always exist: $L(0,1)$ and $L(0,2)$. $L(0,1)$ is the fundamental, axisymmetric wavemode within the longitudinal family. $L(0,1)$ is dispersive in the frequency bandwidth used for GWT therefore transducer arrays and signal transmission algorithms are designed to suppress it and reinforce the transmission of $L(0,2)$. An example of a dispersion curve displaying this frequency dependence is shown in Figure 3.1 and Figure 5.4 shows the dispersive behaviour of $L(0,1)$ when propagated to a distance of 10m in an 8 inch schedule 40 steel pipe (OD = 219mm, wall thickness = 8.18mm).

- **Torsional** - The fundamental member of this wavemode family $T(0,1)$ is non-dispersive and the exception to this rule. All other torsional wavemodes are dispersive. This category of wavemode is analogous to the Shear Horizontal (SH) plate modes [Su and Ye (2009)].

- **Flexural** - This classification of wavemode is attributed to those displaying a displacement pattern which incorporates a harmonic oscillation distributed around

the circumference. The flexural modes are divided into a subset which are coupled to either the longitudinal or torsional family.

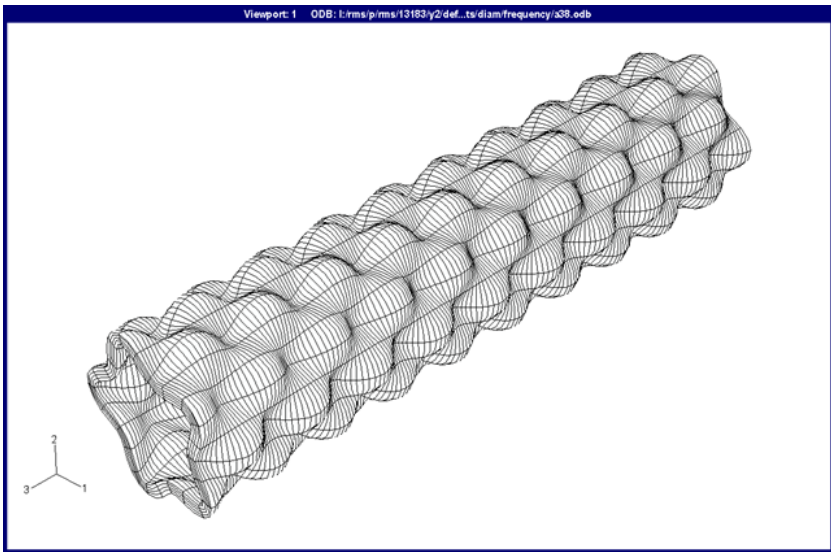

FIGURE 2.5: A Finite Element Analysis (FEA) representation of the $F(5,1)$ wavemode

2.5.1 Wavemode nomenclature for hollow cylinders

The naming scheme for each family of wavemodes for hollow cylinders was first coined in Meitzler (1961). The classification was based upon particle displacement. The longitudinal family were allocated $L(0,n)$ where $n = 1,2,3,4...n$, the torsional family were stated as being $T(0,n)$ where $n = 1,2,3,4...n$ and the flexural family were allocated two variables in the naming scheme $F(m,n)$ where m represents cyclic variation around the circumference. For the longitudinal and torsional modes, regardless of order, the value for m will always be zero. This is because their displacement pattern does not vary around the circumference. They are the so-called axisymmetric modes. Flexural wavemodes display a non-axisymmetric variation around the circumference during propagation and the value of m quantifies this. For example the FEA representation of the flexural mode in Figure 2.5 shows 5 points of rotational symmetry around the circumference and it is first order so therefore the mode is classified as a $F(5,1)$ flexural wavemode. The mode order is dictated by the point at which they appear on the dispersion curves for the structure. The order begins from the origin of the frequency axis and counts each mode as it comes into existence.

2.5.2 Guided wave testing of pipelines

Guided waves are transmitted along pipelines via a pulse-echo system incorporating a pulser/receiver, a laptop PC to control the test and an array of transducers which is designed to transmit an axisymmetric wavemode. The transmission of either $T(0,1)$ or $L(0,2)$ is desired as they are less dispersive, which means that the pulse will not spread out and lose amplitude during propagation. Guided waves within pipes at low frequencies possess very low attenuation which allows them to propagate long distances. A proportion of the energy contained in the transmitted wave front will be reflected back to the tool if an acoustic impedance change occurs due to the presence of a feature or discontinuity (such as a flaw or weld) along the waveguide. If the discontinuity is part circumferential then mode conversion takes place into a given proportion of flexural modes. The FEA representations in Figures 2.6 and 2.7 show the displacement patterns of the

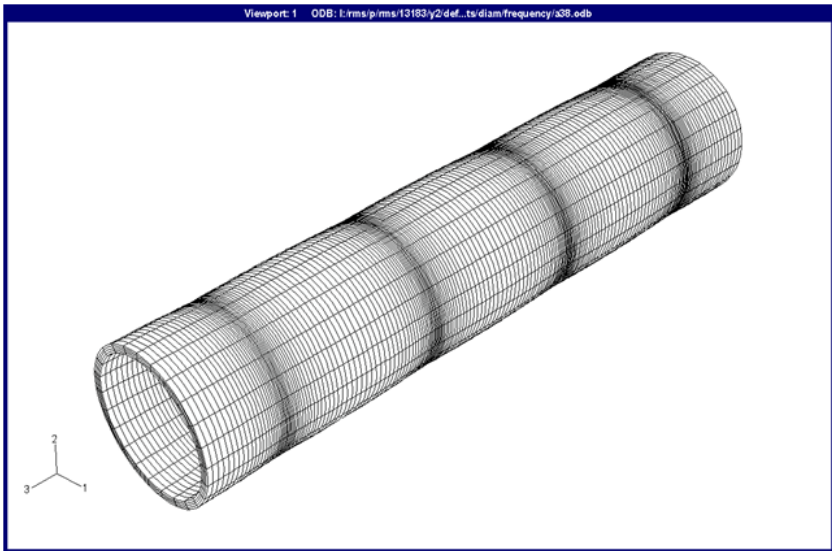

FIGURE 2.6: A Finite Element Analysis (FEA) representation of the $L(0,2)$ wavemode

two axisymmetric wavemodes used for transmission in GWT. It is important to excite a single mode so that selective reception between mode converted signals arising from flaws and known features in the pipe is possible. A single transducer exciting the pipe will generate all wavemodes within the selected bandwidth but by spatially suppressing the majority of flexural modes through a circumferentially distributed transducer array a dominant axisymmetric wavemode is produced.

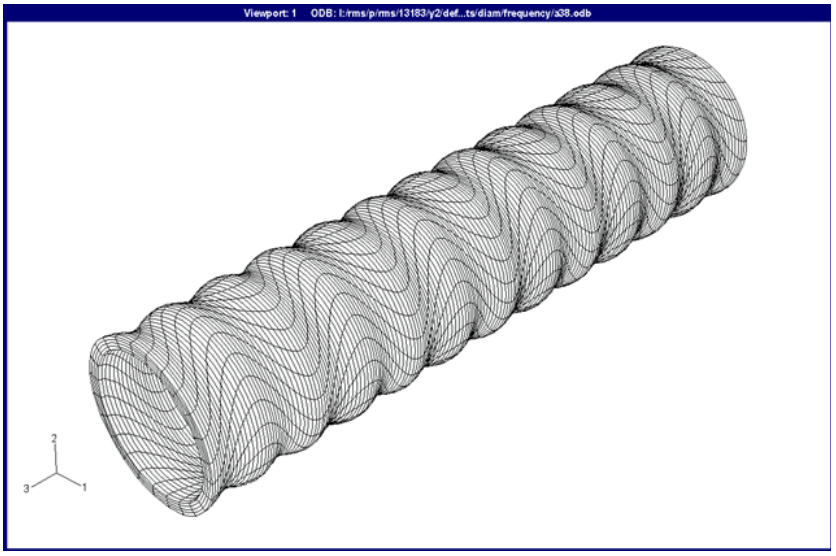

FIGURE 2.7: A Finite Element Analysis (FEA) representation of the $T(0,1)$ wavemode

In order to achieve spatial suppression of unwanted flexural modes, the number of transducers in the array must exceed the points of rotational symmetry around the circumference. For the $F(5,1)$ mode in Figure 2.5 for example, there must be more than $m = 5$ transducers present around the circumference in order to achieve spatial suppression of that particular flexural mode. Ideally, the more transducers possible around the circumference the lower the ratio of flexural to axisymmetric mode becomes during transmission.

The selection between $T(0,1)$ and $L(0,2)$ is achieved through the orientation of the transducer. If a longitudinal test is required then the transducers are aligned to create an axial displacement. If a torsional test is deemed more appropriate for the structure then the transducers are rotated through 90°to generate a circumferential displacement.

The bandwidth of the input signal is currently limited so that the waves propagating become less dispersed over long distances. This is achieved by using a large number of cycles within the pulse (compared to UT), this is usually between 5 and 10 cycles. However, some structures may enhance scattering and dispersion such as coated sections of pipes. A higher number of cycles can reduce the effects of dispersion as it reduces the frequency bandwidth of the pulse. The disadvantage of raising the number of cycles is a reduction in spatial/temporal resolution.

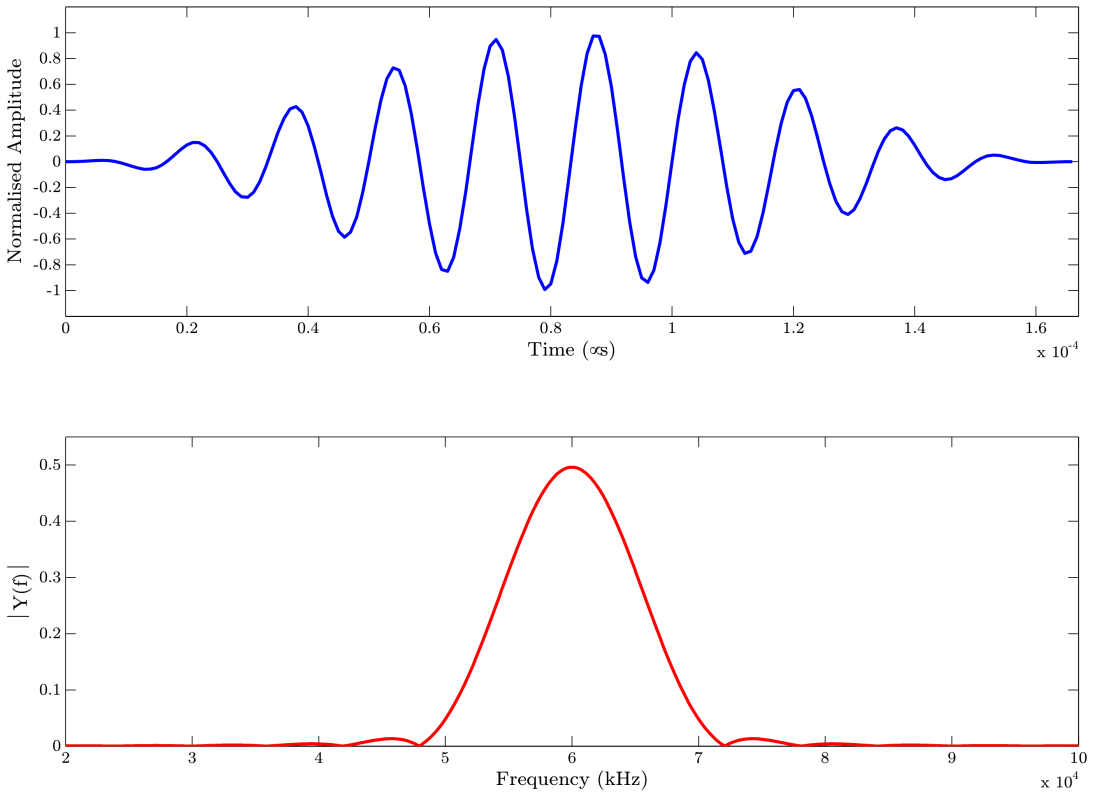

FIGURE 2.8: A narrowband 10 cycle, Hann windowed pulse with the associated frequency response.

Figure 2.8 shows an example of a narrowband transmission signal used in GWT. The pulse is generated by specifying a short sinusoidal pulse train of a specified number of cycles and multiplying this by a chosen window function. There are a number of window functions available to achieve a narrow bandwidth but the two functions in common use for this technique are the Hann and Gaussian windows.

2.5.3 Interpretation of results

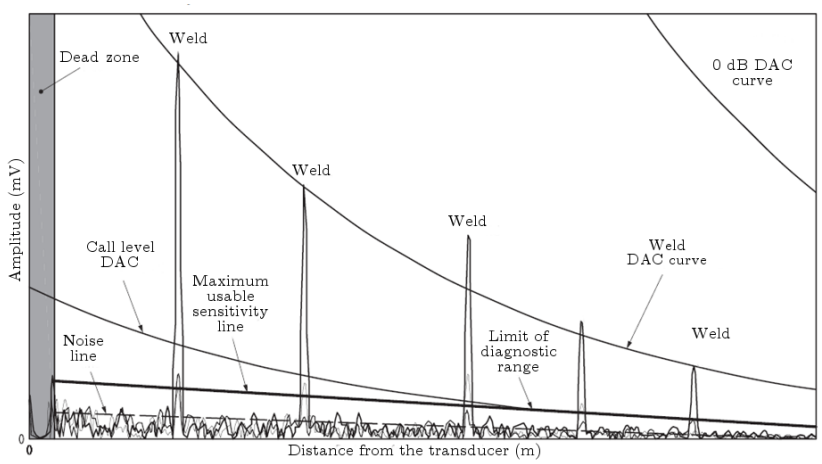

FIGURE 2.9: An example of a typical GWT A-Scan.

Figure 2.9 gives an example of a standard GWT result. The results have been processed in such a way that the features are expressed in terms of distance and not time. In this figure there are three traces present: the darkest trace is the axi-symmetric response and the two remaining shades here represent the first order flexural mode but for two orientations. The tool is divided up into either 4 or 8 parts so it is possible to represent a given flexural mode horizontally or vertically. The responses from the welds are predominantly axisymmetric in nature as the geometry of a girth weld in a pipe is axisymmetric so therefore minimum mode conversion into flexural scatter should occur.

The decay or attenuation of the material is non-linear and is measured as a negative exponential trend in the amplitude of the weld signals shown in Figure 2.9. The weld reinforcement (or weld cap) is considered a consistent reflector and is typically 20% of the cross-section for the thicknesses of pipe commonly encountered when performing GWT (7mm - 13mm thick). The amplitude calibration of a guided wave test relies on this consistency in weld geometry and a Distance Amplitude Correction (DAC) curve is fitted through the peaks of the welds present in a scan. Calibration using the welds as a 20% reflector brings the relative amplitudes of the trace into the correct position and a defined noise threshold is then set at -32dB below the 0dB DAC curve (this curve represents a 100% reflector).

The capability of defect detection is determined by the Signal to Noise Ratio (SNR). Responses from defects, features and discontinuities within the pipe appear above the

background noise threshold set at -32dB. Features within the pipe which are not detectable, therefore outside the limits of sensitivity of the technique, will be lost in the background noise within the scan. Noise in general is variable, therefore a so-called *call line* is required to avoid erroneous reporting of low amplitude peaks (measured within the normal limits of variability for noise) as defects or discontinuities. The call line is set at 6dB above the noise threshold. However, if the amplitude of background noise is particularly low relative to the weld signals (*i.e. much lower than -32dB*) then the inspection engineer will make a judgement on the severity of a discontinuity based upon an estimation of measured amplitude. If the response of the discontinuity is clearly above the level of background noise by 6dB (a ratio of 2:1), then the discontinuity will be reported.

Imposing the 6dB threshold within the scan leads to a sensitivity level which when plotted is known as the maximum usable sensitivity line and is shown in Figure 2.9. As the signal propagates through the structure intensity is lost through attenuation, mode conversion and scatter. As a result the call line eventually coincides with the maximum usable sensitivity line. At this point the limit of defect detectability, also known as the diagnostic range, is reached. Any further assessment on structural integrity beyond the limit of diagnostic range must be made by moving the GWT tool.

2.6 Summary

In summary, this chapter presents the fundamental ideas and some of the theory behind guided wave propagation in elastic solids. Several classes of elastic waves are discussed such as bulk, surface and guided waves but a particular emphasis is given to guided wave propagation within hollow cylinders. Wavemode nomenclature, displacement patterns and desired input parameters for effective guided wave tests of pipelines are covered. To provide the reader with a background on GWT interpretation, the chapter is finalised with coverage and discussion of a typical result from a guided wave inspection.

Chapter 3

Literature Review

3.1 Introduction

This chapter will serve as a review of the developments within the specific area of ultrasonic testing using guided waves in hollow cylinders. It is hoped that the subsequent commentary contained will adequately cover early theoretical progress and briefly chart experimental validation upon which this inspection process is built. The latter part of this chapter concerns the advancement of some of the related signal processing techniques and the strategies adopted to deal with problems such as dispersion and complex received data containing more than one ultrasonic mode.

3.2 Theoretical development of guided wave propagation within Pipes

Theoretical development of guided waves began with plate like structures. However, one of the earliest investigations into suitable testing methods and related theory was carried out by Viktorov (1967). Here Viktorov couples the existing theory laid down by Lamb (1917) and Strutt (1896) with experimental results. Viktorov (1967) also expands the analytical solutions for wave propagation within plates to accommodate for the curvature seen in cylindrical layers using Bessel and Neumann functions and poses several cases for future development of the technique in tubes. Almost a decade before, Gazis (1959a) worked on modelling wave propagation in a hollow cylinder and produced a set

of numerical results in a further paper on the subject: Gazis (1959b). Gazis presented the theory and numerical results for both the torsional and longitudinal family. A full account of these results and the FORTRAN code used can be seen in an accompanying text written a decade later: (Armenàkas et al., 1969). Details of the effects of excitation frequency on wave mode content around the circumference were derived and presented for a cylinder with infinite length. In addition, the more modern text Graff (1991), also recalls the extensive work of Gazis thus highlighting its importance. Further steps were taken by DeVault and Curtis (1959) to classify the modes for bar shaped waveguides. Eventually, this nomenclature was refined and standardised by Meitzler (1961). Although Meitzler states the nomenclature for the longitudinal, torsional and flexural families, torsional excitation was not under investigation and was therefore largely ignored. This is also true for the work of Silk and Bainton (1979) who were investigating guided waves within heat exchanger tubing. To the best of the author's knowledge this is the first example of the direct comparison between the classification of plate and pipe modes, with $L(0,1)$ being directly compared with S_0 and the $L(0,2)$ mode analogous with A_0. Silk and Bainton also commented on the excitability and therefore dominance of a particular mode and the reduction of ultrasonic noise through a more optimum probe design. Earlier in the same decade Zemanek (1972) carried out a thorough comparison between an analytical model of wave propagation in a cylinder with actual test measurements gained via a complex non-contact electrostatic drive/detection arrangement. A non-contact approach during excitation and reception is preferred as variable contact coupling across an array of transducers is eliminated. Eliminating this variability meant that Zemanek was able to make a very close comparison between theoretical and experimental values for the symmetrical $L(0,1)$ and anti-symmetrical $L(0,2)$ dispersion curves. A much later paper, Ditri and Rose (1992), discusses the dynamic behaviour of guided waves under specified loading conditions on the surface of a hollow cylinder. In this paper the author expanded upon the work of Gazis by presenting theory which covered the influence that surface loading has on wavemode excitability and derived predictions to minimise the production of non-axisymmetrical wave modes when implementing a circumferentially distributed, multi-element transducer array. The contribution made by Ditri and Rose can be seen as vital to the practical development of the commercial transducer array used in the generation of axisymmetric modes for guided wave testing of pipelines.

3.3 Transition from Theory to a Valid Pipeline Inspection Technique

Three years previous to the experimental work of Silk and Bainton, Mohr and Höller (1976) produced a paper coupling the theoretical work of Gazis with an experimental procedure to detect flaws in thin-walled tubing. Mohr and Höller also eliminated transducer coupling variability but on this occasion they adopted a non-contact magnetostrictive transducer. The test sample for their experiments was a ferritic tube, the main disadvantage of this method is that magnetostrictive transduction will only work on magnetostrictive materials; *i.e. iron, steel, cobalt and nickel.* Despite this limitation, Mohr and Höller presented satisfactory responses from a range of flaw sizes and geometries using both $T(0,1)$ (represented as $T(0,0)$ in their paper) and $L(0,2)$. South West Research Institute in San Antonio, Texas have since developed a solution with a magnetostrictive (MsS) system which will allow non-ferrous materials to be inspected by bonding a nickel strip around the circumference of the specimen underneath the non-contact EMAT [Kwun and Holt (1995)]. The magnetostrictive displacements experienced in the bonded strip are then transferred into the specimen. This technique is effectively a work around and still experiences coupling variability around the circumference.

It is clear from the trend of journal papers released on this subject during the early 1980s that the nuclear industry saw the potential of ultrasonic guided waves and two papers on the subject stand out as a substantial leap forward for the technology. The first by Schneider (1984) is a proposal for a tube inspection system and contains a desired specification, system overviews and strategies on implementing the technique commercially. The second paper, Böttger et al. (1987), is a follow on from the proposal by Schneider and contains an update on the work with results from a field trial of a prototype EMAT system. The authors begin to make a link between amplitude response and flaw size stating that it may be possible to estimate the depth of a variety of flaws with further research.

The potential use of Lamb waves for ultrasonic inspection was investigated by Imperial College, London in the early 1990s. A notable point in the development of the technology was the PhD thesis of Alleyne (1991). In this document, Alleyne discusses

the measurement of the properties of Lamb waves and the numerical modelling of wave propagation in plates. Defects were added to the models in a later chapter and to conclude the document, experiments were set up to validate the numerical procedure. Some signal processing and transduction methods were presented and recommendations were made to deal with the practical implementation of this technology as a standalone NDT technique. Several publications arose from the research demonstrated by Alleyne (1991). One particular paper, Alleyne and Cawley (1991), pioneers the use of the 2D-FFT technique on a multi-mode Lamb wave response. It was concluded that the 2D-FFT can display the mode content of a given response but its use during a field inspection is not recommended as the receiver used must be moved incrementally several hundred times between scans in order to achieve an acceptable resolution in wavenumber versus frequency. A further paper summarising the conclusions from Alleyne (1991) was published as a guide for the optimisation of inspections using Lamb waves [Alleyne and Cawley (1992)]. The authors cover a range of practical issues related to the generation of Lamb waves within plates; Displacement shapes for $A0$ and $S0$, a discussion on mode selection with modelled results showing propagation time histories, transducer design and a discussion on the merits of generating a pure wavemode via bandwidth control.

3.3.1 Transducer Development

During the late 1990s two research groups in particular led the development of an efficient transduction method for guided wave testing in hollow cylinders. Building on the theoretical work of Ditri and Rose (1992), a group at Pennsylvania State University under the direction of Rose produced feasibility studies on the use of both comb type transducers and wedge probes to produce axisymmetric and non-axisymmetric wave modes in hollow cylinders. The use of an angle beam transducer or wedge probe to produce Lamb and surface waves in plates and planar surfaces by this time had already been established. However, by adapting the wedges used by machining the base so that a flush fitting on the circumference of a cylinder could be achieved, the generation of Lamb waves in pipes was proved possible and evaluated by Li and Rose (2002). Extending the analytical work of Ditri and Rose, Li and Rose also demonstrated that several wedge probes could be held around the circumference in an array in order to generate axisymmetric longitudinal modes. The results from this makeshift tool were not very good in terms of signal to noise ratio, but the paper represents a very important step towards the

generation of a focusing algorithm for enhanced detection of directional features. Polar plots of received echoes prove that the author generates non-axisymmetrical modes in a controlled manner. One of the main disadvantages of using wedge probes however is that their output is frequency dependent as the size of probe is relative to wavelength. For the study carried out by Li and Rose the tests were carried out at 375kHz with an axial size for the element of 50mm. For the frequency range used in GWT the wedges used would be too bulky to be a practical solution for inspection.

Four years earlier, using a novel comb transduction method, Rose et al. (1998) proved that an alternative to the solution proposed by Li and Rose was possible and that the generation of Lamb waves in plates could be achieved using their proposed method. Rose et al. presented an analytical model of the so called comb transducer and experimental results were shown from a 2.25mm thick aluminium plate containing a defect. An investigation of mode contribution and purity was carried out by varying the number of elements and element width. Using a time delay routine the authors were able to control the output of the tool in terms of preferred guided wave mode. In a pulse-echo configuration the tool could be set up to generate and recieve the preferred mode whilst suppressing others at a single frequency. The fixed element spacing limits the tool to the generation of guided waves at a specific wavelength. In practice a range of frequencies are often needed to determine damage within a specimen. The comb transducer spacing would have to be adjusted each time to collect the range of frequencies needed during an inspection. This limitation is unfortunate as the mode purity and contol of the signals generated in the study was high.

As stated previously in (Section 3.3.1), Alleyne of Imperial College, London explored the generation of Lamb waves in plates using wedge probes but extended the idea in Alleyne and Cawley (1994) with the use of a variable angle probe to further establish the input paramters governing the generation of Lamb waves in a steel plate. Futher work carried out by Alleyne [Alleyne and Cawley (1996a)] led to the development of a surface shear piezoelectric element. Initial results from tests where the element was bonded directly to the pipe surface show that the mode of interest (in this case the axisymmetric $L(0,2)$) could be generated with a noise floor on the pulse-echo trace being only 1% of the amplitude of the $L(0,2)$ response measured at the pipe end. One of the key conclusions of this paper is that with such promising results gained in terms of Signal to Noise Ratio (SNR), it became clear that the dry coupled method of transduction for GWT could

be developed further to be incorporated into a commercial GWT tool. It is stated in this paper that with some additional process and fabrication a shear transducer could be produced. This transduction method is capable of producing guided waves efficiently over a wide band of frequencies and has therefore become the most widely used for commercial GWT inspections.

3.3.2 Commercial GWT Tool Development

A subsequent paper, Alleyne and Cawley (1996b), from the same research group begins to refine previous findings during their development of a shear transducer and details of responses from a variety of discontinuities found in industrial pipework are presented. Using a circumferential array of dry coupled shear transducers mounted on one end of the pipe Alleyne and Cawley display responses from two girth welds and a patch of corrosion positioned between the girth welds. The transducers were orientated to excite the longitudinal family the result of which is a response containing a combination of the first two axisymmetric modes within the longitudinal family; $L(0,1)$ and $L(0,2)$. It was observed that the patch of corrosion present between the two girth welds could be detected and produced a so-called mode conversion. A mode conversion is the result of the scattering of an incident pulse containing a given combination of wave modes. This scattering effect is an echo of the incident pulse created by a change in cross-section and if the echo contains a different combination of wave modes to those transmitted then mode conversion has taken place.

Additional to the experimental work carried out during the development of a dry coupled shear element, Imperial College also carried out Finite Element Analysis (FEA) to predict the response of various shapes of notches within cylindrical sections. Lowe et al. (1998) presented results gained from FEA and laboratory based experiments. The author measures the reflection coefficients for the $L(0,2)$ wave mode for a range of defect depths and varying axial extent.

Developments in transducer design, defect response analysis and signal processing led Imperial College to file for several patents on the technology with the overall system being described in Cawley and Alleyne (1996). The tooling described contains more than one circumferential array (hereinafter known as a ring) of transducers. With the application of time delays and phase manipulation between the rings guided wave propagation can

be maximised in one direction and suppressed in the other thus making the output of the tool unidirectional. The unidirectional feature allows the researcher or technician to identify a feature in a given axial direction away from the tool. The segmented dry coupled shear tool described in the Cawley and Alleyne (1996) is the most popular form of commercial tool on the market and is manufactured under licence by Guided Ultrasonics Ltd., Plant Integrity Ltd. and more recently by Olympus. The commercial viability in terms of the transduction method across a wide bandwidth and portability has seen the market for this technology open up.

3.4 Output Normalisation and Control of GWT Tools

It was discovered at an early stage in the development of pipe inspection using UGWs that the isolation of a single axisymmetric wave mode on transmission is a key factor which has an impact on the sensitivity of the technique to flaws and other features of interest. Within the frequency range of this technique (typically 20kHz to 100kHz) it is possible to excite a large number of wave modes in a hollow cylinder (see Figure 3.1 overleaf). Fortunately, a large number of these are filtered out spatially when using a segmented GWT tool as demonstrated by Catton (2008).

Catton also investigated and compared the performance of several methods of balancing the output of a circumferential array of dry-coupled shear transducers contained within a GWT tool produced by Plant Integrity Ltd. Appendix A of the document lists and discusses several further techniques which may be employed to balance the output of a GWT and ensure a near perfect axisymmetric output. However, the current state-of-the-art tooling produced by each of the companies mentioned have a limited number of channels and adjusting the performance of each individual transducer is impossible. This inability to individually address the transducers in the array leads to a circumferential imbalance in input amplitude which results in an unknown proportion and number of wave modes being transmitted during an inspection.

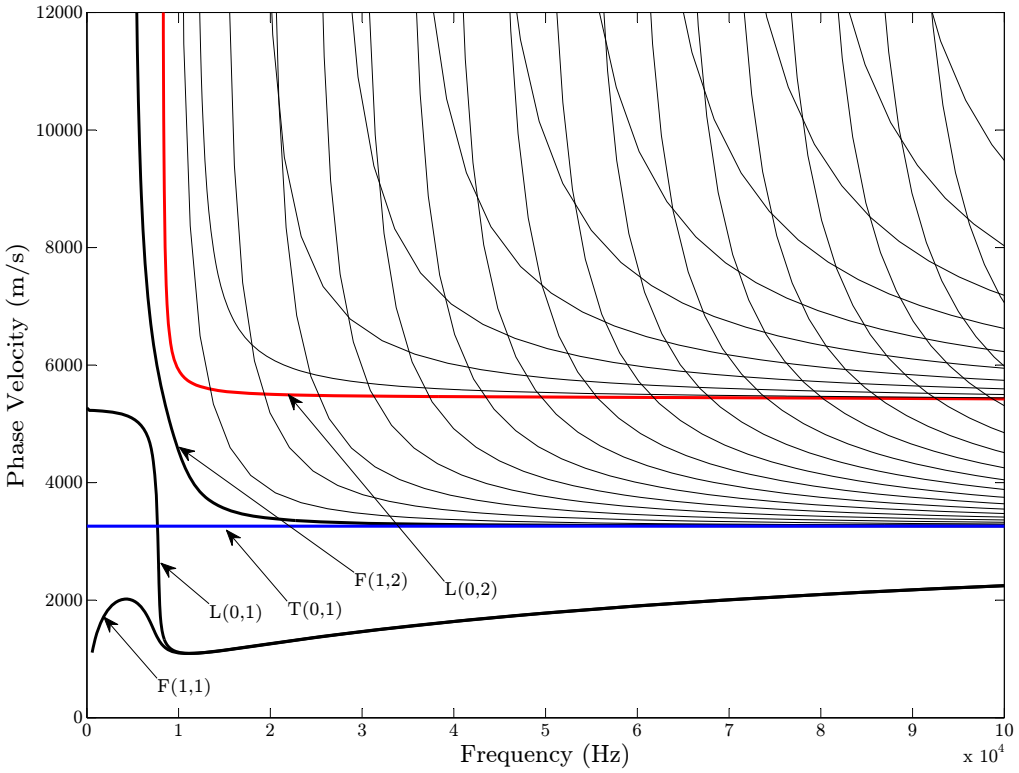

FIGURE 3.1: The phase velocity dispersion curves for an 8inch schedule 40 steel pipe (wall thickness = 8.18mm, outside diameter = 219.1mm). The curves in bold are the five fundamental wavemodes referenced by state of the art GWT equipment to provide an effective pipe inspection

3.5 Applications of Broadband Signals in other Fields

Radar engineers pioneered the controlled usage of broadband signals in an echo-location capacity with many developments being founded just after World War II. One of the limiting factors of radar system performance at the time was detection range. Amplifier and narrowband signal power limitations were overcome by the implementation of a linear Frequency Modulated (FM) signal in Cook (1960). Additional to the development of an optimum broadband input signal for the system, the author proposes a time compression routine to be carried out on the received signal giving better time resolution. The received signals were filtered to resolve narrowband signals and recommendations for filter parameters were suggested. Another notable paper on the subject is Fowle et al. (1963) in which the authors discuss the use of a linear FM transmission signal with a Gaussian envelope with an autocorrelation function at the receiver which was sensitive to the design of the signal transmitted. This allowed the transmission signal to

be differentiated from system and environmental noise within the received time trace, thus improving sensitivity.

In conventional Ultrasonic Testing (UT), linear FM signals (commonly referred to as linear chirp signals) have been implemented to improve the SNR of the received waveform and to overcome power restrictions imposed by pulser/receiver technology. Air-coupled transduction techniques have benefitted greatly from the use of broadband input signals. In Gan et al. (2001) the authors propose the use of broadband capacitance transducers and a wide bandwidth, linearly swept chirp input signal to overcome efficiency issues associated with the transmission of sound between an air-coupled transducer and a test specimen. The results gained showed that combining the broadband input with pulse compression a significant improvement in SNR was achieved. Further work by the same research group led to an improvement in the imaging capability of linearly swept chirp signals through window optimisation [Pallav et al. (2007)]. A thorough discussion on window functions in this paper reveals that by modifying the centre portion of the Tukey window in the time domain to give it an elliptical shape, rather than unity between the rise and fall of the function, undulations (Fresnel ripples) in the frequency domain can be prevented. The reduction of Fresnel ripples leads to improved quality and contrast of any images produced. The authors conclude the paper by comparing the autocorrelation performance of a selection of windows and propose the technique be considered for the optimisation of broadband ultrasound imaging applications. This solution is a compromise between output amplitude, bandwidth and the suppression of any undesired undulations. A more in depth discussion on the suppression of sidelobes and the effects of Fresnel ripples in the frequency domain can be found in Kowatsch and Stocker (1982).

Practical and theoretical recommendations for the employment of a broadband excitation signal for conventional UT transducers that conform to a squared-cosine transfer function were made in Pollakowski et al. (1993). Pollakowski et al. model the transfer function for the transducer and make experimental comparisons to validate their predictions. The authors also provide a guide to the optimum bandwidth of the chirp signal so that the frequencies excited are centred around the resonance of the transducer. Additional observations were made on the comparison of the pulse-compression technique used in radar with the ultrasonic case and according to the research made the radar

equations to calculate the pulse-compression ratio cannot be used for ultrasonics. However, it was found that the ultrasonic transducer acts as a sidelobe reduction filter and after pulse-compression was applied to the received signal a sidelobe improvement of 2.24dB on that of an equivalent radar example was measured. A year later Pollakowski and Ermert continued to explore broadband excitation in UT and demonstrated an improved performance in terms of SNR of pulse-echo mode UT. Matched filters (correlation filters) and so-called pseudochirps (square wave chirps) were used to increase signal amplitude and to further reduce unwanted sidelobes which are produced during pulse-compression.

3.6 Broadband Excitation of Lamb Waves

Due to the high number of wavemodes possible at operational GWT frequencies and associated frequency dependent phenomena *e.g. dispersion*, it was deemed convention to use a narrowband input signal for the inspection of pipes and plates to avoid the excitation of undesired wavemodes that appeared to mask the received time domain signal. In addition to the work already cited here from Alleyne and Cawley (1992), the authors also state that the use of a broadband excitation signal is not recommended for guided wave inspection as the propagation of unwanted modes will result therefore masking the time domain signal with additional noise. Research in contribution to this thesis [Thornicroft and Catton (2010)] has found that an equivalent narrowband signal can be recovered from a broadband trace with minimal error and may offer an alternative excitation and post processing approach to the procedure adopted by the pipeline GWT industry to date.

Almost parallel to the broadband work by Thornicroft and Catton, Georgia Tech reached similar conclusions for the propagation of Lamb waves in aluminium plates using much higher excitation frequencies in Michaels et al. (2011). Michaels et al. provided several snapshots of the wavefield surrounding the transducer showing that chirp signals could be used as an efficient alternative to conducting several narrowband tests. The authors also promote the use of a frequency-wavenumber process to extract non-stationary information within a multimodal signal. The work by Michaels et al. references an earlier brief study on the possible use of chirp signals to excite Lamb waves [Mizutani and

Inokawa (2004)]. The work comprises of a short experimental study in which the transducers are configured in through-transmission on a composite plate comprising of thin bonded sheets of CFRP and Aluminium containing an artificial delamination. Mizutani and Inokawa concluded that measuring the velocity components of Lamb waves using chirp signals was difficult and that further work is needed to refine the technique.

The closest work to the research demonstrated in this thesis is the short overview in Ikeda and Hayashi (2004). The document proposes the use of broadband signals for the guided wave inspection of pipes. The excitation method demonstrated by Ikeda and Hayashi is a linear chirp which is windowed by the Hamming function (The function first derived in (Hamming, 1977, SS. 5.8)). The Hamming function was designed to minimise bandwidth in the frequency domain so it seems that using such modulation for a broadband pulse is not optimum. Multiplying the chirp signal by this window attenuates the frequencies available either side of the centre frequency. This effect can be seen in the scalogram of the input signal produced via a wavelet transform. The mother wavelet was not stated in the paper so it would be difficult to investigate further. The hardware was configured such that the input excitation was applied using a magnetostrictive sensor set up to generate T(0,1) with a second receiving sensor mounted to the pipe 600mm away from the transmitter. The authors do not apply any method of controlling axial direction of propagation away from the transmitting tool. For a commercial system this would not be acceptable as one of the important aspects of GWT is the ability to pinpoint the location of a flaw or feature either side of the tool and thus give the correct time of flight for the response. Ikeda and Hayashi do however provide some interesting experimental results and discussion on the radar-pioneered pulse-compression technique which seems to have good potential.

3.7 Time-Frequency Representations of Lamb Waves

The frequency dependent nature of UGWs manifests itself in many physical variables but a variation of phase and group velocity with frequency means that the response gained from a broadband test is non-stationary. Non-stationary signals have been discussed in length by many scientists and engineers but arguably modern foundations in this area were laid down in Flandrin (1999) and Cohen (1994). There are many

types of distributions which yield results in the time frequency plane. The demonstration the non-stationary nature of Lamb waves in the time-frequency plane by using a two-dimentional Fourier transform (2D-FFT) method in Alleyne and Cawley (1991) but Prosser et al. argued that a large number of closely spaced measurements were required in order to avoid aliasing when carrying out the Fourier transform from the spatial domain [Prosser et al. (1999)]. Prosser et al. combine the use of a broadband excitation signal and chose to display the received signal in the time-frequency plane in a graphite/epoxy composite plate via a Pseudo-Wigner-Ville Distribution (PWVD). The process is more efficient than the 2D-FFT method as there is only one measurement needed via a broadband excitation signal. The time-frequency images presented show the dispersive nature of the plate modes S_0 and A_0 however, due to the interference terms that result when using the PWVD the images are not very defined. The authors have to resort to curve fitting to make a comparison with analytical dispersion curves to good effect. An excellent review paper Niethammer et al. (2001) on the performance of a number of Time-Frequency Representations (TFRs). Niethammer et al. used a Nd:YAG laser to generate Lamb waves over a broad bandwidth (200kHz to 10MHz) which were measured using a high-fidelity interferometer which was resonance free. This means that the measurements collected were not subject to distortion through a varying transfer function. The high resolution experimental set up used in this study was an optimum platform from which to compare the range of TFRs. Niethammer et al. concluded from this study and from a sister paper Niethammer et al. (2000) that the most resolute TFR for use on multi-modal Lamb wave signals was the reassigned spectrogram.

3.8 Summary

The purpose of this chapter is to provide a review of some of the areas of development for the GWT of pipelines and it seems that the use of broadband signals could potentially change the face of the inspection process. The current collection procedure relies on the collection of many frequencies to determine the 'best' frequency from which conclusions on the integrity of the structure at hand can be drawn. This is not an efficient solution but building on the conclusions drawn from the use of broadband transmission signals in other areas a methodology can be derived and applied for the GWT of pipelines.

In addition, the amount of data collected during a test using a broadband excitation is minimal compared with the large array of data currently collected for each test. Given that the GWT industry is currently in the advent of commercialisation of permanently installed monitoring devices collecting large amounts data, it would be sensible to compress the process.

Broadband excitation can also be used as an input to a visualisation and characterisation process for GWT tooling. Due to the non-stationary nature of dispersive wavemodes, broadband excitation highlights these frequency dependent relationships conveniently. It would, for example, be possible to transfer the information contained in a broadband GWT result into the wavenumber-frequency plane so that the contribution of each wavemode generated by the transducer array can be determined.

Chapter 4

Implementation of a Broadband Excitation for Ultrasonic Guided Waves in Hollow Cylinders

4.1 Background

Current GWT technology for pipelines uses a range of narrowband excitation signals which are inputted as separate tests at discrete frequency steps [Mudge (2001); Kwun and Holt (1995); Alleyne et al. (2001)]. A narrowband input signal is used because the majority of the wavemodes that exist within the frequency range of this technique are dispersive *i.e.* they possess a frequency dependent velocity [Alleyne and Cawley (1996a); Pavlakovic et al. (1997)]. The fundamental torsional mode $T(0,1)$ is the only exception to this rule and therefore, a constant phase and group velocity with respect to frequency can be observed for this wavemode [Alleyne et al. (2009)]. Until recently, the idea of broadband excitation in GWT has not been implemented due to a perceived notion that additional complexity caused by dispersion of the broadband carrier signal results in a poor signal to noise ratio (SNR) [Alleyne and Cawley (1992), BS 9690-1:2011].

This chapter proposes a broadband excitation for the propagation of ultrasonic guided waves in hollow cylinders. The derivation of a linear Frequency Modulated (FM) chirp as the carrier signal will be presented along with an appropriate Amplitude Modulation (AM) using an optimised window function. Upon reception of the signals, results of

an adaptive FFT filter with phase modification will show that a narrowband signal of any configuration present within the received spectrum can be emulated with minimum error.

4.1.1 Potential benefits of implementing a broadband signal in GWT

As stated previously in Chapter 3, the potential benefits of the implementation of broadband excitation for GWT can be summarised as:

- A considerable reduction in inspection time. In terms of productivity this can be seen as an increase in efficiency as it would allow a GWT operator to cover more locations per unit time.
- Collection of all frequencies within a wide bandwidth gives the option of selecting any frequency within the excited bandwidth which may be seen as optimum for the situation or most sensitive to a particular geometric feature.
- If the data were to be displayed in the time-frequency plane, some of the non-stationary features of Ultrasonic Guided Waves (UGWs) such as dispersion can be highlighted for further analysis *e.g.* the calculation of time-frequency ridges [Carmona et al. (1997)] and wave mode separation [Xu et al. (2010)].
- Storage and transfer of collected data becomes much more efficient as only one array of numbers is required per sensor in one complete test file as opposed to several separate files for each frequency in the narrowband case. With the GWT technique now being implemented for SHM of pipelines, using a broadband pulse is essentially data compression and will therefore open up the possibility of transmitting collected signals from a remote location periodically via 3G, satellite or any other bandwidth limited networking method.

This study investigates the use of a Linear Frequency Modulation (LFM) excitation signal, whereby a single broadband test *(i.e. one containing a wide range of frequencies)* will provide the same information yielded from a series of separate conventional narrowband tests. A broadband signal approach has been used widely in radar pulse generation as a method of solving the problem of power limitation with respect to spatial resolution

[Mahafza (2000)], but its potential has not been fully investigated for the generation of a variety of elastic wavemodes in solid media.

4.2 Objectives

The aim of the work within this chapter is to establish the feasibility of applying a chosen broadband signal to a single ring of dry-coupled transducers [Alleyne and Cawley (1994)], using commercially available tooling, with a view to recovering an equivalent range of narrowband signals already proven under the framework of standard GWT procedures (see section 6.5 in BS 9690-1:2011).

As such, specific objectives are as follows:

- An appreciation of broadband excitation/reception techniques applied in different fields from the literature
- A procedure for conducting broadband tests under laboratory conditions
- Comparison of chirp tests with conventional tests
- Recommendations for future exploitation/implementation of the broadband excitation approach

4.3 Methodology

4.3.1 Excitation signal generation

The approach taken to validate this proposed shift from the standard narrowband excitation signal currently used, to one containing a wide spectrum of frequencies begins with the design and selection of the proposed signal itself. Properties and limitations of the hardware available will contribute to the outcome of any laboratory trials. It is therefore important to ensure that the hardware is capable of transmitting the proposed signal. The following section introduces theory behind a method which will allow a pulse containing a broad range of frequencies to be transmitted using Plant Integrity's Teletest FOCUS$^+$ low frequency flaw detector.

4.3.2 Laboratory trials

In order to maintain control over this multi variable problem and assess the performance of the proposed excitation method in a pipe it is important that the problem is reduced in complexity. With this in mind a set of experiments were demonstrated using only one ring of dry-coupled piezo-electric transducers orientated such that the dominant wavemode generated is the non-dispersive, fundamental torsional mode; T(0,1). The pipe was defect free and the ends of the pipe were cut square so that the response received at the tool contained minimum coherent noise.

4.3.3 Post-processing

Data collected via laboratory trials contained examples from both the existing narrowband method of excitation and the proposed broadband excitation method. Post-processing procedures were generated which giving a comparison between the two methods. Additional cases are presented which involve other parameters such as variation in pulse length for the broadband method and separate narrowband tests involving a change in the number of cycles used within the pulse. The error between each data set are presented across the frequency spectrum for each comparison.

4.4 Optimisation of a Broadband Excitation Signal

4.4.1 Linear Frequency Modulation (LFM)

Broadband signals are in use across many branches of science including digital comunications, medical ultrasound and electronics. In classical theory the signal which possesses an infinitely wide spectrum whilst being infinitely narrow in time is the Dirac delta function, the fundamentals of which can be found in Bracewell (1986). However, the Dirac delta function cannot be implemented in reality as every signal must be bounded by finite limits. By using the normalised sinc function it is possible to derive an impulse which is an approximation of the Dirac delta function and is wide in frequency and localised in time, an example on this theme can be found in Boashash and Sucic (2003). Due to the localisation of this type of impulse in time it is classified as a monocomponent Frequency Modulated (FM) signal Boashash and Sucic (2000). In GWT a short impulse results in a lower SNR according to Alleyne and Cawley (1996a), it therefore makes sense to seek an excitation signal with a higher time-bandwidth product than that of a monocomponent FM signal. The other main group of FM signals classified by Boashash and Sucic are multicomponent FM signals. An LFM chirp signal is a multicomponent FM signal and in terms of time and frequency there is a high energy distribution across the duration of the pulse which is also observed in its frequency spectrum. According to the observations made by Alleyne and Cawley on the performance of short pulses in GWT, a linearly swept chirp could provide a broadband carrier signal whilst maintaining an envelope which still possesses the energy needed to exceed SNR requirements for the technique.

A chirp signal is a sinusoidal function with a frequency that changes continuously over:

- A stated bandwidth B within a specified excitation time period τ:

$$B : f_1 \leq f \leq f_2 \tag{4.1}$$

$$\tau : 0 \leq t \leq \tau \tag{4.2}$$

The chirp expression used in the tests and to generate the chirp function overleaf in Figure 4.1 can be derived from a sinusoidal toneburst:

$$x_{(t)} = \sin[\omega t + \phi] \tag{4.3}$$

Where $\omega = 2\pi f_c$, f_c is centre frequency and ϕ represents phase in radians.

The introduction of a linear frequency sweep and chirp rate (k) to replace the centre frequency (f_c) results in Linear Frequency Modulation (LFM) within a desired bandwidth: $B = f_2 - f_1$ (f_1 = lower corner frequency, f_1 = upper corner frequency and centre frequency therefore becomes: $f_c = f_1 + B/2$). k is defined as the rate of change of frequency over time.

$$k = \frac{\Delta f}{\Delta t} = \frac{f_2 - f_1}{\tau} \tag{4.4}$$

The linear frequency sweep can be expressed in terms of *instantaneous frequency* as:

$$f_{(t)} = \frac{1}{2\pi}\frac{d}{dt}\phi_{(t)} = f_1 + \frac{k}{2}t \tag{4.5}$$

When substituting this sweep into the sinusoidal toneburst (4.3) the time dependent signal becomes:

$$x_{(t)} = \sin[2\pi(f_1 + \frac{k}{2}t)t] \tag{4.6}$$

Which simplifies to:

$$x_{(t)} = \sin[2\pi f_1 t + \pi k t^2] \tag{4.7}$$

This expression provides a fundamental sine function with a linearly increasing frequency content. The function plotted in Figure 4.1 shows this linear increase in frequency over time. The gradient in this case is known as the *chirp rate*. The expression given in Equation 4.7 yields an *up chirp* as the frequency content is raised upwards in value over time. It is possible to input the chirp rate as a negative value and obtain a *down chirp*, although this was not considered for these tests.

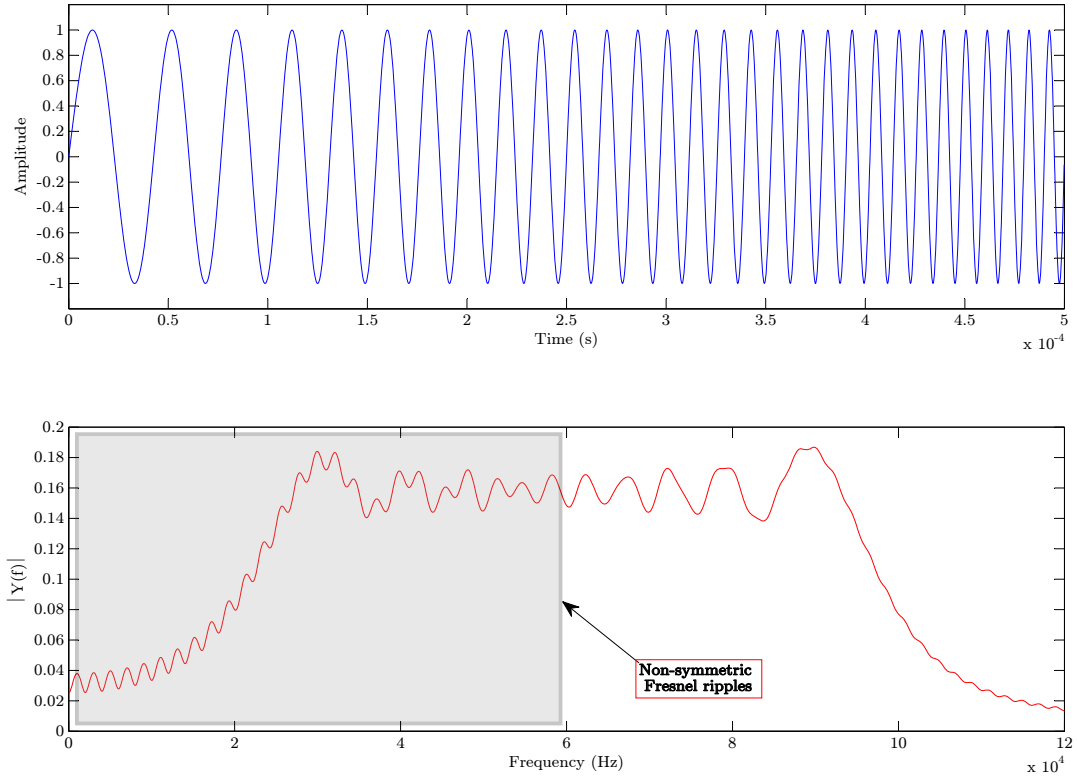

FIGURE 4.1: An LFM chirp signal swept between 20 kHz and 100 kHz with a pulse length of 500μs. The upper axes show the time trace (in blue) with the lower axes revealing the frequency content (in red). The grey area highlights the non-symmetric ringing effect caused by implementing a very low value for the lower corner frequency (f_1)

4.4.2 Amplitude Modulation via a Suitable Window Function

The input signal displayed in Figure 4.1 is unmodulated in terms of amplitude. It can be said that a rectangular window function exists for this signal which bounds it to its signal duration and amplitude limits. This is expressed mathematically as:

$$w(n)_{rect} = 1 \quad \text{if } 0 \leq n \leq (N-1) \tag{4.8}$$

N is the number of digital points and $w(n)$ is used to define a window function in terms of discrete digital points n. This function may be considered as instantaneously switching from a zero state to a sharp rise into the chirp function and again switching off suddenly at a length of N points. This gives rise to the Fresnel ripples observed in the frequency domain plot (the red trace) of the linear chirp in Figure 4.1. The rise

of a rectangular window is effectively an impulse response and when this is mirrored at the centre of the time domain pulse shown in Figure 4.1 it becomes half a cycle of a square wave. The Fourier transform of such a sharp time domain shape gives rise to the Gibb's Phenomenon whereby undulations in the function are created in the frequency domain. This effect was first observed by Wilbraham (1848) but the name was subsequently attributed to Gibbs who wrote a letter to the editor of *Nature* with observations on the Fourier series of the sawtooth function (Gibbs (1899)). In the case of a digital system, such as the Teletest FOCUS$^+$, this effect can produce unstable overshoot behaviour within the electronics causing signal clipping and an increase in load carried by the power amplifiers. Figure 4.2 shows that if the lower corner frequency

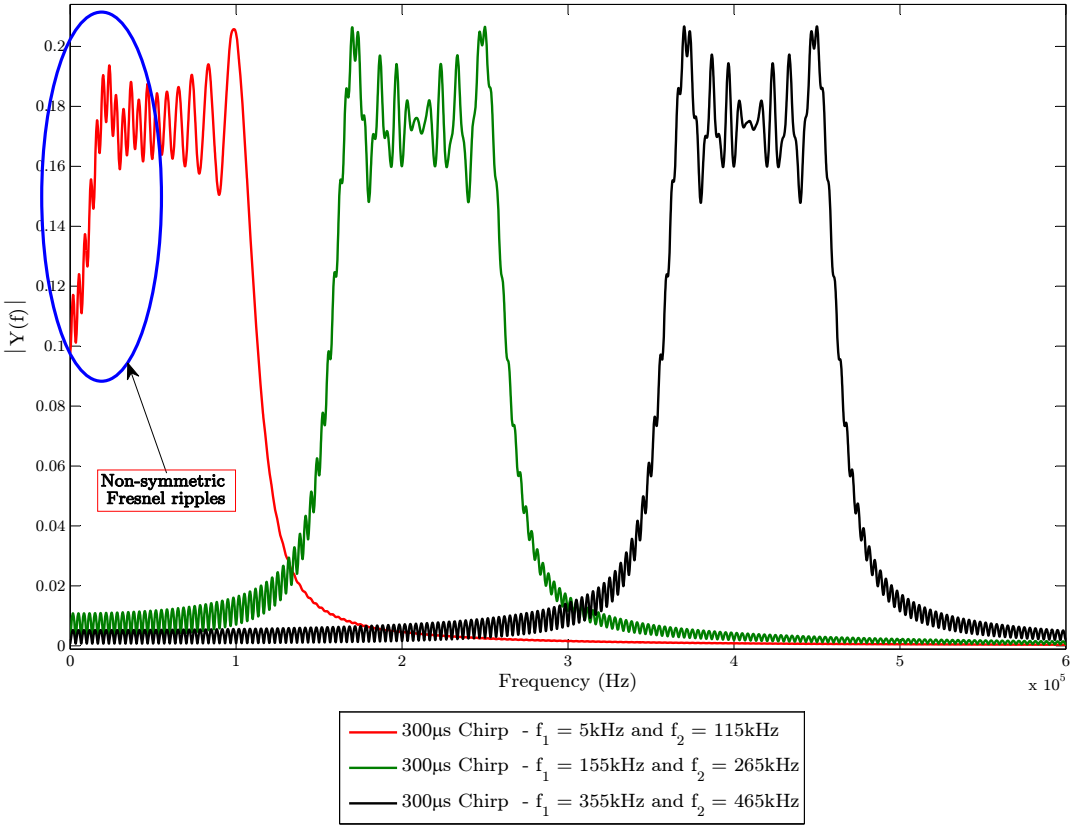

FIGURE 4.2: A demonstration of the effect low frequency chirps have on the symmetry of the Fresnel ripples. All of the LFM chirp signals plotted here have the following parameters kept constant: pulse length = 300μs, $\alpha = 0$ and sample frequency = 10MHz.

(f_1) of the LFM chirp is low enough then the bandwidth below the centre frequency suffers from additional ringing which affects the symmetry of the spectrum. The cause of this is likely to be the fact that the rise up to the magnitude of the lower corner frequency (f_1) in the LFM chirp spectrum is gradual and if the components within that

rise become truncated and therefore less represented, the outcome is additional ringing causing the overall spectrum to be non-symmetric. Figure 4.2 shows two additional LFM chirp spectra, both with higher centre frequencies. The lower corner frequency values for both of these additional spectra do not suffer from this truncation therefore the resulting spectra are much more symmetric.

Fortunately, this ringing effect can be minimised by modulating the pulse with a suitable window function. The frequency response of the proposed linear chirp then becomes almost rectangular. It would therefore be beneficial to preserve the bandwidth by selecting a function which possesses a flat top but also ramps up and ramps down so as to minimise the Fresnel ripples associated with LFM chirp signals. It has been shown in Kowatsch and Stocker (1982) that use of the Tukey window function, also known as the tapered cosine function, can minimise sidelobe ripples and the undulations observed across the main lobe of the LFM chirp whilst maintaining bandwidth. The Tukey window [Tukey (1967)] is described as:

$$w(n)_{Tukey} = \begin{cases} \frac{1}{2}\left[1+\cos\left(\pi\left(\frac{2n}{\alpha(N-1)}-1\right)\right)\right] & \text{if } 0 \leq n \leq \frac{\alpha(N-1)}{2}, \\ 1 & \text{if } \frac{\alpha(N-1)}{2} \leq n \leq (N-1)(1-\frac{\alpha}{2}), \\ \frac{1}{2}\left[1+\cos\left(\pi\left(\frac{2n}{\alpha(N-1)}+1\right)\right)\right] & \text{if } (N-1)(1-\frac{\alpha}{2}) \leq n \leq (N-1). \end{cases} \tag{4.9}$$

Definition in the time domain is therefore as follows:

$$w(t)_{Tukey} = \begin{cases} \frac{1}{2}\left[1+\cos\left(\pi\left(\frac{2t}{\alpha\tau}-1\right)\right)\right] & \text{if } 0 \leq t \leq \frac{\alpha\tau}{2}, \\ 1 & \text{if } \frac{\alpha\tau}{2} \leq t \leq \tau(1-\frac{\alpha}{2}), \\ \frac{1}{2}\left[1+\cos\left(\pi\left(\frac{2t}{\alpha\tau}+1\right)\right)\right] & \text{if } \tau(1-\frac{\alpha}{2}) \leq t \leq \tau. \end{cases} \tag{4.10}$$

The variable α is known as the Tukey ratio. It is a measure of how tapered the slope in and slope out of the function is. When $\alpha = 0$ then the window becomes rectangular as in Equation 4.8, however when $\alpha = 1$ then the Tukey window becomes a Hann window (also known as the raised cosine window [Hamming (1977)]).

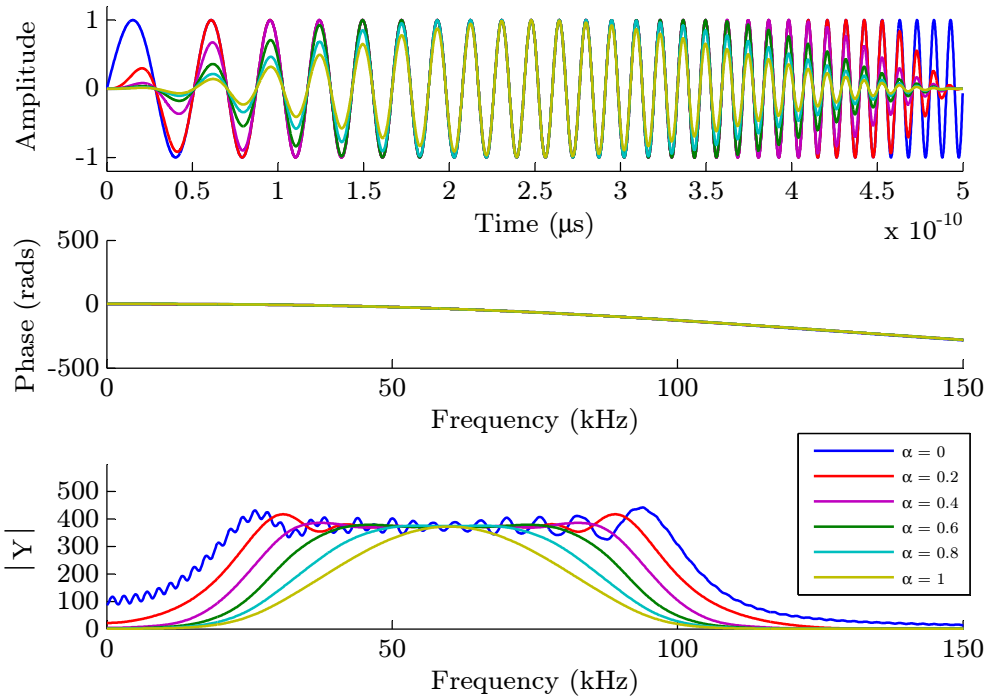

FIGURE 4.3: The effect of varying the Tukey ratio (α) between 0 and 1 on the frequency spectrum. $f_1 = 20$ kHz, $f_2 = 100$ kHz and $B = 80$ kHz. Both unwrapped phase (centre axes) and magnitude (lower axes) are presented.

The plot in Figure 4.3 shows the effect of variation in Tukey ratio α has on the minimisation of Fresnel ripples in the frequency domain. The time domain plot (the upper axes) shows that an increase in α creates a Hann window enveloping the signal with the corresponding Fourier amplitude plot (lower axes) showing a vast reduction in bandwidth due to the application of a Hann window. This relationship reveals a shortcoming in the broadband research carried out by Toiyama and Hayashi. Their approach was to narrow the bandwidth of a broadband excitation signal further by applying a Hann window to the signal before transmission. This effectively reduces the possibilities for broadband imaging and spectral analysis.

The centre axes in Figure 4.3 confirm that because modulation using a window function is an operation which is performed on the amplitude of a signal, the phase remains unchanged. Here, the unwrapped phase is shown for all of the cases displayed in the legend. It is clear that a satisfactory balance is needed between the level of undulations measured in the signal and the effective bandwidth of the pulse. Pollakowski et al. provided recommendations for LFM excitation within compression probe based Ultrasonic

Testing (UT) systems with transducers which conform to a squared-cosine output curve. The authors stated that the LFM bandwidth is 1.14 times the 6 dB bandwidth (7 % per side) of the transducer. This suggests that the signals of importance lie within the 6 dB limits of the output. Dry-coupled shear transducers used in GWT are broadband in nature and acceptable levels of SNR (typically ¿32dB) can be achieved over the recommended inspection bandwidth, which for the Teletest FOCUS$^+$ system is 20 kHz to 100 kHz. It is therefore reasonable to set the output limits to those recommended by Pollakowski et al. when applying the chirp signal for the Ultrasonic Guided Wave (UGW) case.

For an effective bandwidth of 80 kHz between 20 kHz and 100 kHz within -6 dB limit measured from peak magnitude in the frequency domain it was found that using a lower corner frequency value (f_1) of 5 kHz and an upper corner frequency value (f_2) of 115 kHz had to be applied. This ±15 kHz limit holds true for maintaining the effective bandwidth for all of the various broadband pulse lengths examined (see Figure 4.4).

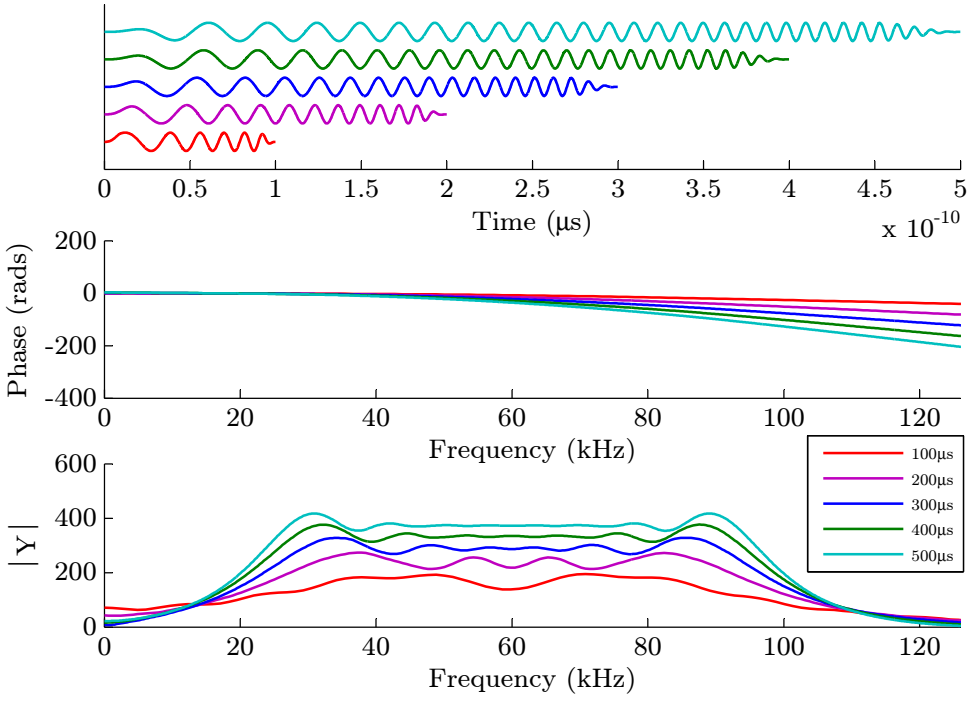

FIGURE 4.4: The effect of a varying LFM chirp pulse length on the frequency spectrum (phase and magnitude). Here the *unwrapped* phase is presented in order to give an idea of the accumulative effect across the spectrum. The input parameters are: $\alpha = 0.2$, $f_1 = 20$ kHz and $f_2 = 100$ kHz

By fixing the Tukey ratio to 0.2 and the frequency limits of the LFM to ±15 kHz of the total proposed excitation bandwidth, it is possible to reveal the effect pulse length (τ) has on frequency content. Figure 4.4 shows a selection of LFM chirp pulses varying in length, thus revealing the effect this parameter has on the frequency spectrum. The unwrapped phase spectrum shows that a shorter LFM chirp pulse possesses a less severe gradient to that of a longer pulse with otherwise identical parameters. This behaviour is attributed to the number of cycles within the carrier signal. If the signal is short in time across a fixed bandwidth then it will possess less cycles and will deviate in phase less across the spectrum than a longer signal possessing more cycles. The use of unwrapped phase is only used to make the visualisation of this behaviour more comprehensive it was not used during derivation of further parameters.

The magnitude of the spectrum shown in Figure 4.4 shows that the pulse length affects the shape and therefore bandwidth of the signal. The red trace in the top axes shows an LFM chirp in the time domain at 100 μs in length with the bottom axes showing the FFT result, again red is used for 100 μs signal. The short pulse is localised in time but not in frequency. This due to the fact that the Fourier transform is a reciprocal relationship as proven by the *similarity* or *stretch* theorem [Bracewell (1986)]. If a signal with a time domain vector t is scaled by a to become at then the apparent *'stretched'* effect on the Fourier transform of $f(at)$ can be described as:

Firstly if $a > 0$:

$$\int_{-\infty}^{\infty} f(at)e^{-2\pi ist}dt = \int_{-\infty}^{\infty} f(u)e^{-2\pi is(\frac{u}{a})}\frac{1}{a}du \tag{4.11}$$

$$(substituting\ u = at)$$

$$= \frac{1}{a}\int_{-\infty}^{\infty} f(u)e^{-2\pi i(\frac{s}{a})u}du \tag{4.12}$$

$$= \frac{1}{a}\mathcal{F}f(\frac{s}{a}) \tag{4.13}$$

In the case of $a < 0$ the limits of integration are inverted when the substitution of $u = at$ occurs, the resulting transform becomes negative: $(\frac{-1}{a})\mathcal{F}f(\frac{s}{a})$. Combining both situations yields the Stretch Theorem:

$$\text{If } f(t) \rightleftharpoons F(s) \text{ then } f(at) \rightleftharpoons \frac{1}{|a|}F\frac{s}{a} \tag{4.14}$$

The Stretch Theorem not only dictates the frequency content of the proposed LFM chirp but it also has an effect on the current narrowband GWT procedure. The aim of conditioning the current excitation signal is to minimise bandwidth to reduce the distortion effects caused by dispersion whilst maintaining an acceptable level of temporal resolution. For example an excitation signal at a given centre frequency containing 20 cycles will be narrow in the frequency domain thus minimising dispersion but in terms of detecting closely grouped flaws or features within a test specimen the pulse length at 20 cycles will have a reduced temporal resolution and the grouped flaws/features will not be detected.

It is not possible to change the behaviour of the Fourier transform, therefore a compromise between magnitude, bandwidth and temporal resolution is to be reached.

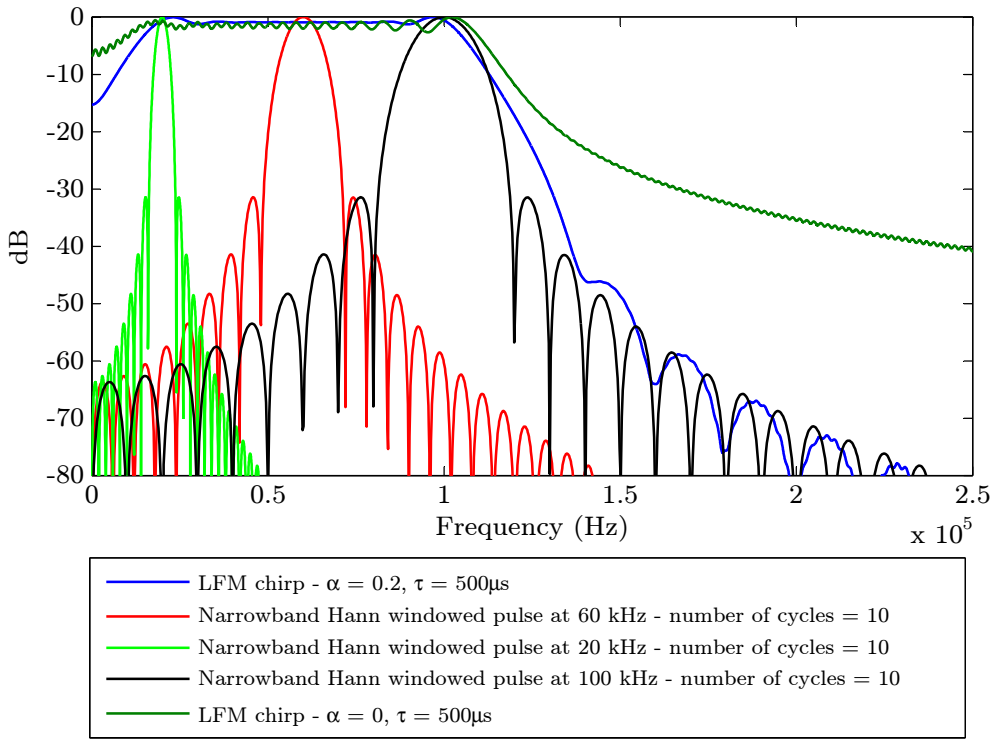

FIGURE 4.5: A frequency domain comparison of three 10 cycle, Hann-windowed pulses used in GWT (20 kHz, 60 kHz and 100 kHz) with two LFM chirp pulses; one with no Tukey window and the other with a 20% Tukey ratio applied

Figure 4.5 shows three narrowband pulses at 10 cycles along with two LFM chirp signals. The narrowband signals at 20 kHz and 100 kHz were chosen as markers to demonstrate that the proposed LFM chirp could span the desired bandwidth. The trace in red is the

narrowband pulse which represents the central frequency within the desired bandwidth; 60 kHz. It is interesting to note that by applying the Tukey window to the LFM chirp signal the upper sidelobe behaviour becomes attenuated just as Kowatsch and Stocker demonstrated. The attenuation rate is similar to that of the 100 kHz narrowband signal. This suggests that if a bandpass filter were applied to the received wideband signal, the narrowband frequency content could in theory be successfully recovered. The same can be said for the 20 kHz end of the spectrum. However at the pulse lengths required by this technique, the LFM chirp sidelobe attenuation observed below 20kHz will not ramp up from zero. The low frequency bias is a direct result of the Stretch Theorem and will not therefore attenuate until the pulse length is increased somewhat. This should not affect the quality of the data beyond the post-processing stage as the bandwidth of interest will be selected using filters in the frequency domain.

4.5 Experimental Validation

To validate the proposed theory an experiment was devised to meet the objectives stated at the beginning of this chapter.

4.5.1 Experimental set up

In order to keep this initial validation simple in terms of wavemode selection and system, a single ring of 24 transducers were loaded into a standard pneumatic Teletest GWT tool. They were orientated such that the displacements of the transducers were circumferential thus predominantly producing the non-dispersive, fundamental torsional wavemode $T(0,1)$. The tool was wired such that the circumference was divided into eight octants with three transducers in each octant representing one transmission/reception (Tx/Rx) channel. A synchronised transmission using an identical excitation signal on all eight channels in theory produces an axisymmetric wavemode. In practice, however, the axisymmetric wavemode is generated along with a measurable of multimode content which, on a defect free specimen, is classified as coherent noise. It is known as coherent because the responses appear within the excitation bandwidth of the wavemode of interest. This phenomenon is not the focus of these particular tests, but it is important that

the narrowband and broadband processed results are comparable to each other including the level and envelope of the coherent noise generated.

The specimen chosen was a 9m long, mild steel, 8 inch schedule 40 pipe (OD = 219mm, wall thickness = 8.18mm) containing no flaws or features and the ends were cut square. Pipes of this size are usually supplied with pre-formed bevelled ends for girth weld preparation, the presence of which cause mode conversion and phase shift problems when used as a reference reflector.

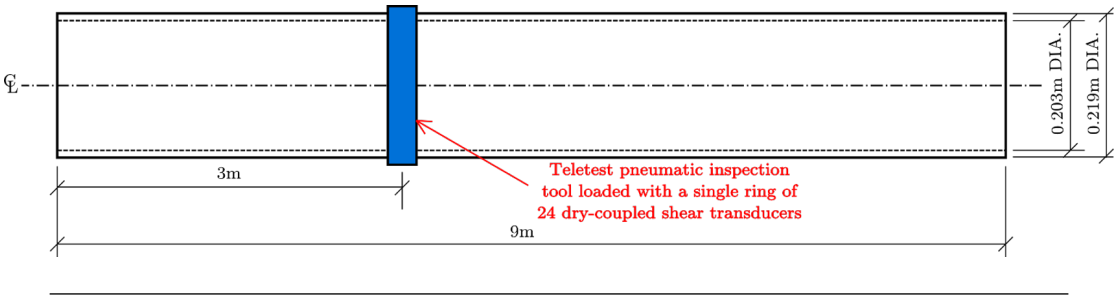

FIGURE 4.6: Experimental set up

Figure 4.6 shows the principle of the experimental set up. The chosen pipe was simply supported on pipe stands but the structure was insulated acoustically from the supports by foam inserts. This insulation process was carried out so that responses created by a local change of stiffness caused by the supports could be minimised. The tool was positioned so that the distance to the near end represented 1/3 of the total length (3m). This distance was chosen so that the time domain responses displayed would not overlap for each of the narrowband tests across the chosen bandwidth.

The coupling force required by the ring of transducers is delivered by a pressurised pneumatic bladder positioned behind the modules containing the transducers. Throughout the experiment this pressure was controlled via a compressed airline and pressure regulator set at 4 bar. Any deviation in pressure during or between tests could have changed the coupling characteristics of the tool and therefore results gained may not have been comparable. In addition a thermocouple was positioned on the surface of the pipe in the region of the tool. It has been shown that temperature affects material properties that govern stiffness and therefore a variation in the speed of sound within a material can be observed [Konstantinidis et al. (2006)]. The experiments for this chapter were carried out in a temperature controlled laboratory space and the thermocouple confirmed this variability to lie within a tolerance of $\pm 1^{\circ}$C.

The pulser/receiver used for the tests was the Teletest FOCUS$^+$ unit which has the ability to accept modified excitation parameters such as the LFM chirp waveforms shown in Figure 4.4.

4.5.2 Initial results

The broadband experiment was divided into six tests each possessing a different value for pulse length (τ). The Tukey ratio for each test was set to 0.2 with a lower corner frequency (f_1) of 5 kHz and an upper corner frequency (f_2) of 115 kHz.

A set of conventional (narrow frequency bandwidth) tests sequentially swept between this frequency bandwidth were then carried out based upon normal test conditions for comparison, which were subsequently used as a baseline for the LFM chirp results.

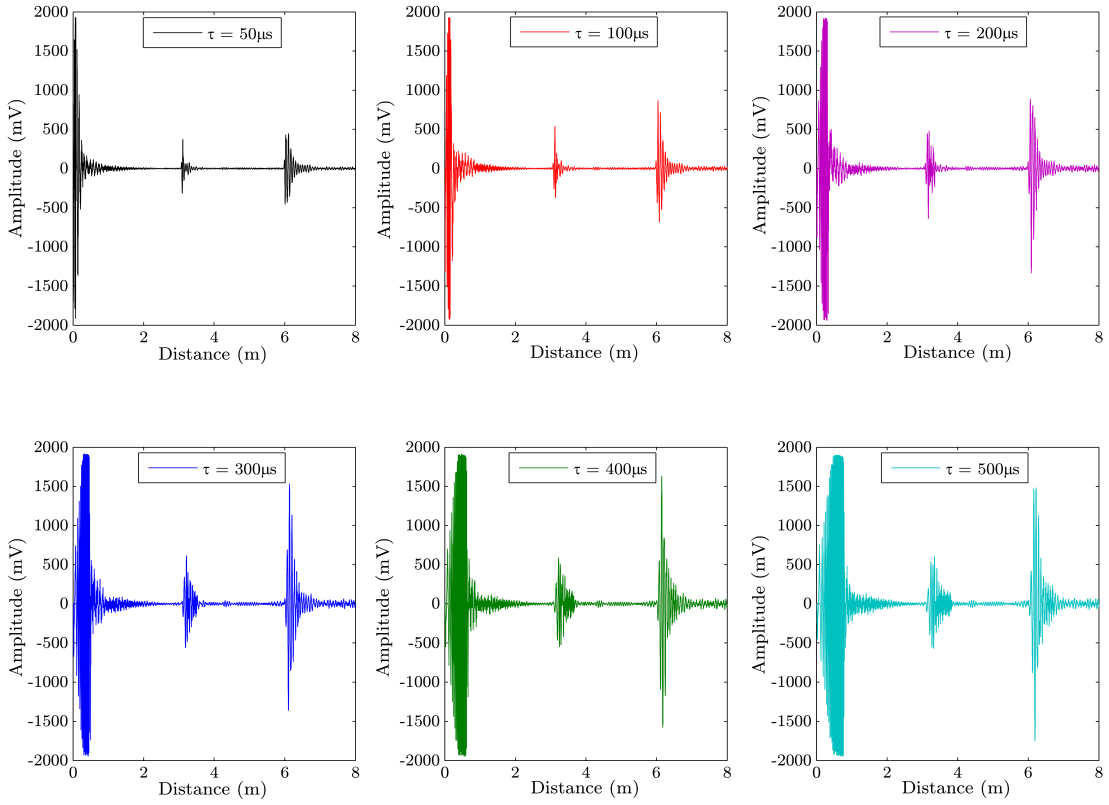

FIGURE 4.7: LFM chirp distance domain responses for the sum of the octants from the 8 inch schedule 40 pipe derived from the time domain using the theoretical group velocity for $T(0,1)$. For each test the pulse length (τ) was varied to be the following: 50μs, 100μs, 200μs, 300μs, 400μs and 500μs. The bandwidth used here was 5 kHz - 115 kHz.

The initial distance domain results in Figure 4.7 shows that by increasing the pulse width an increase in overall amplitude can be measured. The unit for the x axis has been chosen to be distance in metres (based on the group velocity of the wavemode presented: $T(0,1)$) since the GWT technique relies upon distance measurements along a given pipe to identify responses within an A-scan. The data presented is the sum of the 8 octants (24 transducers ganged into 8 groups of 3 wired to operate in unison). At the very beginning of each of the six traces is a high amplitude signal. This signal is an electronic artifact which is produced during transmission. Because the system is set up to transmit a high voltage input signal (300V peak to peak) but receive at low voltage (mV) using the same channel within a confined space, crosstalk or interference between channels occurs. Crosstalk and interference can be reduced through screening and spatial separation but it is a electronic design topic and is not the focus of this thesis. Once the transmission period is complete, the hardware switches the channel over to reception mode. Two further artifacts can be present at the beginning of the reception: *(a)* a switch-on spike and/or *(b)* transducer ringing.

- The so-called switch-on spike is present due to an instant switching from high voltage transmission to a low voltage reception. Because of its shape in the time domain (*i.e. it equates to a very short pulse*) it is usually broadband and without further processing can contribute to false readings when measuring the spectral content of GWT signals.
- Transducer ringing is frequency dependent and is often caused by poor coupling. During transmission the transducers are vibrating intensely, therefore upon switchover to reception there is a settling time, as is the case with any other underdamped vibrating system. If the transducer is not coupled or damped adequately then the settling time increases and the system continues to measure the resulting displacement.

These factors that can often occur at the beginning of the signal may mask the time domain results (often this is known as the dead zone) but also because of their amplitudes and associated frequency content, they dominate the measured spectra. It is therefore important to apply blanking or zero padding to reveal the true ultrasonic information within the received signal. Figure 4.7 shows that minimising the excitation pulse length also minimises the length of the so-called dead zone. This may open up the opportunity

to apply short LFM chirp signals to inspect areas close to the tool which would have otherwise been masked by Tx/Rx artifacts. The disadvantage of using short pulses is that transmission range is shortened, but if the signals are implemented specifically to collect responses close to the tool then the quality of the 50 μs scan shown in Figure 4.7 demonstrates that short LFM chirps can be used for this purpose.

Other than the Tx/Rx artifacts, the two main responses within each trace shown in Figure 4.7 are the near end reflection at 3m behind the tool and the far end reflection at 6m in front of the tool (assuming a test direction of forwards being towards the far pipe end). Because there is only one ring of transducers present there is no directional control hence the presence and amplitude of the two measured responses. The distance axis was determined by using the theoretical value for the group velocity (v_{gr}) of $T(0,1)$ as 3260m/s.

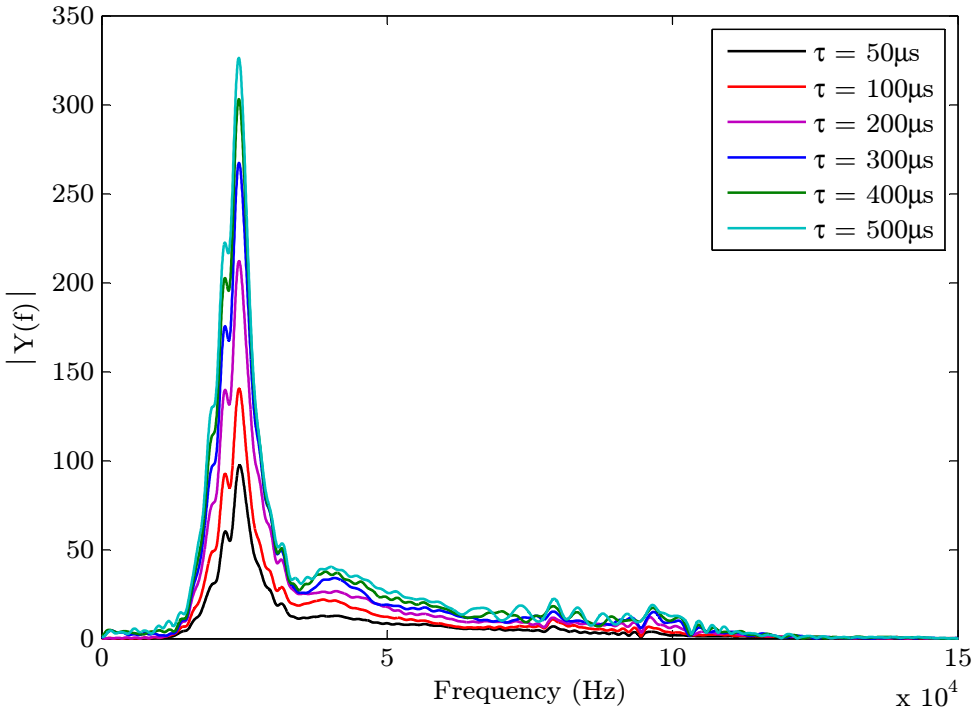

FIGURE 4.8: This is the frequency response of the chirp pipe-end reflection. The excitation bandwidth was 5 kHz - 115 kHz

Figure 4.8 represents the magnitude of the frequency response for the pipe end reflection at 9m. The response was isolated by setting lower and upper limits in the time domain (a process known as gating) and applying an FFT. Gating the response allows a more

representative spectrum for the output of this system as considering the spectrum of the complete received signal can result in distorted results. What is immediately apparent upon examination of Figure 4.8 is that the frequency response does not conform to the input spectrum seen in the ideal broadband excitation signal (Figure 4.4). This suggests that the transfer function of the system as a whole (which includes the electronics, the tool, the waveguide and transducers) acts as a sharp bandpass filter whose magnitude peaks at approximately 25 kHz for this experimental set up. This system behaviour will hamper the performance of any broadband imaging used in post processing. Within the excited bandwidth there is a raised magnitude which may suggest that narrowband signals may be recovered. As predicted via the stretch theorem, the shortest pulse length has yielded the lowest magnitude and conversely the longest pulse length has resulted in the highest magnitude.

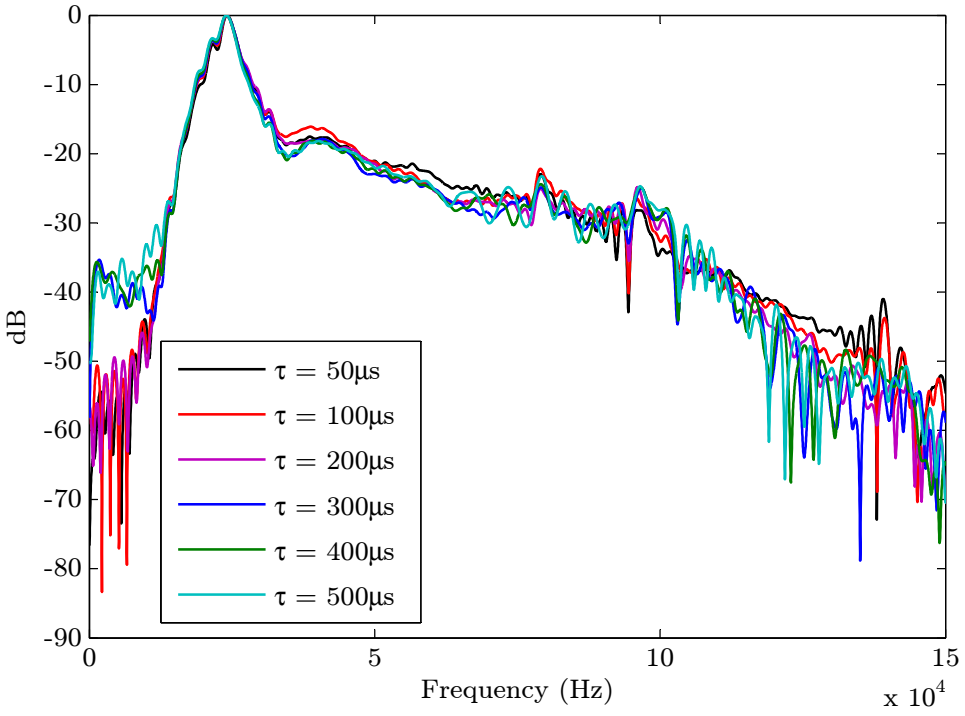

FIGURE 4.9: This is the frequency response of the chirp pipe-end reflection in dB. The excitation bandwidth was 5 kHz - 115 kHz

Figure 4.9 shows the spectrum displayed previously in Figure 4.8 but on the decibel scale. The maximum value now for each trace becomes zero making the data set comparable in terms of relative magnitude with respect to frequency. Displaying the data set using this method shows that the envelope of the spectrum regardless of pulse length is

approximately the same shape within the bandwidth of interest. This further confirms that regardless of input signal bandwidth, or shape in the time domain, the envelope of the transfer function will be constant. For example, if the system was excited with a series of narrowband impulses across a given bandwidth and a subsequent test was carried out with a broadband test using the same given bandwidth, the transfer function or ratio of input versus output peak amplitudes for each case would be approximately equal. Any modification of this spectrum would require changes in tool, electronics and transducer design. Measurement of the individual contributions of these components to the overall transfer function would have to be measured separately in a set of more in-depth experiments. Modelling could assist this process and may bring better understanding of the parameters influencing the response of the system.

4.6 Post-Processing

4.6.1 Filtering using FFT Convolution

The methods in which GWT data is gathered, displayed and interpreted are not in real time as with short range ultrasonic testing techniques such as phased array UT. This is due to the long propagation distances covered during a GWT inspection and therefore large amounts of data handled using this technique. For example, if an inspection with a diagnostic length (x) of 50m was carried out using the fundamental torsional mode $T(0,1)$ (V_{gr} = 3260 m/s) with a sample frequency (F_s) at 1MHz then the number of points (N) in the data set would be:

$$\begin{aligned} N &\approx \frac{F_s x}{v_{gr}} \\ &\approx \frac{1 \times 10^6 \times 50}{3260} \\ &\approx 15337 \; \textit{points} \end{aligned}$$

In addition to the large amount of data collected, offline or batch processing within a specified directory on the PC controller is used as the time delays associated with long range propagation do not allow real time processing or display. The current Teletest system implements an FFT filter within the post-processing routine in order to attenuate frequencies outside of the desired bandwidth. An FFT method is chosen because

the filter kernel (the desired frequency response shape used during convolution) is easily generated and can be customised to bandwidth requirements. Digital filtering using FFT convolution is a method widely implemented for offline data [Smith (2011)]. FFT convolution is implemented by multiplying a desired frequency *template* (the time domain representation of which is known as the kernel) by the raw received signal in the frequency domain. The underlying principle is that multiplication in the frequency domain corresponds to convolution in the time domain. Pre-1965 this was carried out by using the Discrete Fourier Transform (DFT) and was a time-consuming process as it was computationally heavy.

The DFT is a digital implementation of the Fourier transform presented in Equation 4.11 and can be described as [Lempriere (2002)]:

$$F_m = \sum_{n=0}^{N} f_n e^{-in\Delta tm\Delta\omega} \tag{4.15}$$

Where f_n represents the time domain signal digitally sampled to be discrete values of n between 0 and N, Δt is the time interval and $\omega_m = m\Delta\omega$ is the frequency bandwidth sampled at the frequency increment $\Delta\omega$. The set of complex values produced is the DFT of the time function f_n. The Cooley-Tukey algorithm was developed to improve the efficiency of the DFT [Cooley and Tukey (1965)]. By changing the input parameters in the exponent the DFT the process becomes the Fast Fourier Transform (FFT):

$$F_m = \sum_{n=0}^{N} f_n e^{\frac{-i2\pi mn}{N}} \tag{4.16}$$

The FFT algorithm is most efficient when N is a power of 2, *i.e.* $N = 2^p$ where p is a whole integer.

Figure 4.10 overleaf shows the spectrum of a narrowband GWT axisymmetric test at 60 kHz using the experimental set up shown in Figure 4.6. The blue trace is the filter kernel currently used by the Teletest system for a 60 kHz pulse containing 10 cycles, the red trace is the ideal transmission spectrum for a 60 kHz Hann-windowed pulse again containing 10 cycles. The black dashed trace is the unfiltered received signal from the test at 60 kHz. The width of the filter response is set to only include the first sidelobe of the ideal transmission spectrum. The upper and lower frequency limits (f_1 and f_2) at any sidelobe minimum for a Hann-windowed pulse can be expressed as [Oppenheim

and Schafer (1975)]:

$$f_1 = f_c - \frac{f_c(k+2)}{n} \tag{4.17}$$

$$f_2 = f_c + \frac{f_c(k+2)}{n} \tag{4.18}$$

Where f_c is the centre frequency, k represents the number of sidelobes to be included in the desired bandwidth ($k = 0$ considers only the main lobe) and n is the number of cycles within the pulse.

Using FFT convolution, the filter response is then multiplied by the magnitude of the received spectrum in the frequency domain. This operation only operates on the magnitude spectrum leaving the phase intact. One advantage of the FFT convolution method is that the desired spectrum can be defined. The filter in this case is defined as an approximation to a top hat or rectangle function with a sloped transition in and out of the desired bandwidth. The filter must be this shape in order to preserve the shape of the Hann-windowed pulse transmitted. However, because there is no curvature which ramps up to a maximum value across the bandwidth during the filtering process ringing occurs within the sidelobes. Figure 4.10 shows this effect in the green trace. This effect could be minimised by applying a similar shape to that of the Tukey window where the raised cosine transition provides a smooth slope in and out thus reducing ringing. Although the ringing observed within the sidelobes changes the spectrum slightly, the main lobe of interest remains identical which means that the time domain signal will only contain minor errors.

4.6.2 Adapting FFT Convolution for Broadband Excitation

In the previous section the design of the current narrowband FFT filter used within the Teletest system was discussed. This design is effectively a smoothed rectangle function which is set to preserve the information within the main lobe in the frequency domain with transition regions which attenuate the first sidelobe above and below the mainlobe. The shape of the received response shows that during the transmission and reception of sound in the specimen the spectrum conforms well to the theoretical spectrum (the red trace in Figure 4.10). In order to extract an emulated equivalent narrowband result from a broadband test using the same experimental set up, the existing smoothed rectangle

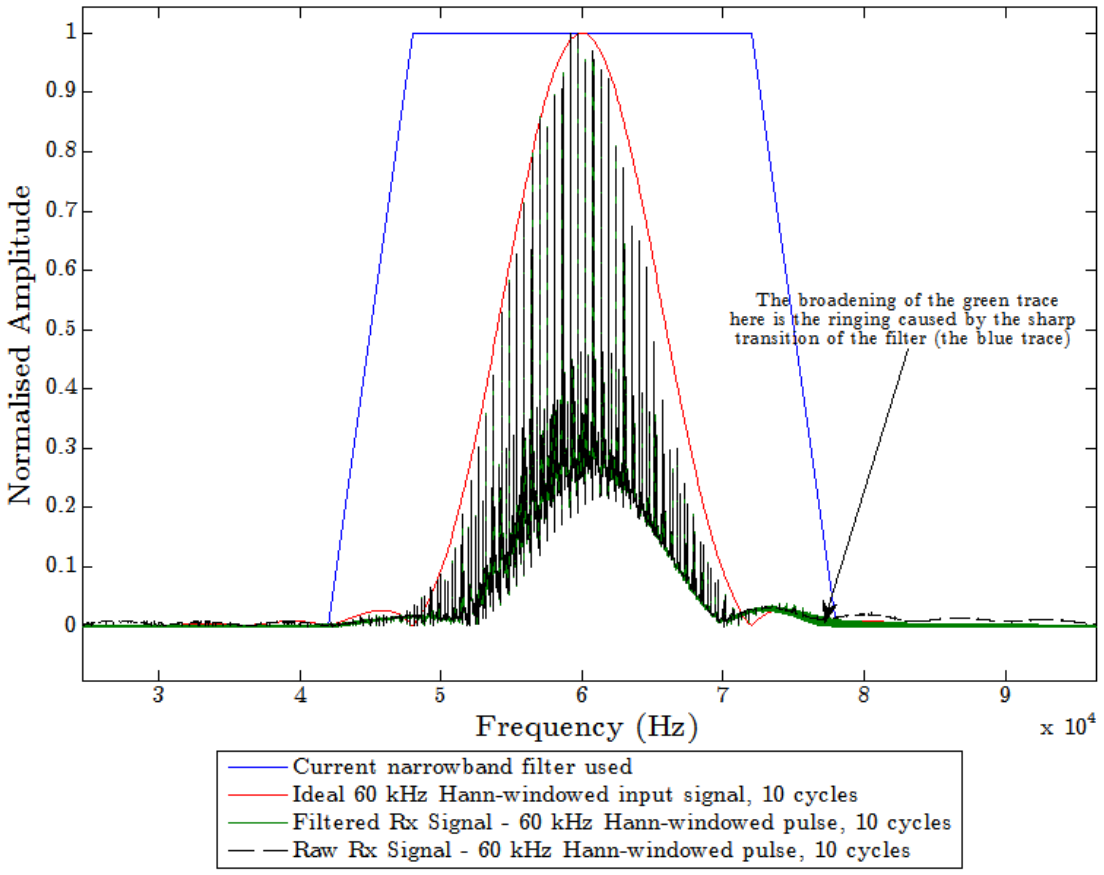

FIGURE 4.10: The normalised spectrum of an example narrowband GWT signal at 60kHz. The filter kernel is shown in blue, the ideal Tx spectrum in red, the raw Rx spectrum in black and the result of the FFT convolution in green

FFT filter would be unsuitable as spectral leakage would occur either side of the centre frequency. It would therefore be more appropriate to use the ideal magnitude spectrum from the desired narrowband input signal as the FFT filter. This would ensure that the filter attenuates the result correctly. In addition, ripples in the frequency domain caused by the sharp truncation of the spectrum in the currently implemented filter would not occur as the proposed FFT filter would be applied with the sidelobes intact. The example case stated here in Figure 4.10 is a narrowband input signal at 60 kHz with 10 cycles but the principle holds true for any combination of these parameters. The current input signal used for narrowband GWT using the Teletest system can be defined as a sinusoidal toneburst modulated using the Hann window. The Hann window is chosen as it gives a reasonable compromise between bandwidth and sidelobe attenuation [Blackman and Tukey (1959)].

The red trace in Figure 4.10 is the desired shape for the FFT filter in terms of magnitude.

However, during FFT convolution the phase spectrum remains untouched within the bandwidth passed by the filter. This is a major advantage of using FFT convolution for filtering. The proposed method for this work uses a phase manipulation process which computes the difference in phase between the ideal input broadband signal and the desired narrowband signal to be emulated. This difference in phase spectrum is then used to reconstruct the FFT before an inverse is applied to reveal the filtered time domain result. In a sense it can almost be viewed as a form of manipulated matched filtering.

4.6.3 Proposed FFT Phase Manipulation

The proposed phase manipulation method for the filtering of broadband GWT signals down to an equivalent, emulated narrowband result operates by comparing two template signals; the ideal broadband input signal and the desired, ideal narrowband template. Firstly, the FFT of both the broadband transmission signal ($x_{n(LFM)_{TX}}$) and the desired narrowband signal ($x_{n(Hann)_{TX}}$) to be extracted are calculated. The time domain signals here are expressed in digital points (n) as the FFT is a discrete function.

$$X_{m(LFM)_{TX}} = \sum_{n=0}^{N} x_{n(LFM)_{TX}} e^{\frac{-i2\pi mn}{N}} \tag{4.19}$$

$$X_{m(Hann)_{TX}} = \sum_{n=0}^{N} x_{n(Hann)_{TX}} e^{\frac{-i2\pi mn}{N}} \tag{4.20}$$

The results of both equations 4.19 and 4.20 are complex numbers with the phase spectrum of each being represented by the following relationships:

$$\phi(\omega_m)_{(LFM)_{TX}} = \arctan\left[\frac{\Im(X_{m(LFM)_{TX}})}{\Re(X_{m(LFM)_{TX}})}\right] \tag{4.21}$$

$$\phi(\omega_m)_{(Hann)_{TX}} = \arctan\left[\frac{\Im(X_{m(Hann)_{TX}})}{\Re(X_{m(Hann)_{TX}})}\right] \tag{4.22}$$

A measure of phase difference between the two reference signals is then obtained:

$$\phi(\omega_m)_{(diff)} = \begin{cases} \phi(\omega_m)_{(LFM)_{TX}} - \phi(\omega_m)_{(Hann)_{TX}} & \text{if } \phi(\omega_m)_{(LFM)_{TX}} > \phi(\omega_m)_{(Hann)_{TX}}, \\ \phi(\omega_m)_{(Hann)_{TX}} - \phi(\omega_m)_{(LFM)_{TX}} & \text{if } \phi(\omega_m)_{(LFM)_{TX}} < \phi(\omega_m)_{(Hann)_{TX}}, \\ \phi(\omega_m)_{(LFM)_{TX}} = \phi(\omega_m)_{(Hann)_{TX}} & \text{if } \phi(\omega_m)_{(LFM)_{TX}} = \phi(\omega_m)_{(Hann)_{TX}}. \end{cases} \tag{4.23}$$

Once the phase difference ($\phi(\omega_m)_{(diff)}$) has been calculated it can be used as an operator to shift the phase spectrum of a received broadband signal thus emulating a narrowband test.

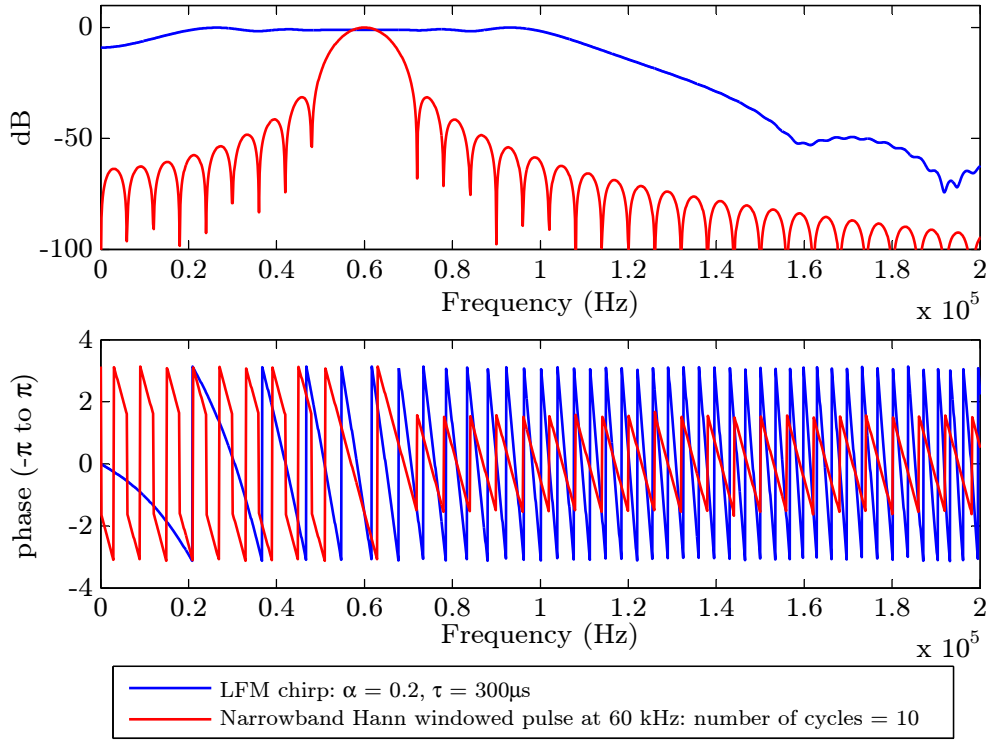

FIGURE 4.11: The magnitude and phase spectrum of two example transmission signals used as templates in the FFT phase manipulation process. The red trace is the narrowband signal, in this case it is a Hann-windowed, 10 cycle pulse with a centre frequency (f_s) of 60kHz. The blue trace represents the spectrum of a broadband LFM chirp. ($\tau = 300\mu$s and a Tukey ratio of $\alpha = 0.2$)

Figure 4.11 shows the broadband and narrowband spectra in terms of their magnitude and phase. The example trace in red is the frequency response of a Hann-windowed, 10 cycle pulse at 60 kHz. Before FFT convolution the magnitude part ($X_{m(Hann)_{TX}}$) is normalised so that the peak at the centre frequency becomes 1. This function, $X_{m(Hann)_{filt}}$, becomes the filter which when multiplied with the received broadband signal in the frequency domain attenuates the undesired spectral information in terms of magnitude. The resultant spectrum contains two parts however; magnitude and phase. The phase is left untouched during convolution as the filter at this stage only operates on magnitude. The phase is then corrected using the phase difference operator calculated in Equation 4.23. The proposed FFT filter can be described using the following process:

The FFT of the received broadband signal is calculated as:

$$X_{m(LFM)_{RX}} = \sum_{n=0}^{N} x_{n(LFM)_{RX}} e^{\frac{-i2\pi mn}{N}} \tag{4.24}$$

This signal is then convolved with the normalised filter derived from Equation 4.20 to create a narrowband signal without phase correction:

$$X_{m(Hann)_{Initial}} = X_{m(Hann)_{filt}} * X_{m(LFM)_{RX}} \tag{4.25}$$

The magnitude and phase of this derived spectrum are expressed as:

$$|X_{m(Hann)_{Initial}}| = \sqrt{\Re(X_{m(Hann)_{Initial}})^2 + \Im(X_{m(Hann)_{Initial}})^2} \tag{4.26}$$

$$\phi(\omega_m)_{Initial} = \arctan\left[\frac{\Im(X_{m(Hann)_{Initial}})}{\Re(X_{m(Hann)_{Initial}})}\right] \tag{4.27}$$

Phase manipulation is carried out by using the phase difference operator:

$$\phi(\omega_m)_{(adjusted)} = \begin{cases} \phi(\omega_m)_{Initial} - \phi(\omega_m)_{(diff)} & \text{if } \phi(\omega_m)_{(LFM)_{TX}} > \phi(\omega_m)_{(Hann)_{TX}}, \\ \phi(\omega_m)_{Initial} + \phi(\omega_m)_{(diff)} & \text{if } \phi(\omega_m)_{(LFM)_{TX}} < \phi(\omega_m)_{(Hann)_{TX}}, \\ \phi(\omega_m)_{Initial} & \text{if } \phi(\omega_m)_{(LFM)_{TX}} = \phi(\omega_m)_{(Hann)_{TX}}. \end{cases} \tag{4.28}$$

The final step in the filtering process is to reconstruct the convolved signal ($X_{m(Hann)_{Initial}}$) using the corrected phase spectrum ($\phi(\omega_m)_{(adjusted)}$). Applying the inverse FFT yields a time domain result which emulates the result of a narrowband test.

4.7 Results

A variety of tests were carried out to determine the suitability of LFM excitation signals to GWT. These tests are catalogued in Tables 4.1 and 4.2 below.

No. Cycles	Frequency Range (kHz)	Frequency Increment
5	20 - 100	1 kHz
10	20 - 100	1 kHz
15	20 - 100	1 kHz
20	20 - 100	1 kHz

TABLE 4.1: Narrowband tests carried out

Tx Signal Length (μs)	LFM Parameters
50	
100	All tests were carried out with a
200	Tukey ratio of $\alpha = 0.2$, lower corner
300	frequency $f_1 = 5$ kHz and an upper
400	corner frequency $f_2 = 115$ kHz
500	

TABLE 4.2: Broadband tests carried out

The total number of possible results, based upon a 1 kHz frequency increment, is 6 x 81 x 4 = 2430 comparison A-Scans. Therefore, in order to keep the results section concise, results at 20 kHz, 60 kHz and 100 kHz for each of the narrowband signals listed in Table 4.1 are presented and compared with a filtered LFM signal 300μs in length. These frequencies have been selected as they are key points across the defined bandwidth. 20 kHz and 100 kHz represent the lower and upper frequency limits for this chosen GWT technology. 60 kHz represented the centre frequency within the selected bandwidth.

Figures 4.12 to 4.23 display the A-scans in terms of distance and show that a narrowband signal can be emulated by using the broadband received signal. For each case the filter was derived to suit each individual set of parameters. A 20m collection length has been presented showing several pipe-end reflections. The far end (6m away from the transducer array) is shown as a substantial response on each trace. In addition the so-called *round-trip* signal can be seen at 9m. The round-trip is the summation of the backwards and forwards travelling guided wave, the time of flight of the two signal paths for a distance of 9m converge at this point giving a much larger amplitude than either of the end reflections observed at 3m and 6m. The exception to the rule in this case appears to be the data collected at 20kHz for each input signal configuration (Figures

4.12, 4.15, 4.18 and 4.21). The near end (3m) and round-trip signals appear to be attenuated within the data collected at 20kHz. It is thought that during propagation of the guided wave transmission under the transducer array on the near end side, signal is damped by the material within the tool which is in contact with the pipe. This effect must be frequency dependent as data from the other frequencies presented (60kHz and 100kHz) do not display this behaviour.

4.8 Conclusions

A broadband excitation transmission signal based on an LFM chirp has been chosen and optimised to suit the propagation of the fundamental torsional mode $T(0,1)$ in a laboratory based pipe specimen. It was determined that in order to maintain a transmission bandwidth between the lower corner frequency of 20 kHz and an upper corner frequency of 100 kHz a tolerance of ± 15 kHz has to be applied to the total specified bandwidth. One influencing parameter on the value of this tolerance is the Tukey ratio value. In order to strike a balance between useable bandwidth, overshoot in the form of Fresnel ripples in the frequency domain and operating within the limits of the electronics, a value of 0.2 was chosen as the ratio of tapered window section to constant section.

An FFT filter was developed which not only operates on the magnitude of the received signal as in many common applications of an FFT filter but also an adjustment of phase is applied based upon the difference in phase between two template signals; the transmission LFM chirp used in the test and the desired narrowband signal to be extracted during the filtering process. In this case, various lengths of Hann windowed pulses were used at every 1 kHz over the entire bandwidth. In principle, this method can be applied ant two signals providing the bandwidth is available in the transmission signal and that the narrowband template signal lies within the transmission frequency spectrum.

One key observation from the initial received broadband results is that the transfer function of the system attenuates certain frequencies whilst promoting others (Figure 4.8). This is largely due to the resonance of the transducers themselves, this effect has been characterised experimentally [Engineer (2013)]. This will affect the outcome of any imaging carried out in the time-frequency plane. It may be possible to alter the frequency modulation of the excitation signal to actively deal with this problem. The

direction for solving this issue is explained in more detail with accompanying initial results in Chapter 7.

The results in Figures 4.12 through to 4.23 show that as predicted an equivalent narrowband signal can be recovered showing little error. Any error existing in the scans presented can be attributed digitally through a slight difference in sampling causing a slight numerical difference or environmentally as some of the data were acquired with a substantial time in between. In such a time gap it seems feasible that a natural rise in ambient temperature through the day could explain the time of flight difference observed in Figure 4.23.

Establishing a broadband excitation for the guided wave testing of pipes will make the inspection technique more efficient in terms of data acquisition and storage and could lead to a more informed defect detection methodology.

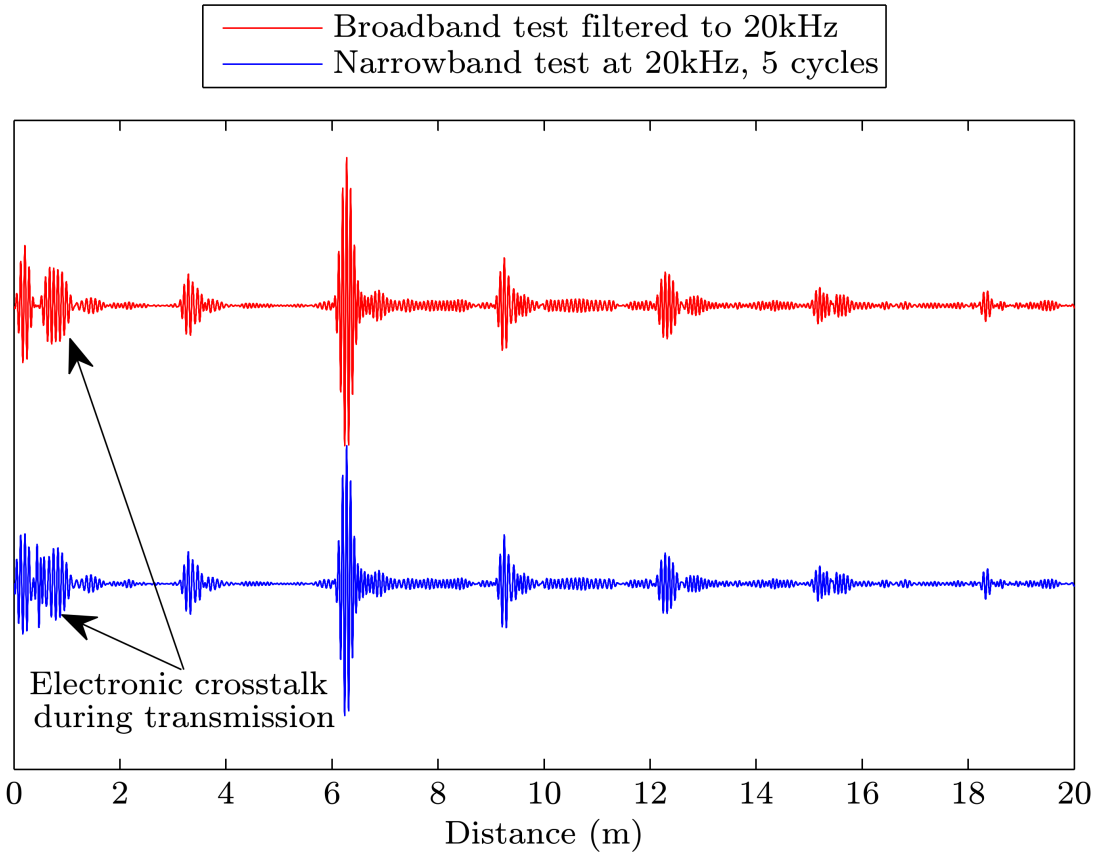

FIGURE 4.12: A Comparison of the narrowband test at 20 kHz, 5 cycles and the emulated narrowband result filtered down from a 300μs (α= 0.2, f_1=5 kHz and f_2 = 115 kHz)

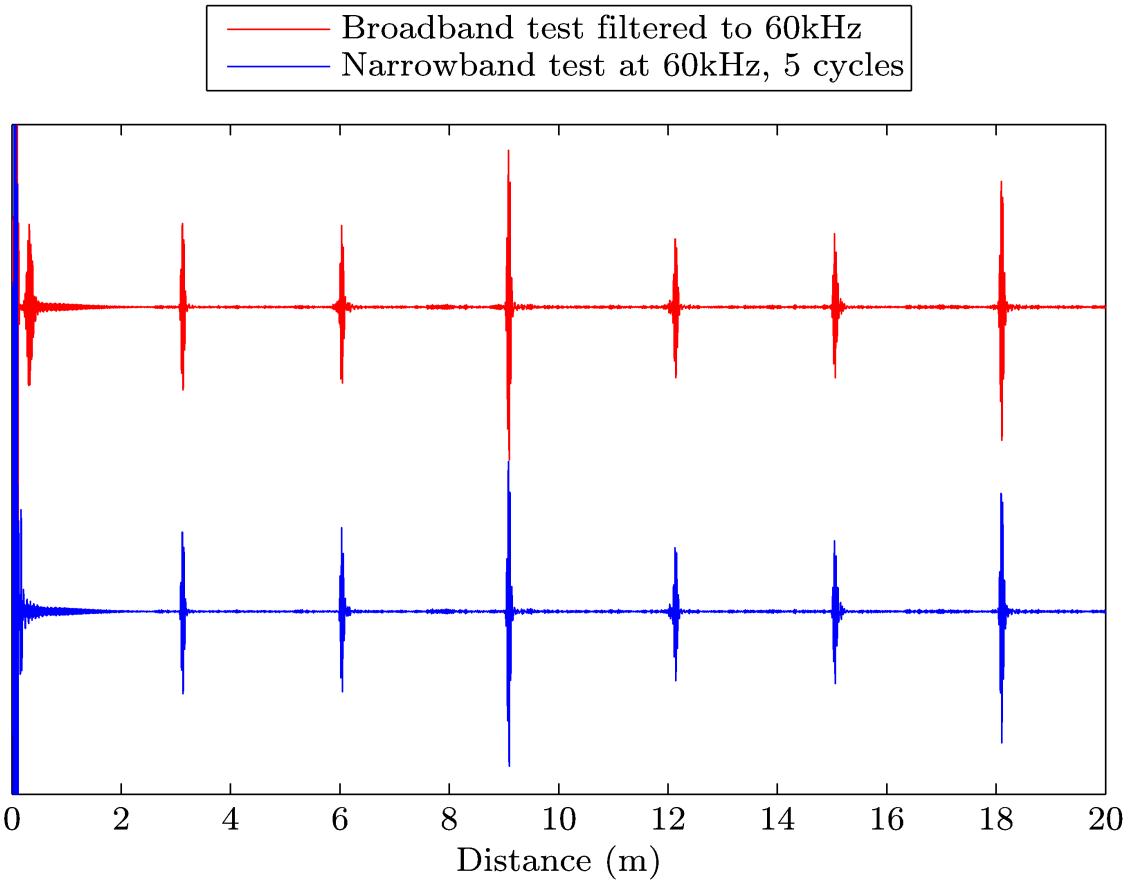

FIGURE 4.13: A Comparison of the narrowband test at 60 kHz, 5 cycles and the emulated narrowband result filtered down from a 300μs (α= 0.2, f_1=5 kHz and f_2 = 115 kHz)

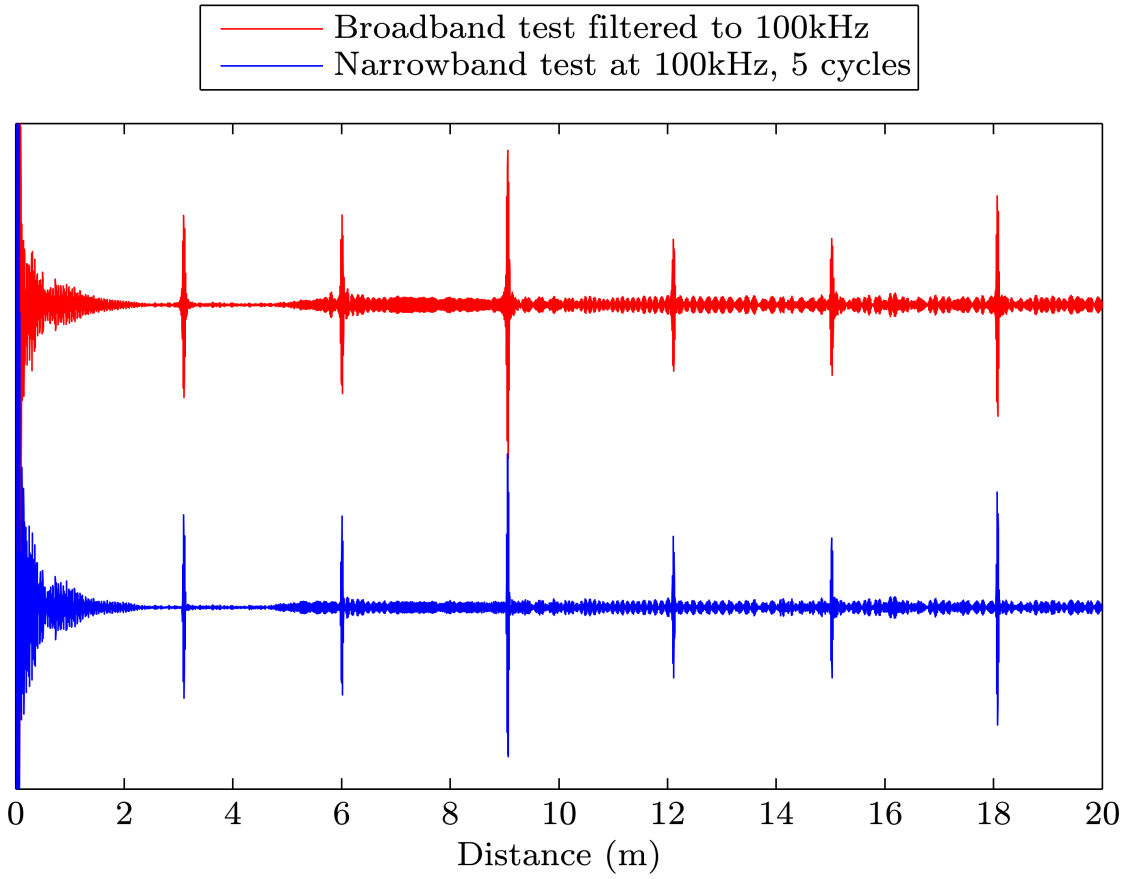

FIGURE 4.14: A Comparison of the narrowband test at 100 kHz, 5 cycles and the emulated narrowband result filtered down from a 300μs (α= 0.2, f_1=5 kHz and f_2 = 115 kHz)

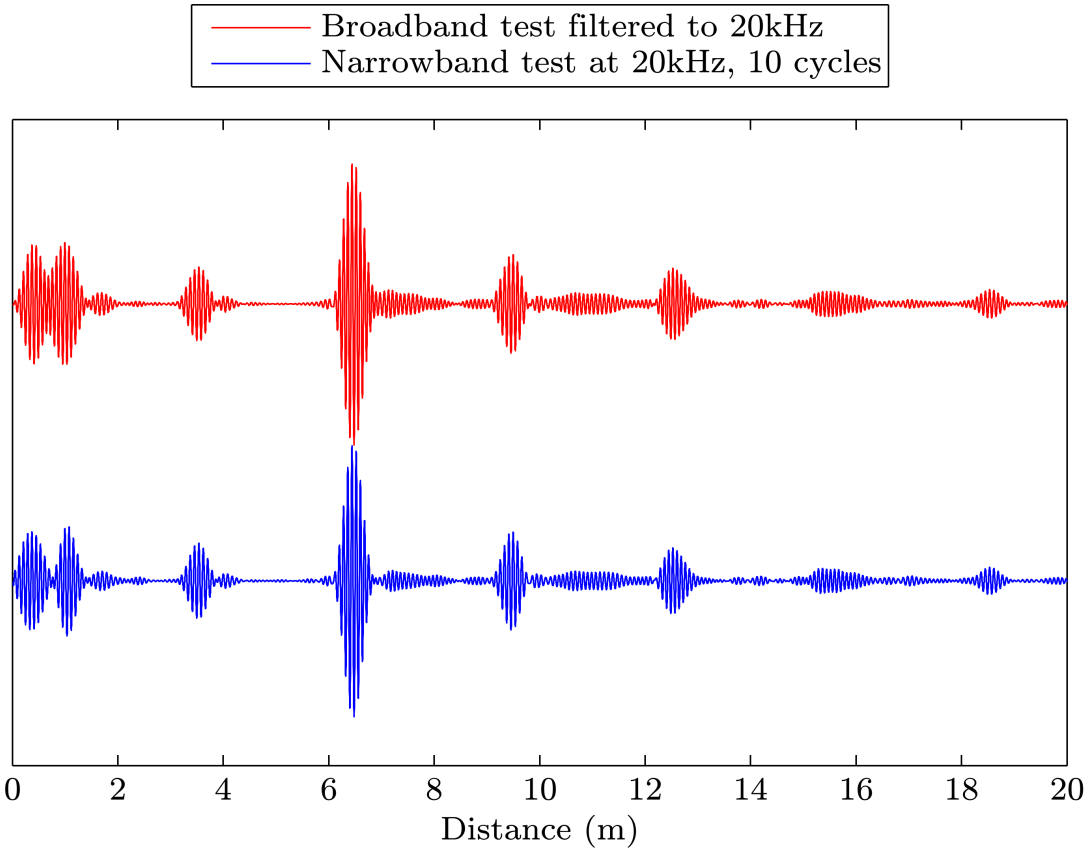

FIGURE 4.15: A Comparison of the narrowband test at 20 kHz, 10 cycles and the emulated narrowband result filtered down from a 300μs (α= 0.2, f_1=5 kHz and f_2 = 115 kHz)

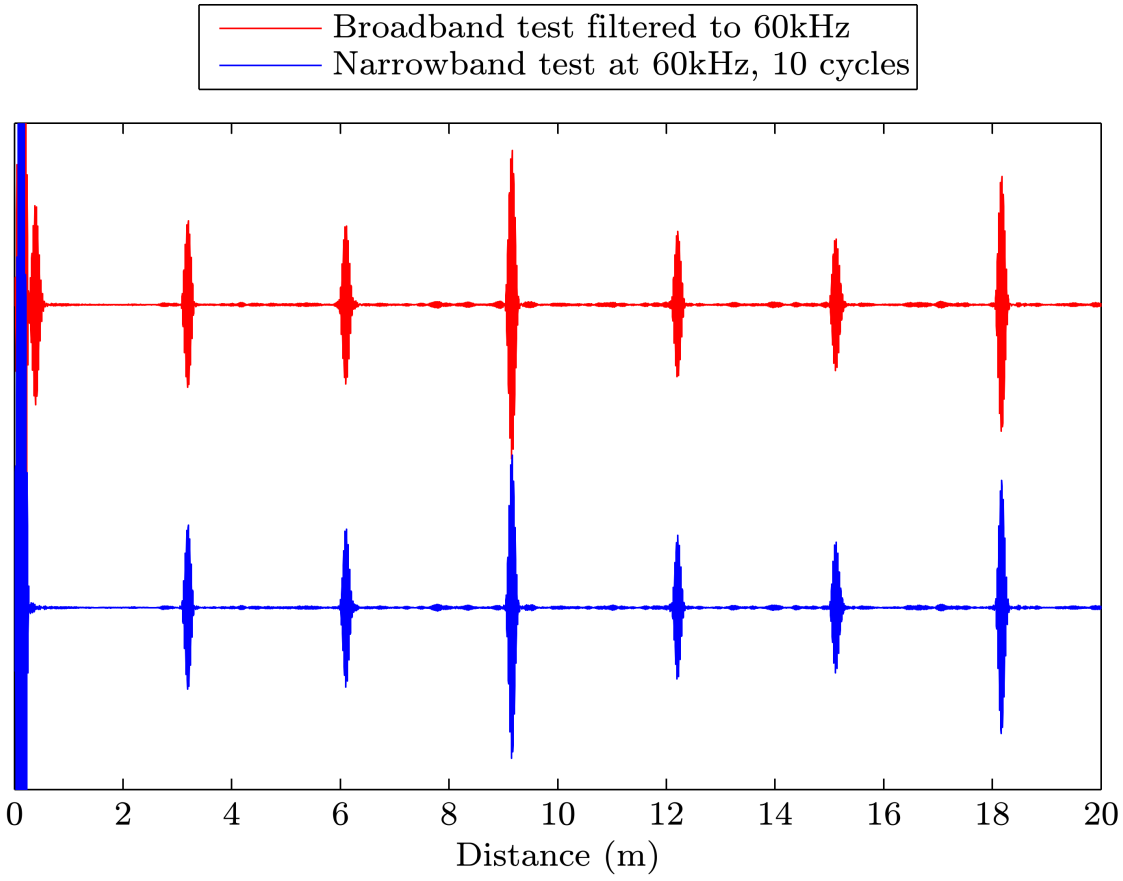

FIGURE 4.16: A Comparison of the narrowband test at 60 kHz, 10 cycles and the emulated narrowband result filtered down from a 300μs (α= 0.2, f_1=5 kHz and f_2 = 115 kHz)

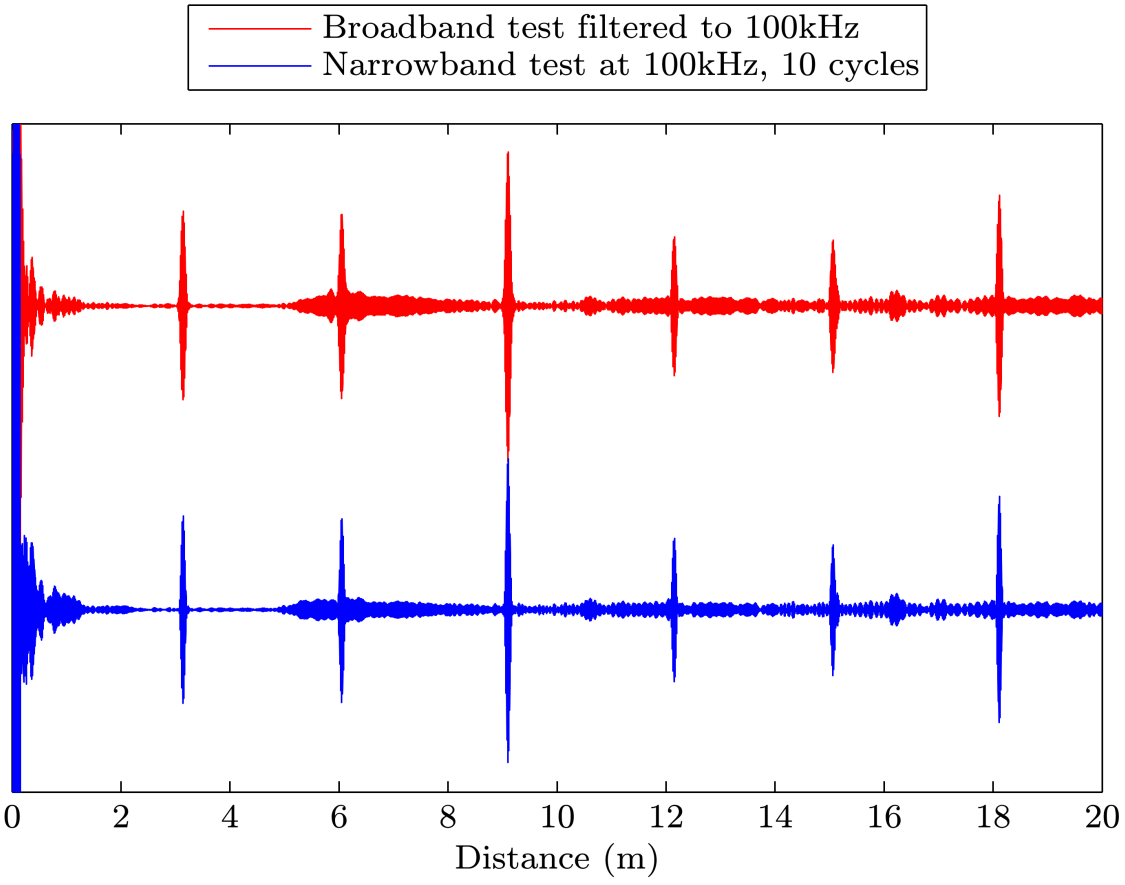

FIGURE 4.17: A Comparison of the narrowband test at 100 kHz, 10 cycles and the emulated narrowband result filtered down from a 300μs (α= 0.2, f_1=5 kHz and f_2 = 115 kHz)

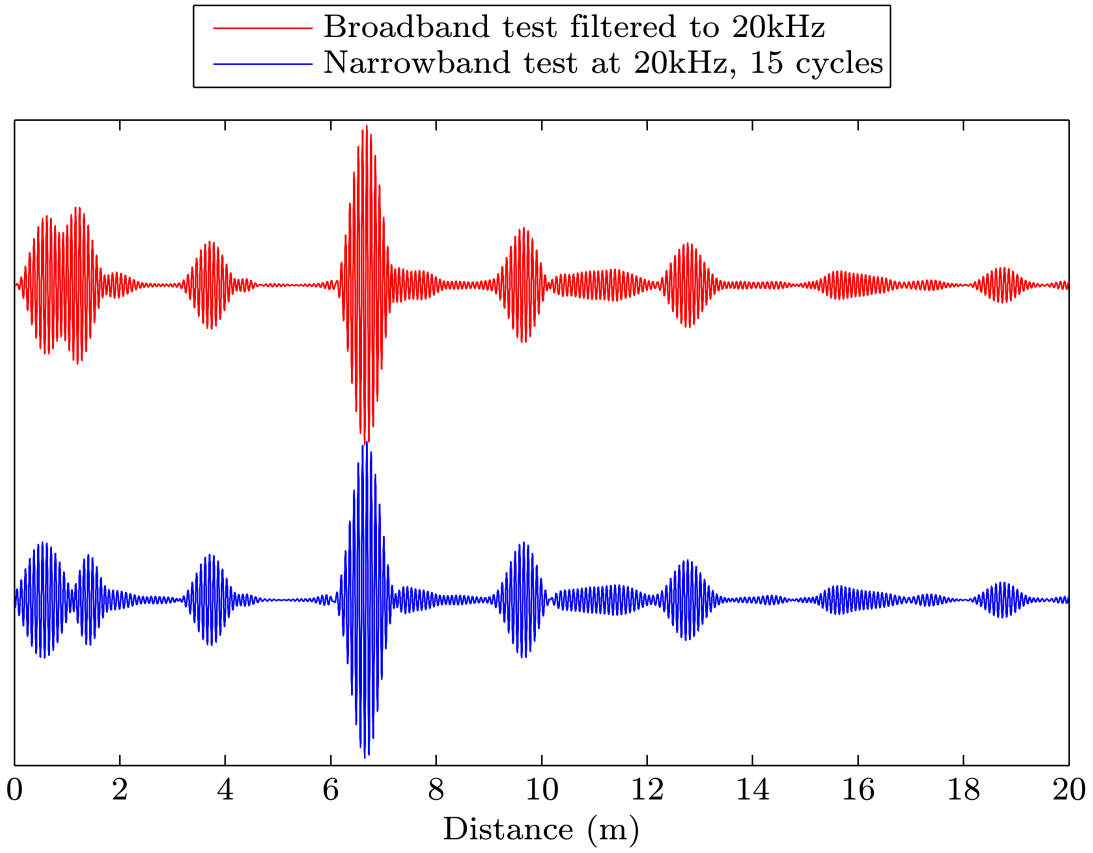

FIGURE 4.18: A Comparison of the narrowband test at 20 kHz, 15 cycles and the emulated narrowband result filtered down from a 300μs (α= 0.2, f_1=5 kHz and f_2 = 115 kHz)

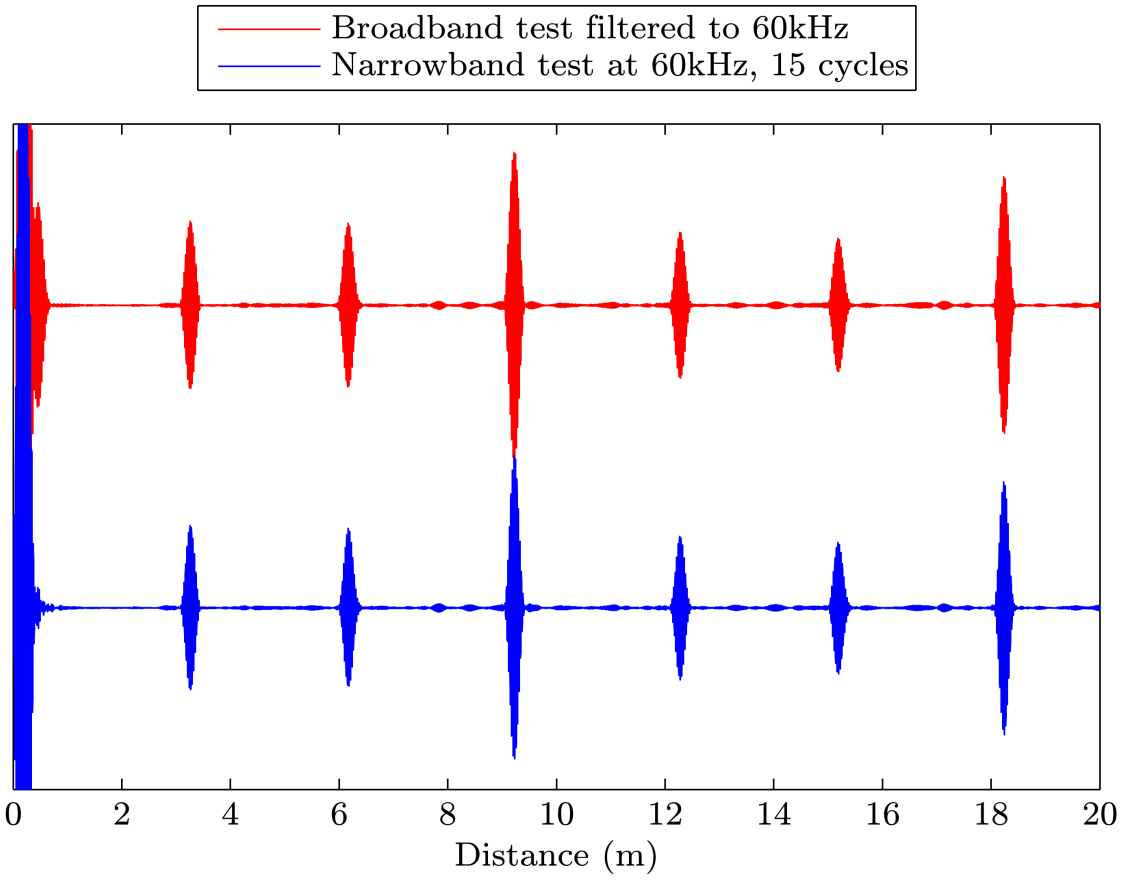

FIGURE 4.19: A Comparison of the narrowband test at 60 kHz, 15 cycles and the emulated narrowband result filtered down from a 300μs (α= 0.2, f_1=5 kHz and f_2 = 115 kHz)

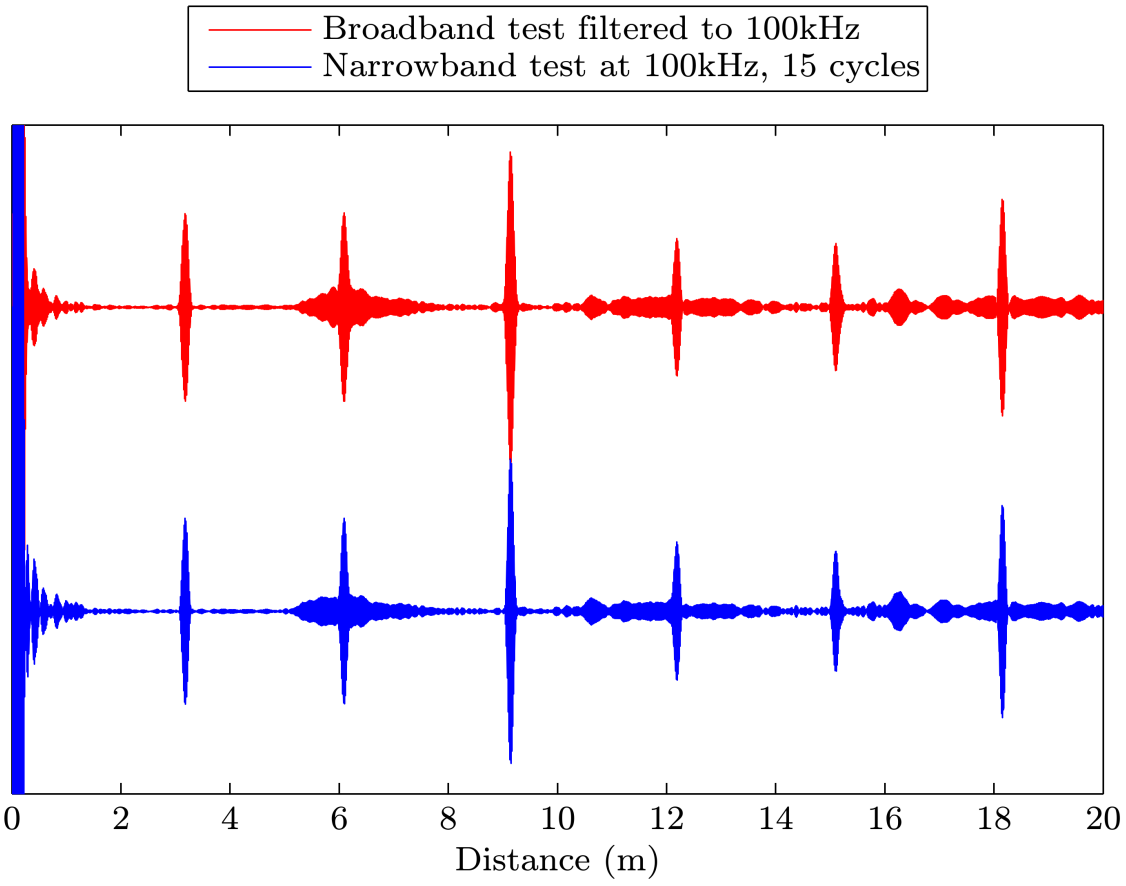

FIGURE 4.20: A Comparison of the narrowband test at 100 kHz, 15 cycles and the emulated narrowband result filtered down from a 300μs (α= 0.2, f_1=5 kHz and f_2 = 115 kHz)

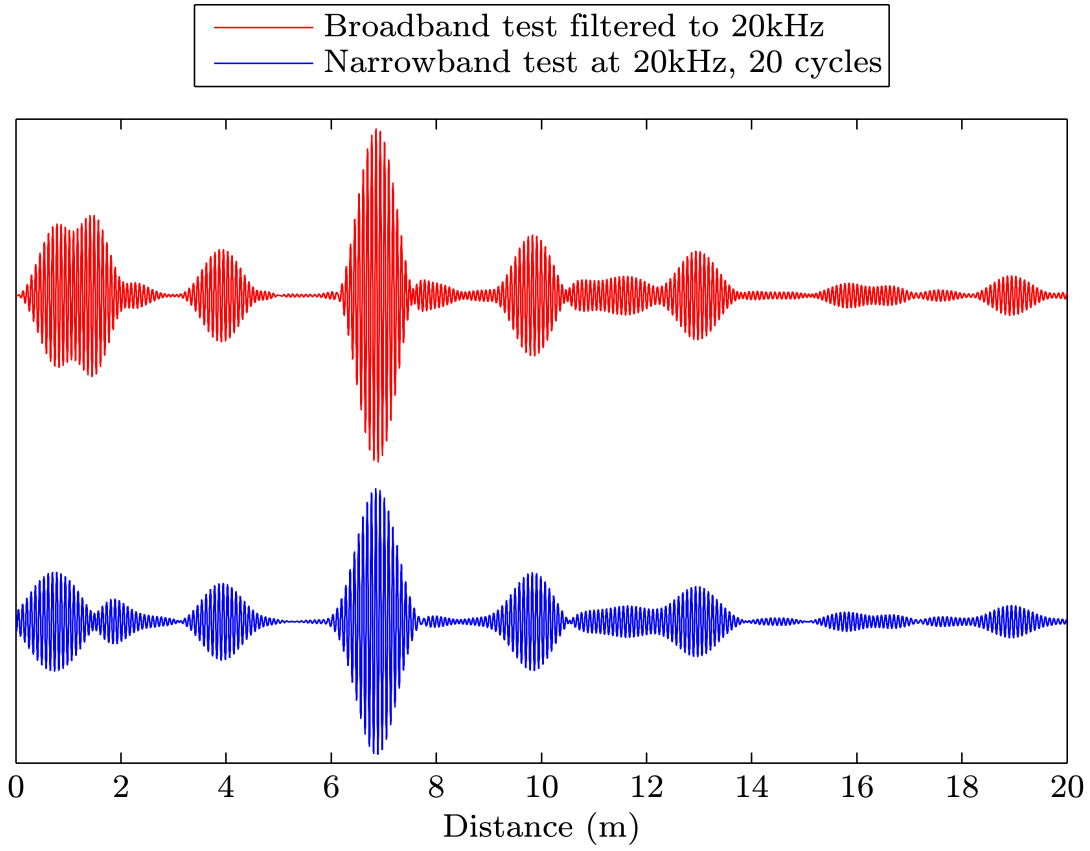

FIGURE 4.21: A Comparison of the narrowband test at 20 kHz, 20 cycles and the emulated narrowband result filtered down from a 300μs (α= 0.2, f_1=5 kHz and f_2 = 115 kHz)

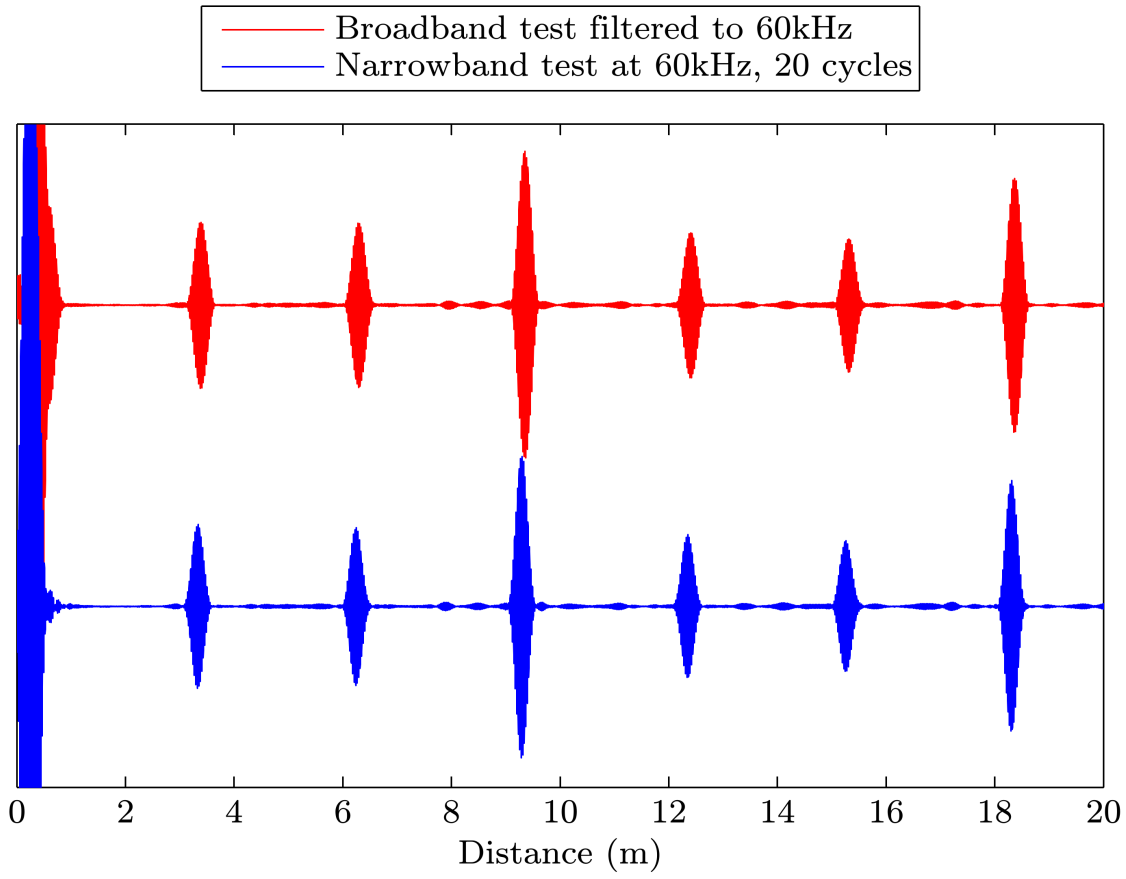

FIGURE 4.22: A Comparison of the narrowband test at 60 kHz, 20 cycles and the emulated narrowband result filtered down from a 300μs (α= 0.2, f_1=5 kHz and f_2 = 115 kHz)

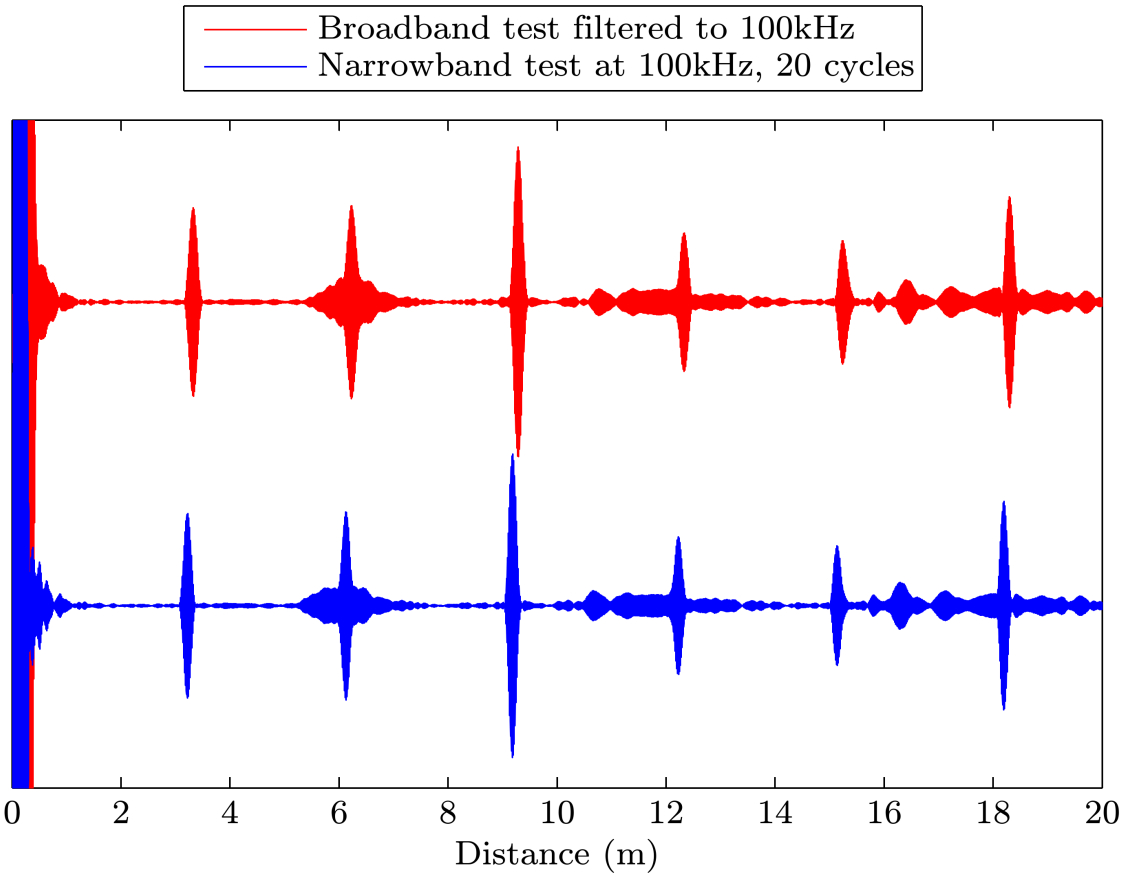

FIGURE 4.23: A Comparison of the narrowband test at 100 kHz, 20 cycles and the emulated narrowband result filtered down from a 300μs (α= 0.2, f_1=5 kHz and f_2 = 115 kHz)

Chapter 5

The Application of a Broadband Excitation to a Commercial Guided Wave Inspection System

5.1 Background

In the previous chapter it was shown that a broadband excitation can be used to generate UGWs in a hollow cylinder and that by using an optimised FFT filter incorporating a phase compensation, an equivalent narrowband response of any specified configuration could be extracted from the broadband response providing the frequencies required were present within the transmitted bandwidth. The proposed idea was tested using a single ring of circumferentially distributed dry-coupled shear transducers exciting the fundamental torsional mode $T(0,1)$. The fundamental torsional mode was chosen because it is non-dispersive and is therefore the simplest case to analyse. The test was set up in a single ring of transducers in order to eliminate any complexity associated with the superposition of signals between the 2 or 3 transducer rings. These rings are essential for producing unidirectional guided waves within a Teletest GWT system.

This chapter presents a solution to the problem of assigning the broadband excitation method demonstrated in Chapter 4 to a multi-ring GWT inspection system. The chosen GWT system utilises both the fundamental torsional mode $T(0,1)$ and the fundamental longitudinal mode $L(0,2)$. In order to assess confidently the location of a defect or

feature within an inspected length, the output of the GWT tool must be unidirectional *i.e. sound must propagate away from the tool in one direction.* Results shown in this chapter will demonstrate that the use of an LFM chirp transmission signal for both $T(0,1)$ and $L(0,2)$ tests is possible. A further hardware design recommendation will be given which improves the output of the existing commercial torsional tool over the available bandwidth.

5.2 Objectives

The aim of the work within this chapter is to establish the feasibility of applying a chosen broadband propagation routine to each configuration of the commercial tools manufactured and designed by Plant Integrity Ltd.

As such, specific objectives are as follows:

- A unidirectional broadband propagation routine is to be derived for commercial torsional and longitudinal GWT tools.
- A procedure for assessing these routines under laboratory conditions is to be stated.
- A comparison between the existing narrowband and proposed broadband technique will be made.
- Recommendations on subsequent direction for implementation will be stated.

5.3 Methodology

5.3.1 Unidirectional propagation of an LFM chirp

There are two parallel tasks which must be covered here. The first is the solution to the problem of a broadband unidirectional propagation routine for the fundamental torsional mode $T(0,1)$ and the second is a broadband unidirectional propagation routine for the slightly dispersive, fundamental longitudinal mode $L(0,2)$. The dynamics of these two wavemodes are very different, therefore they must be considered as two separate cases. The torsional tools available in the Teletest GWT system exist in two variants; a 2 ring

tool and a 3 ring tool with two different ring spacing options. There are therefore three cases in total to derive for the torsional case and one 3 ring case for excitation of the longitudinal wavemode (Section 5.7). Details of the axial layout of each transducer array configuration are given in the early sections of this chapter. Broadband transmission signals will be derived for all cases and compared with all of the existing ideal directional output curves for narrowband excitation.

5.3.2 Laboratory trials

Each of the possible Teletest inspection configurations were tested on the simply supported, 9m long 8inch nominal diameter schedule 40 pipe used for the initial feasibility study documented in Chapter 4. One main advantage of using this experimental set up is that the effectiveness of the unidirectional process can be assessed by comparing the results gained to those collected using only a single ring of transducers in the previous chapter. The cut ends of the pipe will serve as large reflecters of the sound energy thus exposing the performance of the unidirectional routines developed.

5.3.3 Post-processing

Data collected will be recombined using specified propagation routines to optimise guided wave energy from a chosen direction for the test mode of interest. The two test modes are $T(0,1)$ and $L(0,2)$. The results presented will be in a similar format to those presented in the previous chapter but the test frequencies used will reflect those used in the commercial system for both test modes and all tooling configurations. The broadband received signals will be filtered using the FFT approach recommended in Chapter 4.

5.4 Unidirectional Propagation of Guided Wave Signals in a Pipeline

The first demonstration of unidirectional propagation of ultrasonic guided waves in a hollow cylinder was given by Böttger et al. (1987). The transducer array used was an EMAT and the system operated with two axially distributed transmission coils which operated in a delay sequence based on specific fractions of the cycle period T within the input pulse. In theory this array could completely cancel out sound propagating in one direction, the remaining energy therefore propagates in the other direction (the test direction). In reality however, experimental results revealed that the amplitude ratio between the maximum peak in the test direction and the poorly cancelled backwards travelling peak observed within the data collected from in front of the tool was approximately -60dB. The generation of unidirectional UGWs in pipelines using a dry-coupled shear transducer array was first demonstrated in Alleyne and Cawley (1997). The authors used a multi-ring tool with a sequence of delays to provide an adequate unidirectional signal. Here total theoretical cancellation was based upon the use of the centre frequency only with recommendation that a narrowband signal be used so that any error that occurred either side of that value was negligible. However, the wavemode used by Alleyne and Cawley was $L(0,2)$ which is dispersive over the bandwidth causing lack of effective cancellation either side of the centre frequency.

The process of forming the unidirectional signals demonstrated in this chapter will account for the whole bandwidth excited and not just the centre frequency.

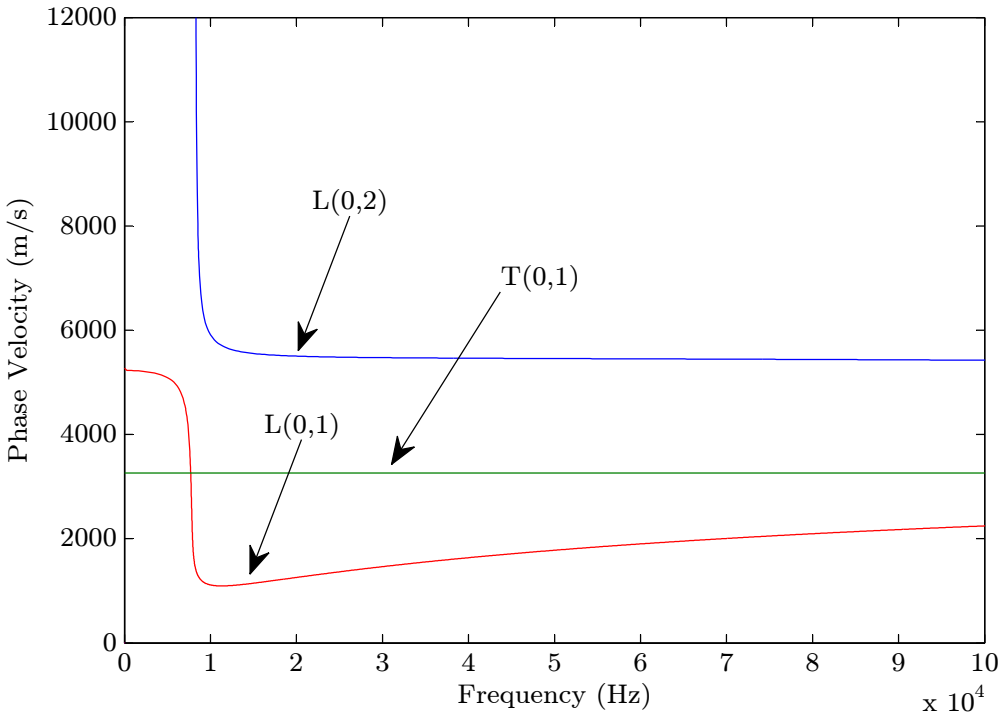

FIGURE 5.1: The fundamental axisymmetric wavemodes transmitted during an ultrasonic inspection using guided waves

5.4.1 Using the dispersion curves to model wave propagation

Figure 5.1 shows the dispersion curves for each of the possible axisymmetric wave modes excited during a guided wave test between 20kHz and 100kHz. It should be noted that the longitudinal and the torsional modes are produced in separate tests and not concurrently. It is clear to see that the torsional mode $T(0,1)$ has no variation in phase velocity (v_{ph}) with frequency and is therefore deemed *non-dispersive*. However, the longitudinal modes $L(0,2)$ and $L(0,1)$ do exhibit variation in their phase velocities with frequency and are thus deemed *dispersive*. The curves in Figure 5.1 were produced using the *DISPERSE* software [Pavlakovic et al. (1997)]. The software has the ability to provide analytical solutions to the wave equations for plates and cylindrical members.

In order to present the curves in terms of phase velocity, the circular wavenumber $k(\omega)$ is calculated for each angular frequency value ω across the bandwidth of interest. Phase velocity is then determined by using the following relationship:

$$k(\omega) = \frac{\omega}{v_{ph}(\omega)} \tag{5.1}$$

The dispersion phenomenon is not exclusive to ultrasonic guided waves. It has also been observed in seismology [Kulesh et al. (2005) and Kulesh et al. (2008)], it is also an area of great interest in optical communications. A review of the behaviour of a pulse as it propagates in a dispersive medium from an optical fibre point of view can be found in Sjöberg (2010). The author provides a thorough description of the relationship the envelope and carrier signal have during propagation and mentions some modelling optimisation techniques for pulse propagation. When a pulse propagates within a dispersive medium it becomes distorted and can spread out destroying temporal resolution. Approaches were taken in Wilcox (2003) and Alleyne et al. (1993) to reverse the unavoidable effects of dispersion but they only deal with a single wavemode. Multimodal signals cannot currently be corrected. However, the following propagation equation stated in both Wilcox (2003) and Sjöberg (2010) can be utilised to create broadband transmission signals needed for a multi-ring guided wave test providing the dispersion curves for the pipe are available.

$$u(x,t) = \int_{-\infty}^{\infty} F(\omega) e^{i(k(\omega)x - \omega t)} d\omega \tag{5.2}$$

Equation 5.2 above operates on the time domain signal $u(x,t)$. Using the phase shift of each frequency component within the excited bandwidth, a point in time (t) and space (x) can be defined according to the dispersive nature of the media and the chosen wavemode. $F(\omega)$ represents the Fourier transform of the time domain signal $u(x,t)$.

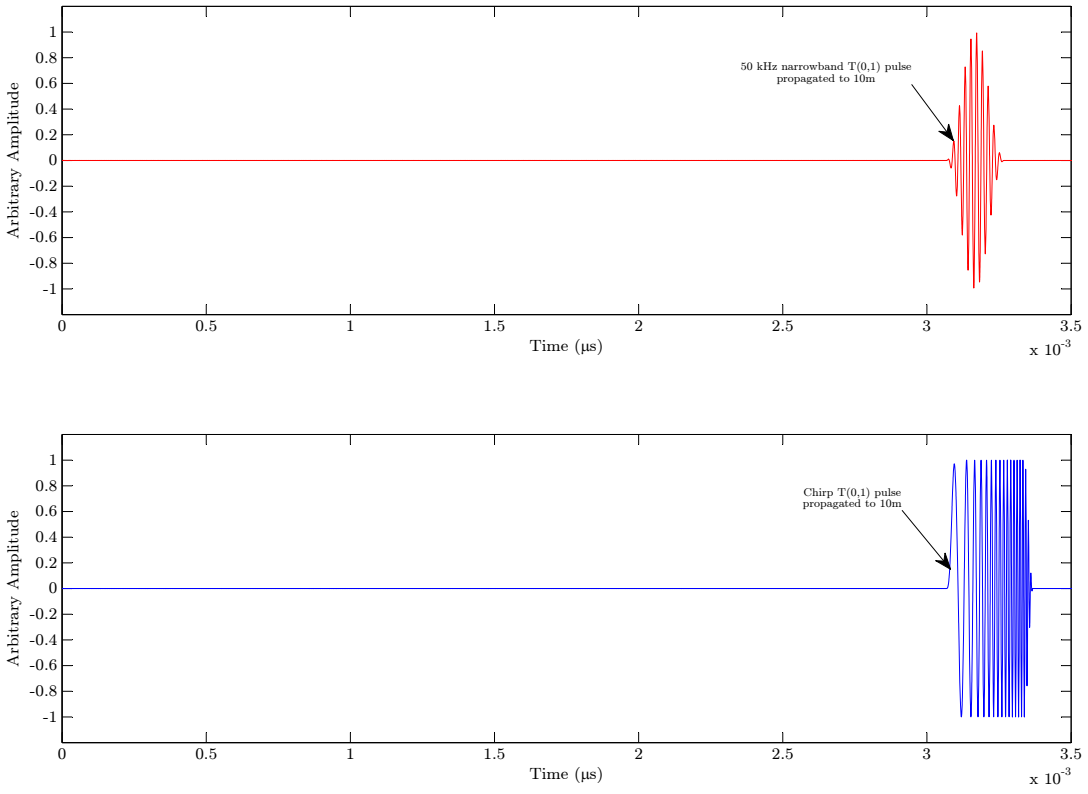

FIGURE 5.2: Propagation of a 10 cycle Hann windowed pulse at 50kHz and an LFM chirp (α= 0.2, f_1=5 kHz and f_2 = 115 kHz). The phase velocities used here were extracted from the $T(0,1)$ dispersion curve

The signals presented above in Figure 5.2 were produced using the dispersion curves for an 8inch Schedule 40 steel pipe. The plot represents a 10 cycle Hann windowed pulse at 50kHz (in red) and a 500μs long LFM chirp swept between 5kHz and 115kHz (in blue) propagated to a fixed distance of 10m. The phase velocity used in this case as an input to Equation 5.2 was the theoretical value for $T(0,1)$. For steel this is 3260m/s and does not vary with frequency. This is the reason why both sets of signals (carrier and envelope) remain unchanged despite having propagated several metres.

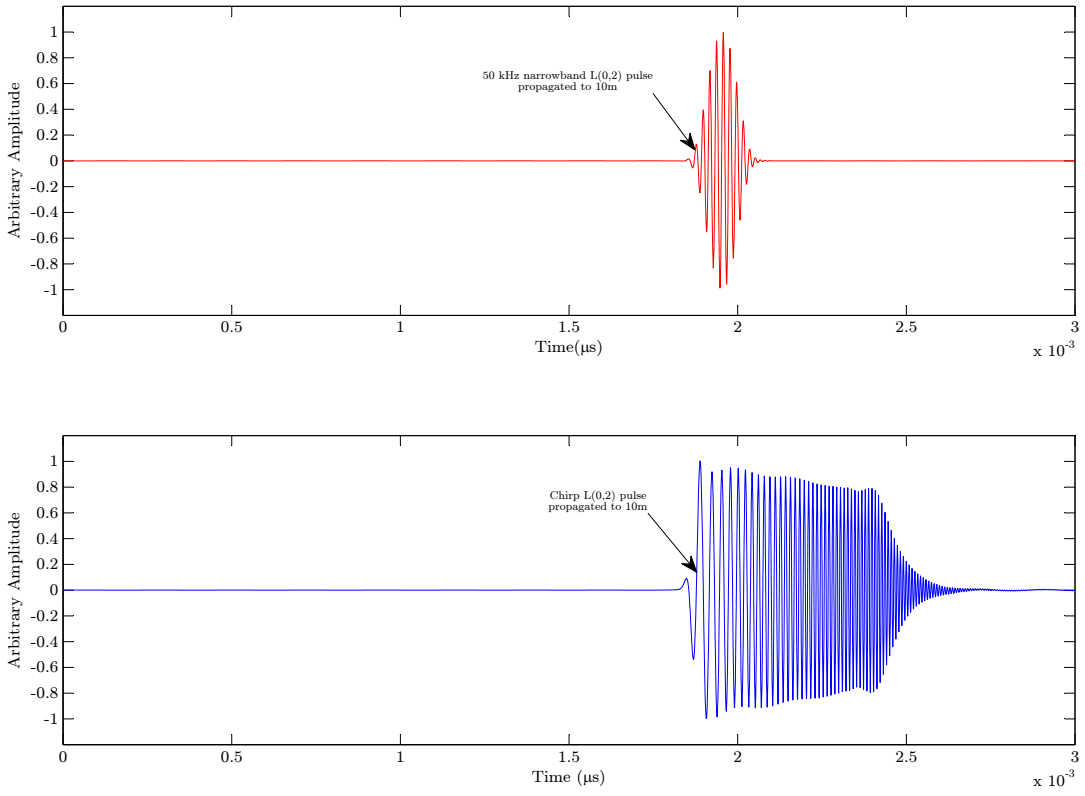

FIGURE 5.3: Propagation of a 10 cycle Hann windowed pulse at 50kHz and an LFM chirp (α= 0.2, f_1=5 kHz and f_2 = 115 kHz). The phase velocities used here were extracted from the $L(0,2)$ dispersion curve

Figure 5.3 shows an equivalent propagation example to those displayed in Figure 5.2 but the slightly dispersive $L(0,2)$ is demonstrated here. The blue trace in Figure 5.1 is the dispersion curve for the $L(0,2)$ mode. Within the bandwidth utilised in GWT the gradient of the curve is relatively shallow which results in minimum distortion of the transmitted narrowband pulse. An time/distance animation of this plot shows a phase change within the carrier signal for the narrowband pulse (in red) but the distortion of the envelope is negligible. However, the LFM signal distorts both in phase and envelope. This is due to the fact that each point in frequency possesses a different phase velocity which causes an overlapping effect in time, this results in constructive/destructive interference and thus creates amplitude variation. Despite the broad range of frequencies transmitted in the LFM chirp pulse though it is still coherent.

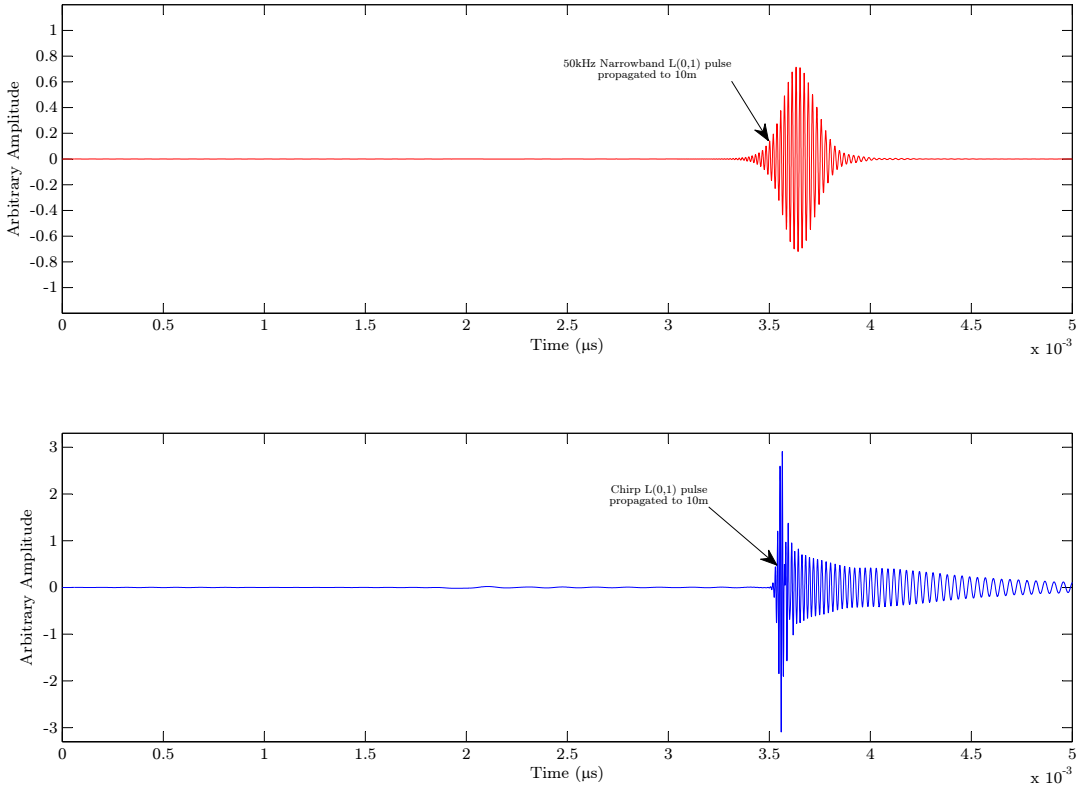

FIGURE 5.4: Propagation of a 10 cycle Hann windowed pulse at 50kHz and an LFM chirp (α= 0.2, f_1=5 kHz and f_2 = 115 kHz). The phase velocities used here were extracted from the $L(0,1)$ dispersion curve

Again the plot shown above in Figure 5.4 uses the same process as the previous examples given. The only difference here is that the phase velocity for the very dispersive $L(0,1)$ has been used as an input for the propagation equation. The interference through the superposition effect described previously is quite apparent here in the LFM chirp pulses. The propagated narrowband pulse becomes distorted and more spread out than the dispersion-free $T(0,1)$ case shown in Figure 5.2. The earlier arrival of the 50kHz narrowband signal can be attributed to the fact that the velocity of $L(0,1)$ at that frequency is higher than that of the lower corner frequency (f_1) of the LFM chirp. This results in the LFM chirp appearing to arrive later. It should be noted that currently in GWT inspection the $L(0,1)$ wavemode only appears as an undesired bi-product when testing using the $L(0,2)$ wavemode.

5.5 The two ring torsional propagation routine

The simplest method of achieving unidirectional guided wave propagation in a pipe using dry coupled shear transducers is to use two circumferentially distributed transducer arrays, also termed as rings. These so-called rings are set at an axial distance apart known as the ring spacing (shown in Figure 5.5 below as the parameter d).

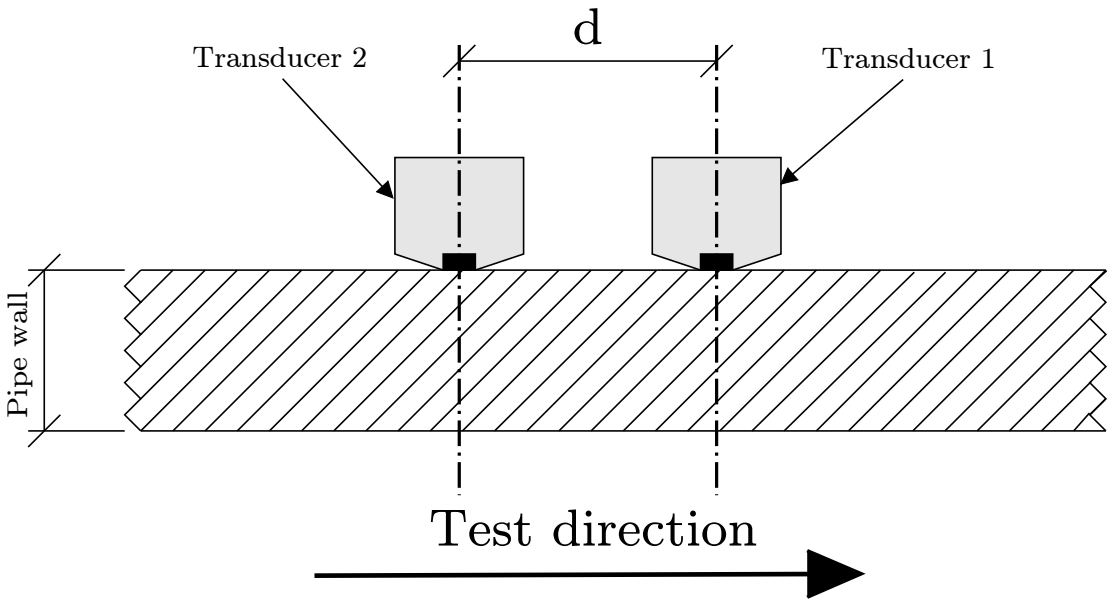

FIGURE 5.5: A simplified schematic showing the axial distribution of the transducers in a two ring tool

Figure 5.5 shows the axial distribution of 1 transducer from each ring along a pipe wall. Transducer 1 represents ring 1 and transducer 2 represents ring 2. This configuration is used for a basic unidirectional torsional test using $T(0,1)$. In order to propagate sound in the test direction shown in Figure 5.5 the transmission signals should be set up as follows:

- Ring 1 - This signal should remain unchanged. *i.e. it should be the desired excitation signal*
- Ring 2 - In order to cancel any backwards propagating sound from ring 1 for $T(0,1)$, the signal supplied to ring 1 is propagated using Equation 5.2 to a distance equalling the ring spacing. This signal is then inverted. The values for $v_{ph}(\omega)$ can be calculated using either *DISPERSE* or the Plant Integrity's FocusApp software.

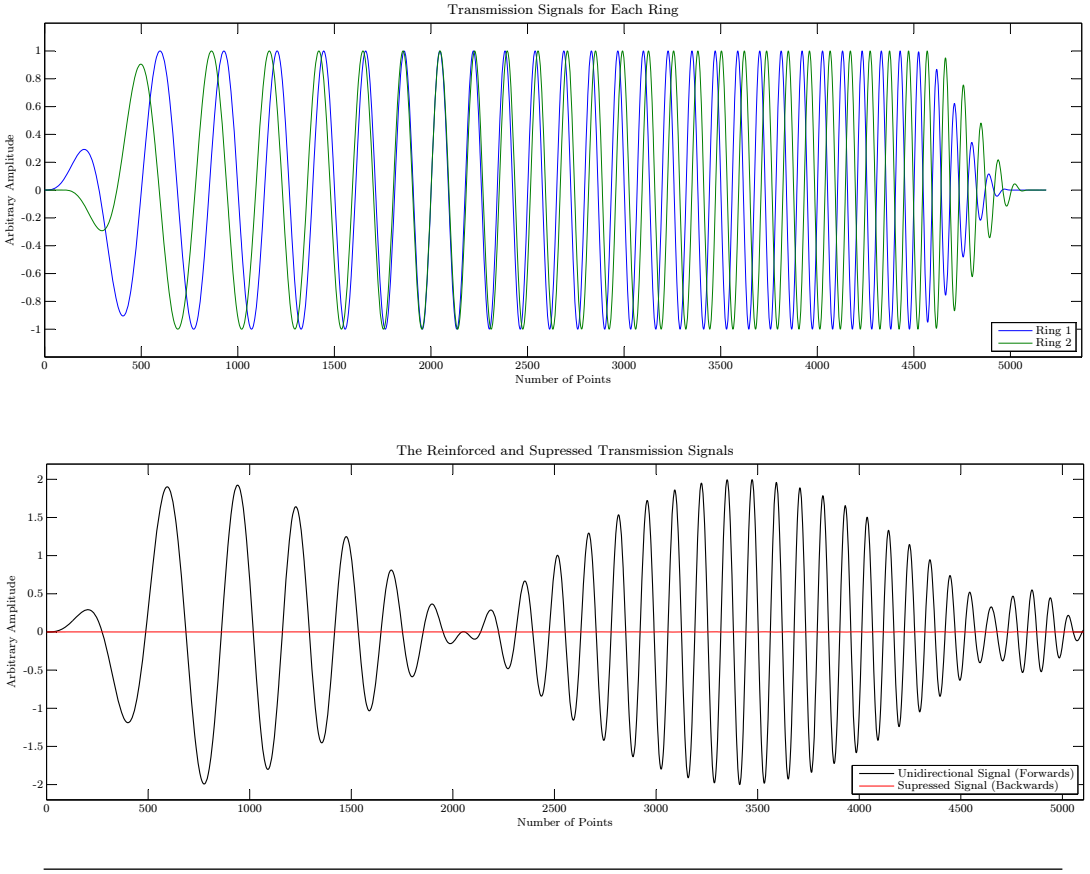

FIGURE 5.6: Torsional 2 ring 30mm ring spacing input signals, unidirectional signal (forwards) and the resulting suppressed signal (backwards)

Figure 5.6 shows two sets of axes containing signals related to the transmission of a broadband 2 ring torsional guided wave test at a ring spacing of 30mm. The upper axes show the transmission or so-called input signals for each ring. The trace in blue is the signal sent to ring 1 (transducer 1 in Figure 5.5). This signal is not delayed and is not inverted. However, the signal in green which is transmitted from ring 2 (transducer 2 in Figure 5.5) possesses a phase and group delay associated with a 30mm ring spacing at the velocity of the chosen wavemode $T(0,1)$. The transmission signal supplied to ring 2 is also inverted to provide destructive interference upon transmission, thus generating a unidirectional, torsional guided wave transmission. The signal for ring 2 can also be created using a group delay in the time domain and inversion. This is possible due to the fact that the group and phase velocity for $T(0,1)$ are equal. There is no change in the form of the carrier or envelope during the propagation of this mode, so in a digital sense a number of zeros can be added to the beginning of the signal (a process known as *padding*) and inversion of the signal is then carried out. This is not as accurate as performing propagation via phase manipulation in the frequency domain.

The axes below shows the predicted physical outcome of the signals created by rings 1 and 2. This signal was produced by propagating the traces in the above axes to a fixed point along the test direction and summing them. In practice this is the shape of the pulse which travels along the waveguide. If one were to monitor for signals behind the tool *i.e. in a direction opposite to the test*, the result in theory would be zero. However transducer efficiencies and coupling variation prevent absolute destructive interference.

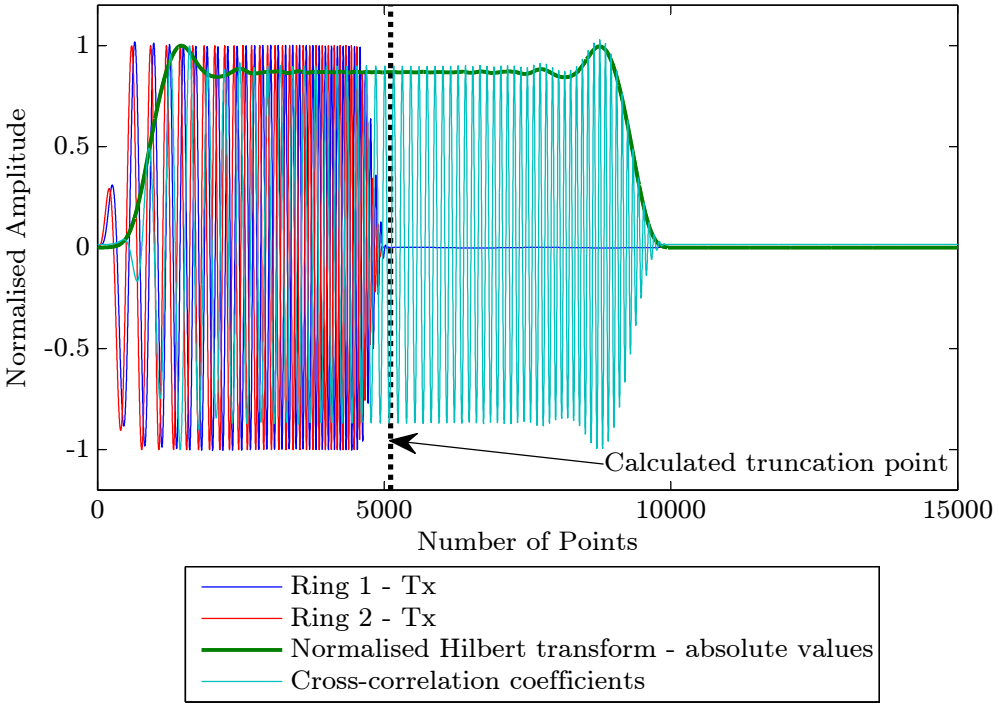

FIGURE 5.7: Demonstration of how cross-correlation can be used to detect the end of a propagated pulse

In normal inspection mode for GWT all pulser/receivers are set in a pulse echo mode. This means that for the duration of the excitation pulse the pulser/receiver is set to transmit only. It is not possible with current hardware to transmit and receive concurrently. Beyond this transmission all of the channels switch over to receive. The transmission time is also known as the dead zone as nothing is detectable within this range. The time domain signal $u(x,t)$ calculated when producing a propagated transmission trace is the result of an inverse FFT. This means that it will be as long as the number of FFT points. To achieve good frequency resolution this could exceed the number of points in the pulse itself by several hundred points. For a pulse echo GWT system the end of the propagated pulse must be detectable so that it can be truncated.

If the signal is not truncated, the result would be the transmission of the pulse and the associated FFT zero padding thus masking any useful information within the affected part of the trace. In addition hardware constraints will only allow a finite number of digital transmission points which can be exceeded if a long transmission signal were to imported.

It is impractical to truncate the FFT pad manually so for efficiency this process must be automated. A combination of cross-correlation and an application of the Hilbert transform can help achieve this. Figure 5.7 shows an example of the method applied to the propagated signals generated throughout this chapter. The traces in blue and red are rings 1 and 2 respectively of a two ring torsional system at 30mm ring spacing. The process adopted for truncation is as follows:

- The signal which has been propagated trace is reversed *i.e. the sequence of y values with respect to the x axis is reversed.* This is achieved by using the *flipud* command in MATLAB.
- The cross-correlation coefficients between the original propagated signal and the flipped signal calculated in step one are found.
- If a narrowband pulse is propagated then the maximum of the cross-correlation coefficients will line up with the end of the propagated pulse. In the case of the LFM chirp the maxima sit either side of the centre of the cross-correlation values.
- The Hilbert transform for the cross-correlation values was calculated and the absolute values were used to extract the maxima/maximum. In Figure 5.7 the maxima are easily identifiable and the truncation point sits at the midpoint between these two peaks. Logic was applied in the MATLAB program written for this to handle the detection of maximum values for either case. The calculated truncation point is shown as the vertical black dashed line in Figure 5.7.
- Once the index for the truncation point is found then a new variable is created which only contains the values for the propagated pulse up to the truncation value.

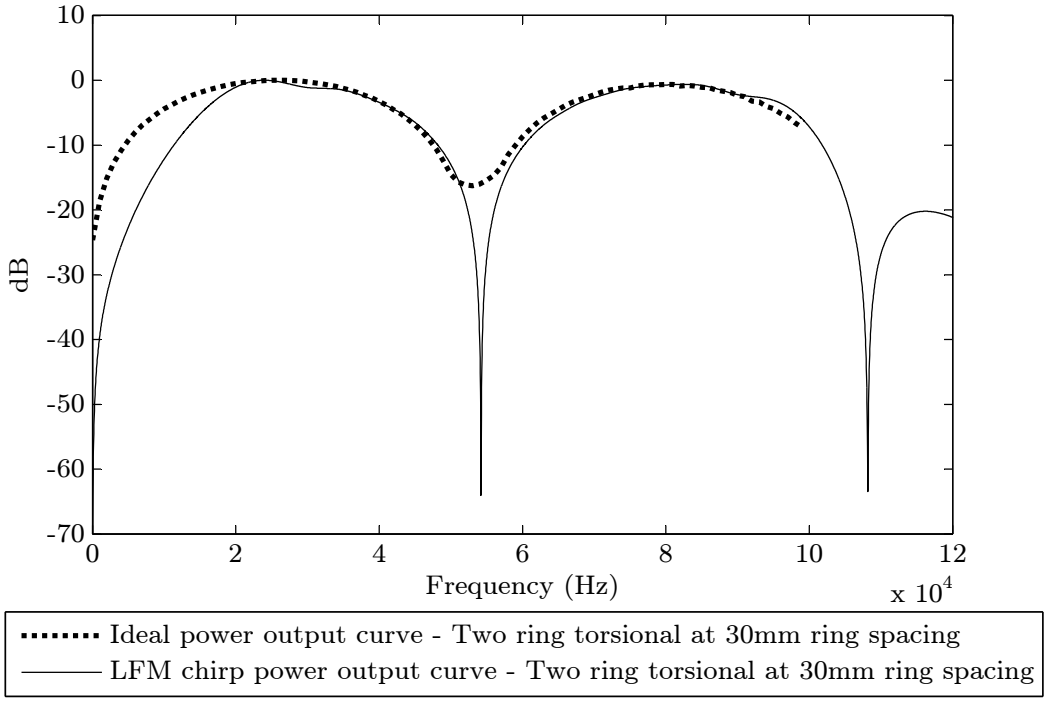

FIGURE 5.8: Two ring output curves for $T(0,1)$

Figure 5.8 shows the frequency dependence of the output of the two ring torsional tool at 30mm spacing. If the test direction is considered to be forwards then through the propagation routine developed the sound propagating backwards is minimised but due to the fixed ring spacing there is a cyclic frequency dependent intensity of the sound propagating forwards away from the tool. The problem is fully defined in space therefore when a transmission signal containing a range of linearly increasing frequencies (therefore variety of wavelengths) is used the envelope varies across the pulse width. This effect is seen in the unidirectional LFM chirp plotted as the black trace in Figure 5.6. The solid black line in 5.8 is the FFT of the unidirectional LFM chirp. The shape of the frequency response has good agreement with the theoretical curve produced using a range of peak values for the narrowband Hann windowed pulse utilised in the current commercial application. The two traces have been plotted on the dB scale to gain an equal comparison. Variations between the two curves exist where the modulation of the LFM chirp appears outside of the bandwidth of interest and at the troughs at approximately 55kHz. The troughs in the LFM chirp frequency response are sharper than those in the narrowband dashed curve. This is because the results were obtained from one broadband pulse, this can be considered a continuous result where as the

narrowband trace is calculated using many narrowband results at a given step. This effect here is minimal but it is effectively a sampling issue.

5.6 The three ring torsional propagation routine

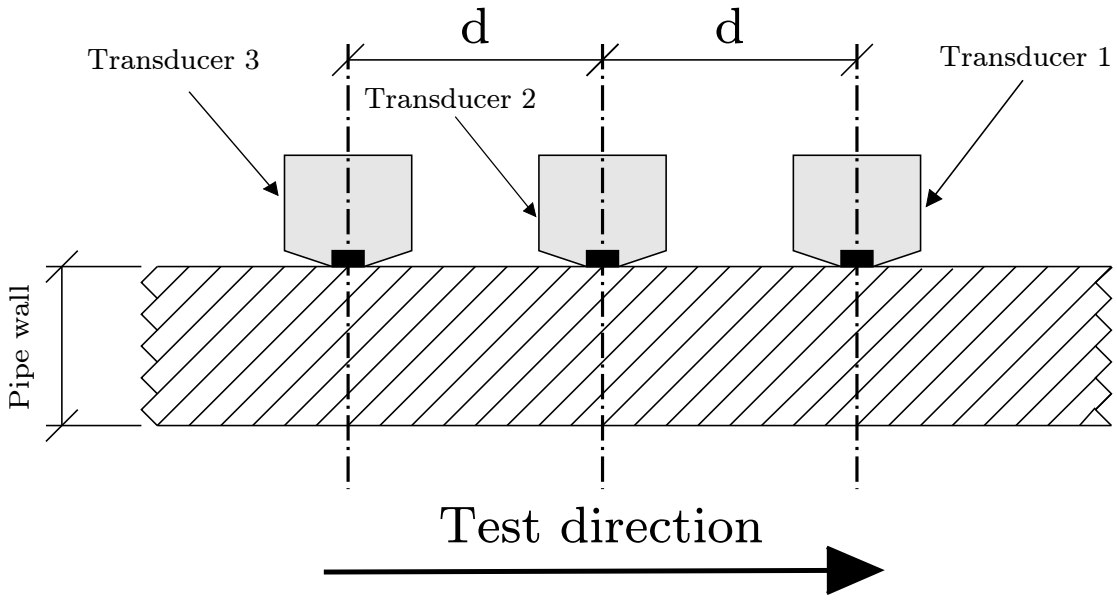

FIGURE 5.9: A simplified schematic showing the axial distribution of the transducers in a three ring torsional tool

The principle of three ring excitation stemmed from a technical report recommending a four ring excitation method to provide a solution for the testing of thick walled pipe using the longitudinal mode $L(0,2)$ [Lank (2001)]. The document explains in detail how pairs of axially spaced rings can be configured to cancel the undesired $L(0,1)$ wavemode in both directions whilst maintaining a unidirectional excitation of the desired $L(0,2)$ wavemode. Extending this idea Lank developed a configuration whereby the two inner rings of the four ring case were combined spatially so that the array contained three axially spaced rings only [Lank (2002)]. At time of the publication only the centre frequencies were considered. The signals supplied to each ring can be described as:

- Ring 1 - This signal remains unchanged in terms of delay and inversion *i.e. it is the desired excitation signal*
- Ring 3 - This signal is the desired excitation but delayed using the propagation equation (Equation 5.2) to a distance d shown in Figure 5.9.

- Ring 2 - This signal is the inverted sum of those applied to rings 1 and 3.
- Normalisation - If the signals applied to rings 1 and 3 possess amplitude limits of -1 to 1 then the amplitude limits of the signal applied to ring 2 will exceed this. The current hardware will only accept signals possessing an amplitude within a range of -1 and 1. All three rings are then scaled to the maximum amplitude seen across all of the transmission signals.

5.6.1 Three ring torsional using a 30mm ring spacing

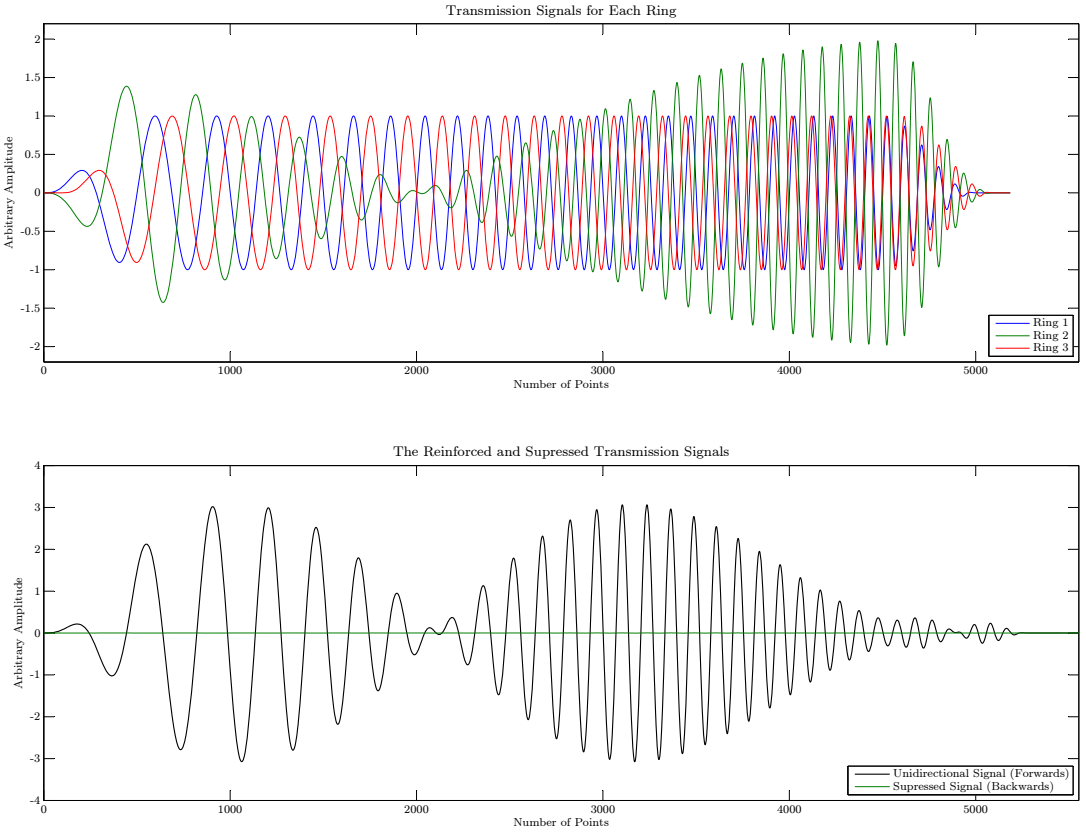

FIGURE 5.10: Torsional 3 ring 30mm ring spacing input signals and unidirectional signal (forwards) and the resulting suppressed signal (backwards)

Figure 5.10 shows the broadband input signals and the resulting unidirectional pulse. The upper axes show the individual ring signals before normalisation. The envelope of the unidirectional transmission signal is once again affected by the fixed ring spacing. The original reason for the development of the three ring torsional system was to increase output in terms of amplitude. The shape of the unidirectional trace in Figure 5.10 looks similar to that of the unidirectional trace shown in the 2 ring system (Figure 5.6) but

the amplitudes produced are approximately a third higher. This increase is due to the presence of a third ring of transducers in the system providing extra constructive superposition upon transmission of sound into the workpiece.

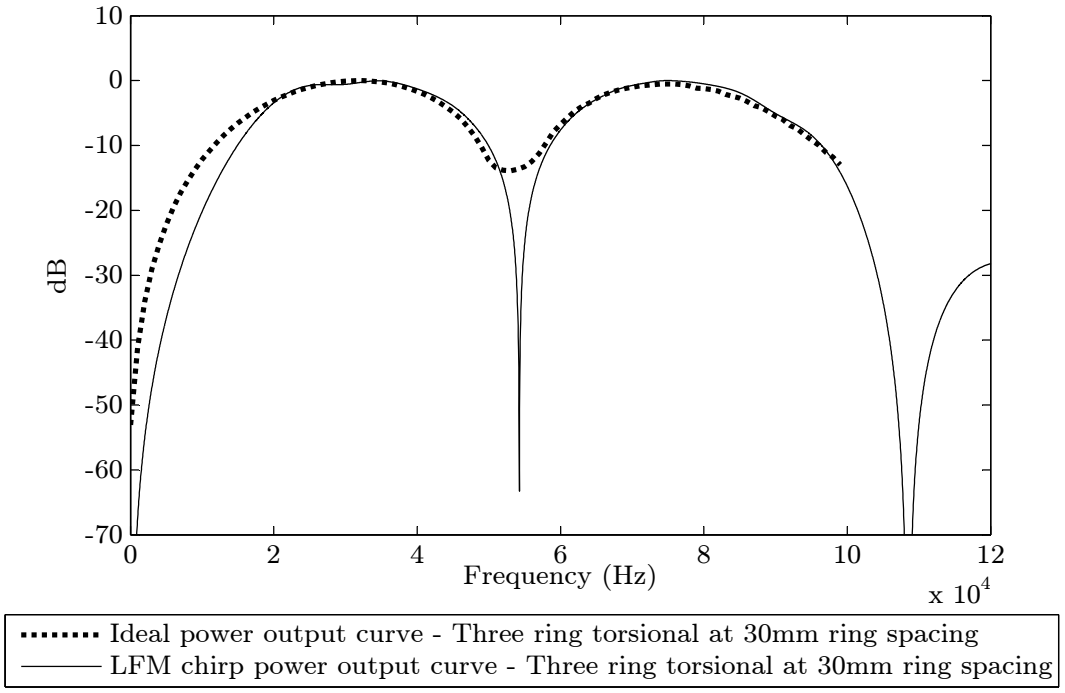

FIGURE 5.11: Three ring output curves for $T(0,1)$ at a ring spacing of 30mm

Figure 5.11 above displays the frequency dependence on the transmission output of $T(0,1)$ caused by the axial configuration of the tool. The solid black trace is the FFT of the unidirectional LFM chirp input signal. There is again good agreement between the broadband output curve and the equivalent narrowband output curve in dashed black. The trough in the output curves just below 60kHz represents a region whereby a narrowband unidirectional pulse becomes distorted through destructive interference between the ring signals produced during transmission. Tests performed within this trough are not recommended as the quality of the input signal is severely diminished.

5.6.2 Three ring torsional using a 45mm ring spacing

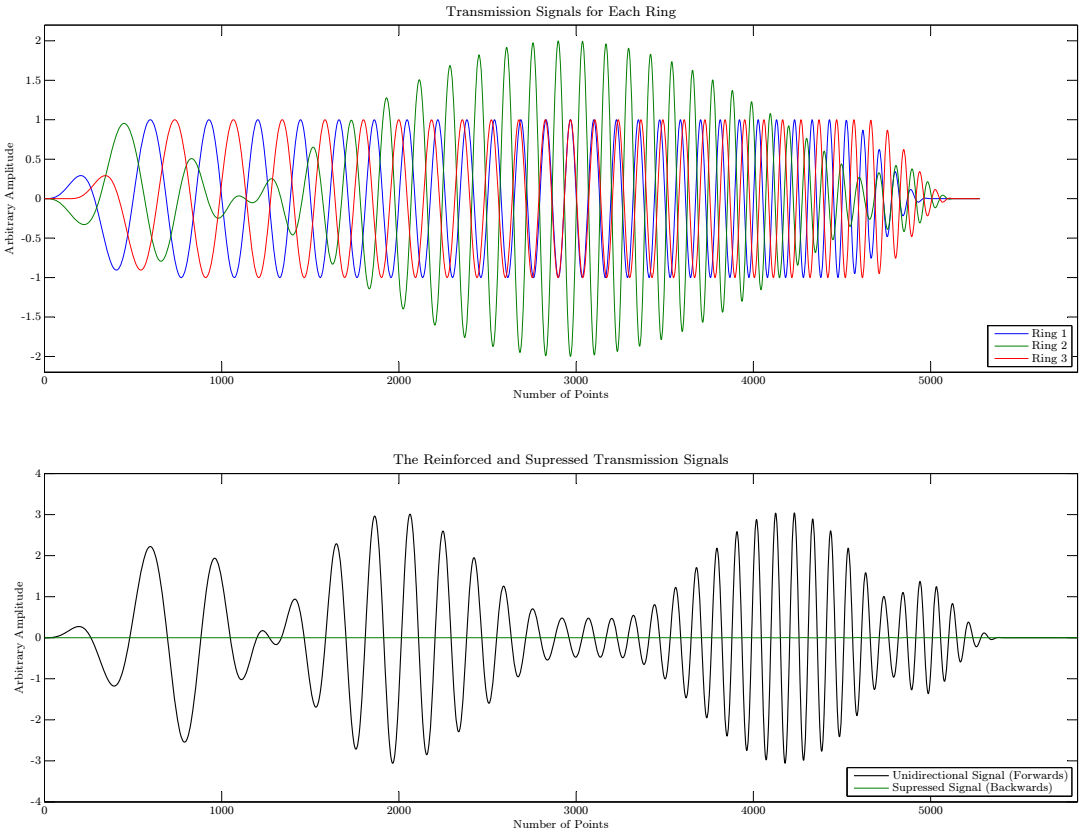

FIGURE 5.12: Torsional 3 ring 45mm ring spacing input signals and unidirectional signal (forwards) and the resulting suppressed signal (backwards)

The upper axes in Figure 5.12 above show the input signals derived for the three ring torsional tool with a 45mm ring spacing. This configuration of ring spacing is designed to bridge the trough in the power output curve displayed in Figure 5.11. In this case the tool is loaded with a total of 5 rings which are switchable into two different configurations: a 30mm spacing configuration with three axially distributed rings and a 45mm ring version. For both settings the centre ring is common leaving four transducers either side of the common centre ring which have 30mm and 45mm offset dependent upon the required frequency. The unidirectional signal plotted on the lower axes looks to be distorted but this is due again to a cyclic interference pattern being generated during transmission.

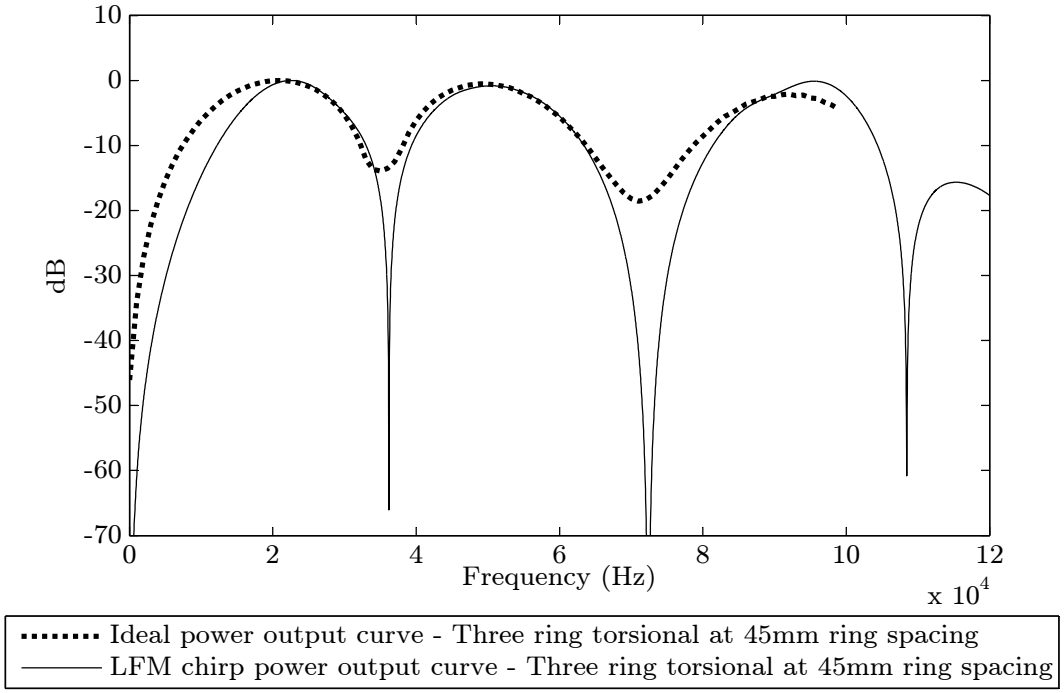

FIGURE 5.13: Three ring output curves for $T(0,1)$ at a ring spacing of 45mm

Figure 5.13 shows the power output of a three ring torsional tool configured with a 45mm ring spacing. The dashed line represents the current narrowband output for this tool and the solid line represents the proposed broadband solution. There are subtle differences in the curves particularly just outside the bandwidth of interest (20kHz - 100kHz). This is due to the variation in amplitude present at the leading edge and trainling edge of the Tukey window that is used to modulate the LFM chirp, Chapter 4 covers the parameters selected for this window.

5.7 The three ring longitudinal propagation routine

The use of the longitudinal mode $L(0,2)$ within a GWT system employing dry-coupled transducers was first proposed by Alleyne and Cawley (1995). At this time some of the practical advantages of the non-dispersive $T(0,1)$ wavemode had not yet been discovered. Alleyne and Cawley transferred knowledge of Lamb wave propagation in plate-like structures to cylinders and since the longitudinal modes which exist within the bandwidth for commercial GWT are analogous to the Lamb modes in plates, it was an obvious choice of wavemode. There are some disadvantages when using $L(0,2)$ for an GWT such as reduced performance in pipelines with high pressure liquid contents and limitations in operating frequency when inspecting thick-walled pipes. Within the bandwidth of interest both $L(0,1)$ and $L(0,2)$ exist and are generated with similar energy simultaneously (*note: they possess different wavelengths*). As demonstrated in Figure 5.4, the dispersive nature of $L(0,1)$ has the potential to corrupt an $L(0,2)$ result. The purpose therefore of the third ring of transducers is to eliminate the propagation of the $L(0,1)$ wavemode. However, this destructive interference is only effective at one frequency whereby the $L(0,1)$ wavelength is equal to the ring spacing (in this configuration it is 30mm). This *mixed mode* transmission limits a useful longitudinal test to an operational compromise with two specific objectives:

- Suppression of the $L(0,1)$ wavemode
- Unidirectional propagation of the less dispersive $L(0,2)$ wavemode

In light of these constraints it seems that $T(0,1)$ is a more convenient choice of wavemode. However, the way in which torsional and longitudinal guided waves interact with the structure within which they are propagating is fundamentally different. Some geometrical features may not be suited to a particular choice of wavemode *e.g.* the torsional mode produces poor results when inspecting pipes with axially welded pipe supports at low frequencies due to the torsional stiffness increase created by this design of feature [Alleyne et al. (2009)]. An equivalent longitudinal test will not be as sensitive to this effect, the results therefore will possess a higher SNR. There are other issues associated with the choice of the longitudinal wavemode such as the double mode conversion effect and limits when testing liquid filled pipelines [Alleyne et al. (2009)] but in general it

is important to have both wavemodes available as it is not always clear ahead of time which will be optimum when carrying out an initial inspection on a structure.

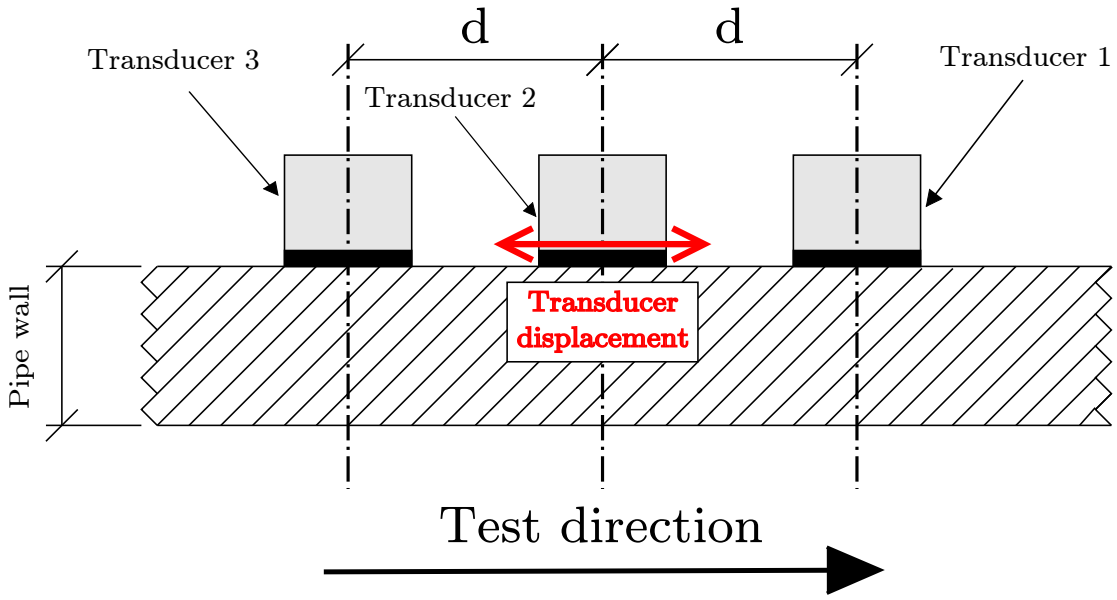

FIGURE 5.14: A simplified schematic showing the axial distribution of the transducers in a three ring longitudinal tool

5.7.1 Three ring longitudinal using a 30mm ring spacing

Due to the dispersive nature of the $L(0,2)$ wavemode it important to use the portion of the dispersion curve within the excited bandwidth to predict the input signals on rings 2 and 3. The propagation of the $L(0,2)$ wavemode was modelled using Equation 5.2 and demonstrated in Figure 5.3. The envelope for a propagated LFM chirp using the $L(0,2)$ dispersion curve does distort but is predictable. The distance of propagation when setting up the excitation rings is only 30mm which in effect minimises any large accumulative errors associated with long distance propagation. The proposed set up for the excitation of an LFM chirp during a longitudinal test is as follows:

- Ring 1 - This signal remains unchanged in terms of delay and inversion *i.e. it is the desired excitation signal*
- Ring 3 - This signal is the desired excitation but delayed using the propagation equation (Equation 5.2) to a distance d shown in Figure 5.14. The key difference for longitudinal excitation is that the wavenumber $k(\omega)$ is frequency dependent and is therefore applied as a matrix of numbers and not a single value.

- Ring 2 - This signal is the inverted sum of those applied to rings 1 and 3.
- Normalisation - The amplitude here still needs scaling as the hardware will only accept signals possessing an amplitude within a range of -1 and 1. All three rings are then scaled to the maximum amplitude seen across all of the transmission signals.

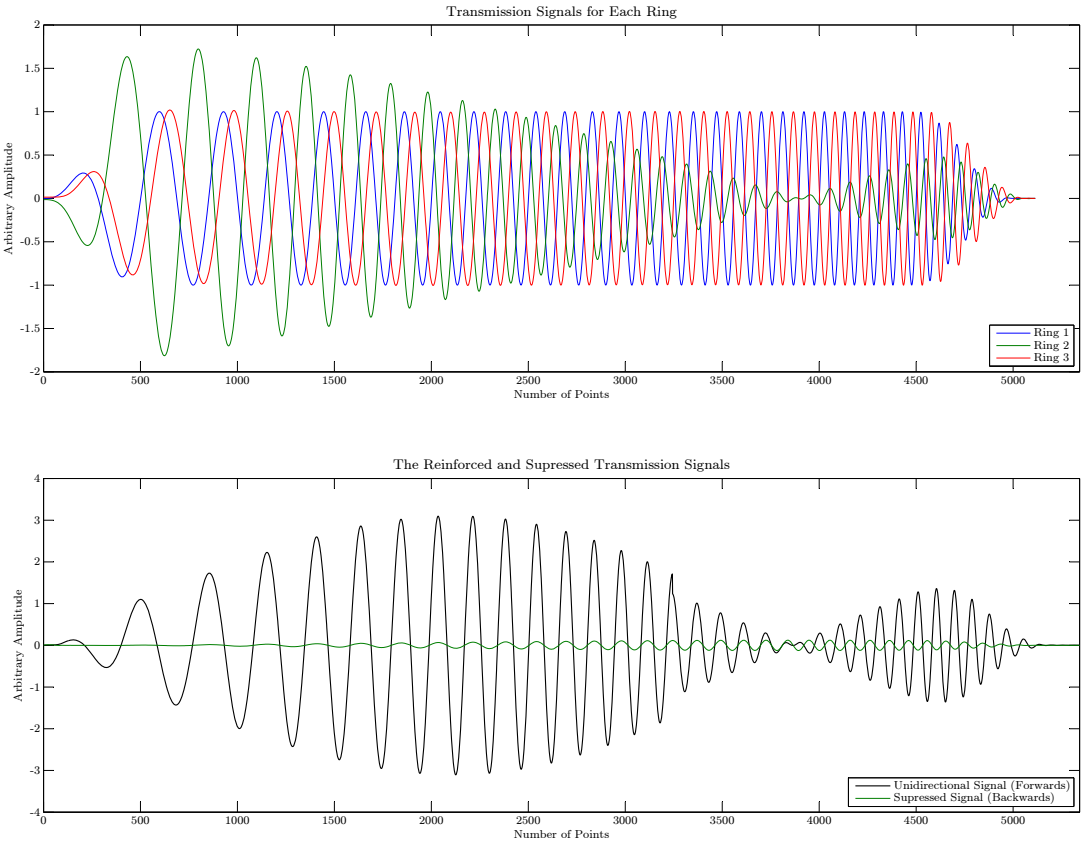

FIGURE 5.15: Longitudinal 3 ring 30mm ring spacing input signals and unidirectional signal (forwards) and the resulting suppressed signal (backwards)

The upper axes in Figure 5.15 shows the three transmission signals (pre-normalisation) which are sent to the transducers in their respective rings. The blue trace is ring 1 which remains unchanged with respect to phase and amplitude; it is the desired excitation signal. The red trace represents the signal applied to ring 3. This signal has been propagated 30mm using the phase velocity ($v_{ph}(\omega)$) for $L(0,2)$ within the bandwidth of the LFM chirp. The bandwidth of the LFM chirp was matched with the phase velocity values for $L(0,2)$ in order to input the correct range of vales for $k(\omega)$ into Equation 5.2. The trace for ring 2 is calculated as the inverted sum of the traces applied to rings 1 and 3 as specified in Lank (2002). The unidirectional LFM chirp plotted in black on the

axes below is the result of a sum of the modelled signals for rings 1, 2 and 3 propagated to a fixed reference distance in the test direction. The frequency dependence of a fixed ring spacing is revealed as a varying envelope along the pulse length. The destructive interference when creating a unidirectional $T(0,1)$ transmission (Figures 5.6, 5.10 and 5.12) is almost perfect but in the longitudinal case numerical error when propagating the signal in the frequency domain has resulted in minor leakage of a backwards propagating signal (seen in Figure 5.15 as the green trace in the lower axes). The error amounts to approximately -28dB below the maximum of the transmission signal propagation in the test direction. During transmission destructive interference occurs on all of the multi-ring GWT tools but due to the difference in wavelength between $L(0,2)$ and $T(0,1)$ the power output curves for these two wavemodes from a three ring tool with a 30mm spacing are different.

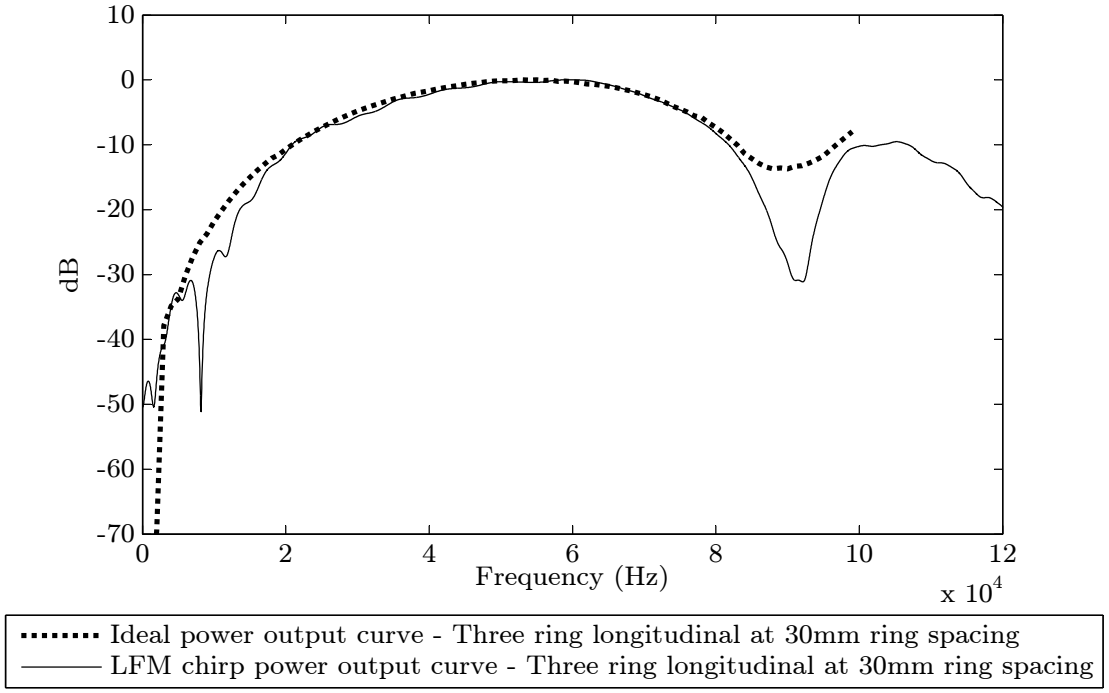

FIGURE 5.16: Three ring output curves for $L(0,2)$ at a ring spacing of 30mm

Figure 5.16 shows the comparison between the power output of the unidirectional narrowband signal and the proposed LFM chirp using the $L(0,2)$ wavemode and a three ring tool with a 30mm ring spacing. Despite the complexity introduced by referencing a dispersive wavemode using a broadband signal over the three rings to produce a unidirectional signal, there is good agreement between the broadband and narrowband

outputs. Outside of the bandwidth of interest (20kHz - 100kHz) a difference in amplitude modulation exists between the two methods so they are not expected to correlate very well.

5.8 Experimental Set Up

The pipe and tool position used to test out the possibility of successfully applying unidirectional signals using an LFM chirp for each configuration of GWT tool stated was stated in Figure 4.6. For simplification this pipe contains no defects, has square cut ends and is simply supported on two pipe stands.

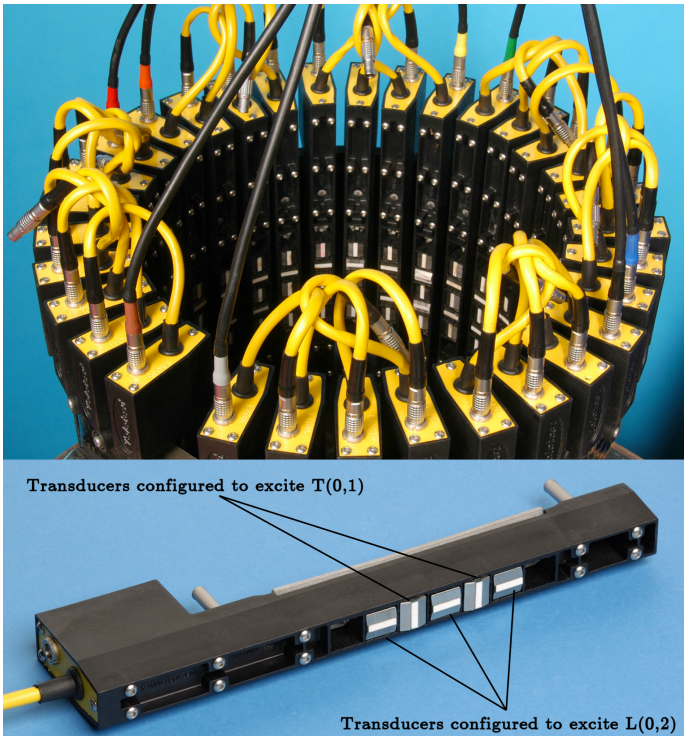

FIGURE 5.17: An example of a *multi-mode* GWT tool produced by Plant Integrity Ltd.. The lower image shows the orientation of the transducers within the transducer module for torsional and longitudinal excitation

Figure 5.17 shows a *multi-mode* tool used in GWT. The lower image shows the orientation of the transducers for both a two ring torsional and a three ring longitudinal test. The three ring torsional tests were carried out using a variant of this tool where each module is loaded with five transducers all orientated to achieve a circumferential displacement, a 3D representation is shown overleaf in 5.18. This tool has a common central ring which serves both a 30mm and 45mm ring spacing configuration.

The tool was mounted to a 9m long, mild steel, 8 inch schedule 40 pipe (OD = 219mm, wall thickness = 8.18mm). The distance to the near end of the pipe was 3m and the far end of the pipe (the test direction) was 6m away from the tool. These distances were chosen so that there was no 'round-trip' effect within the time/distance of interest. The more central the tool is the more chance there is for pulses of interest to overlap thus masking phase and amplitude information.

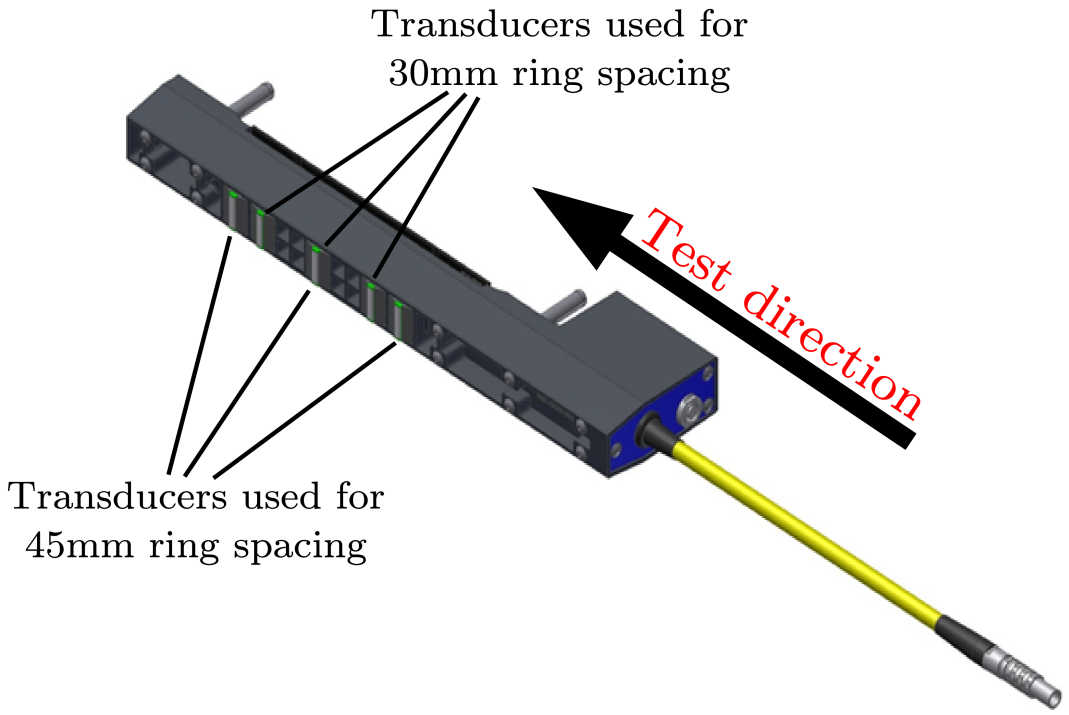

FIGURE 5.18: An example of a *torsional* module produced by Plant Integrity Ltd..

Figure 5.18 shows a CAD representation of a torsional module used for the 3 ring torsional experiments. The arrow indicating test direction shows the directionality of the experiment only. These tools can be configured to fire in either direction. During a GWT inspection both directions are used in separate tests increasing the amount of pipeline covered from a single tool location. It is clear from Figure 5.18 that the transducers are all aligned in the same direction, this is a different configuration to the multi-mode tool shown in Figure 5.17.

5.9 Discussion of Results

Table 5.1 displays the reported narrowband test schedule used to compare the performance of a unidirectional broadband excitation. The number of cycles used for all tests was 10. The asterisk beside the centre frequency denotes an optimum test frequency for the specified tool configuration. In terms of power output in the test direction these frequencies are found at the peak of the power output curves displayed in Figures 5.8, 5.11, 5.13 and 5.16.

Wavemode	No. Rings	Ring Spacing (mm)	Frequency (kHz)	Plot Ref.
Torsional	2	30	27*	Figure 5.19
Torsional	2	30	81*	Figure 5.20
Torsional	3	30	36*	Figure 5.21
Torsional	3	30	72*	Figure 5.22
Torsional	3	45	24*	Figure 5.23
Torsional	3	45	48*	Figure 5.24
Longitudinal	3	30	51	Figure 5.25
Longitudinal	3	30	61	Figure 5.26
Longitudinal	3	30	65*	Figure 5.27
Longitudinal	3	30	71	Figure 5.28

TABLE 5.1: Schedule of tests carried out

Figures 5.19 to 5.28 show the result of an axisymmetric, unidirectional test for both narrowband excitation and the filtered down emulated version using an LFM chirp (τ = 500μs, f_1 = 5kHz, f_2 = 115 and α = 0.2). The blue trace in each case is the narrowband result at a specified centre frequency and the red trace is the emulated broadband equivalent. Each trace has been normalised to be within -1 and 1 using the far end response at 6m. Using this method of presentation the traces become directly comparable. Across the range of signals displayed the responses are agreeable beyond the excitation signal which differs because the excitation conditions are not identical. One anomalous result appears however, in Figure 5.22. The low level response observed just before 6m in the red trace is thought to have occurred due to a slight disturbance of the test piece between tests causing a change in the response near to the far end.

As mentioned previously these responses were gathered from the same specimen used in Chapter 4 using an identical tool location. When comparing the unidirectional plots to those collected using only a single ring it is clear that the propagation routine for each configuration is effective in cancelling out the near end signal (expected here at 3m), reducing the round trip signal (expected at 9m) and reinforcing responses expected within

the test direction. This is true for both the non-dispersive torsional mode $T(0,1)$ and the slightly dispersive longitudinal mode $L(0,2)$. One key observation to make when comparing these signals is the level and nature of the responses within each comparable trace. It is clear that at some frequencies the level of coherent noise would be unacceptable for guided wave inspection but the fact that the broadband filtered version presents the same levels of coherent noise across the results presented and beyond proves that this choice of excitation is a valid replacement. A good example of this equivalence is the two responses displayed in Figure 5.20. It is known that for torsional excitation a circumferential Lamb wave propagates during transmission and at the current circumferential module spacing the circumferentially propagating Lamb wave continues to be received masking the time base (Figure 5.20 exposes this effect beyond 6m). The trace is clearly unusable but despite this the LFM chirp equivalent has yielded almost identical results. The proposed LFM chirp excitation method, the broadband unidirectional propagation routine and the FFT filter with incorporated phase compensation have proven to be capable of providing an efficient alternative to the current narrowband GWT method which requires several individual tests.

5.10 Conclusions

A unidirectional broadband excitation method using an LFM chirp has been presented. A selection of commercial GWT tools were used to prove that directionality and equivalence to the current excitation method could be achieved. In order to meet this objective a propagation routine was established for each tool configuration which incorporated the dispersion curve for the given transmission wavemode and produced phase compensated broadband excitation signals which were applied to the designated transducer ring. This routine considers the whole bandwidth of each signal and not just the centre frequency ensuring that each frequency component propagating in the opposite direction to the test is cancelled out.

The test schedule (the list of test frequencies in Table 5.1) was chosen based upon optimum test frequencies for each configuration of GWT tool. Based upon this schedule, the broadband received signal was filtered to present an emulated narrowband signal for each case using the FFT filter derived and proposed in Chapter 4.

Results have shown the technique to produce equivalent results and that directionality has been achieved even when considering the dispersive $L(0,2)$ wavemode. Furthermore the material within this and the previous chapter is currently being implemented within Plant Integrity's Teletest inspection software for use worldwide on oil and gas industry pipeline.

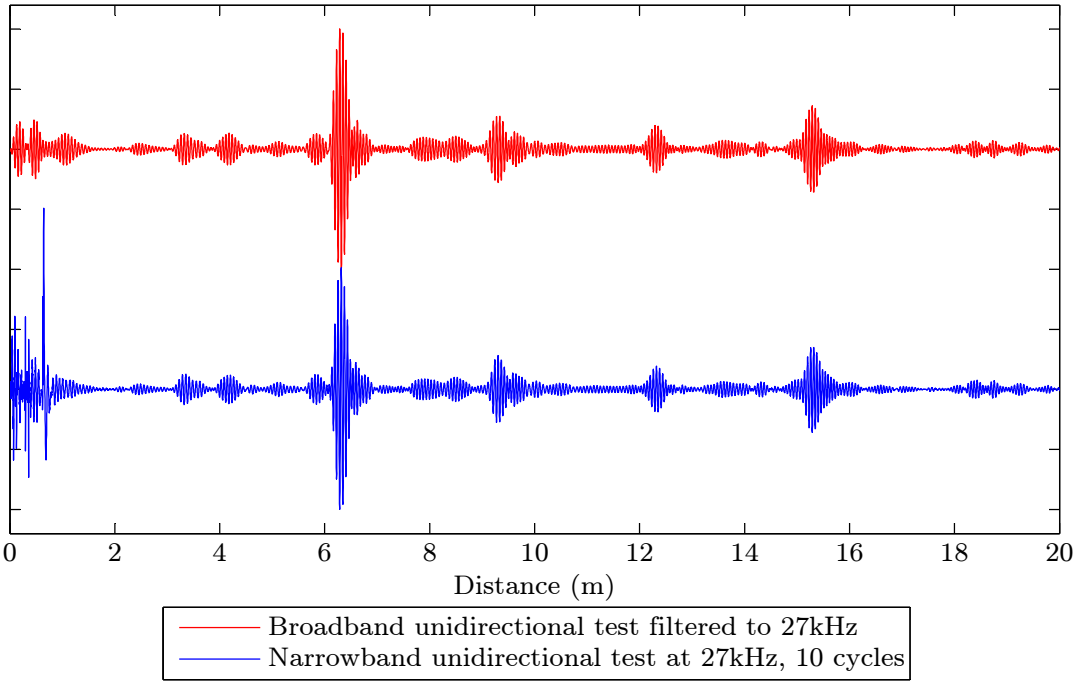

FIGURE 5.19: Two ring torsional unidirectional result at 27kHz

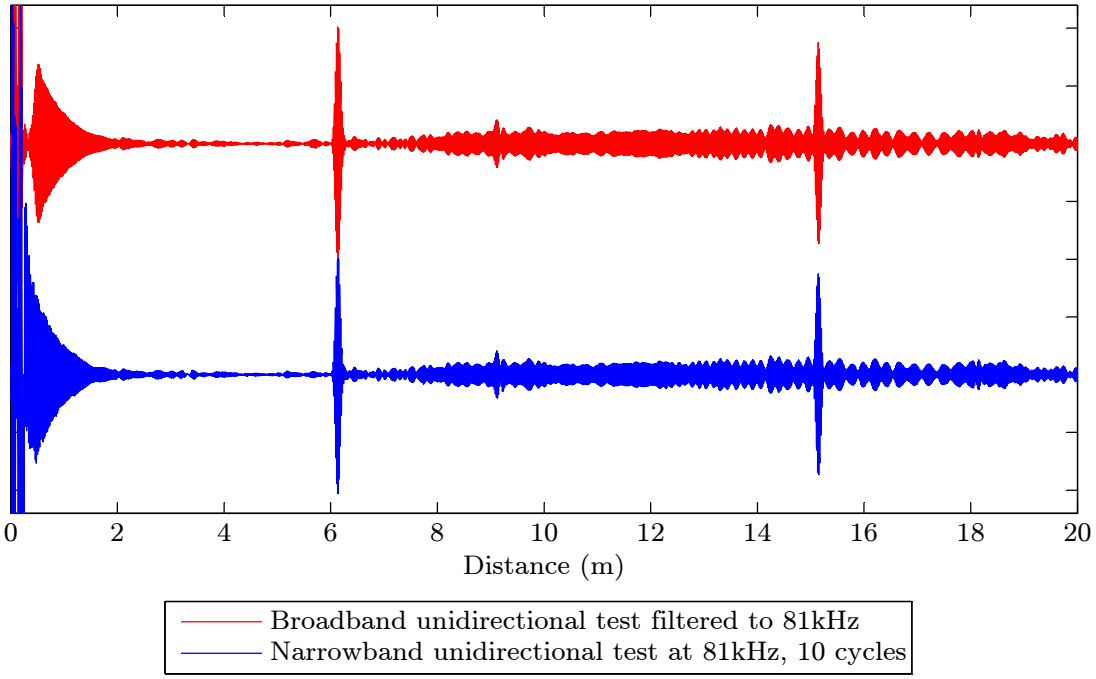

FIGURE 5.20: Two ring torsional unidirectional result at 81kHz

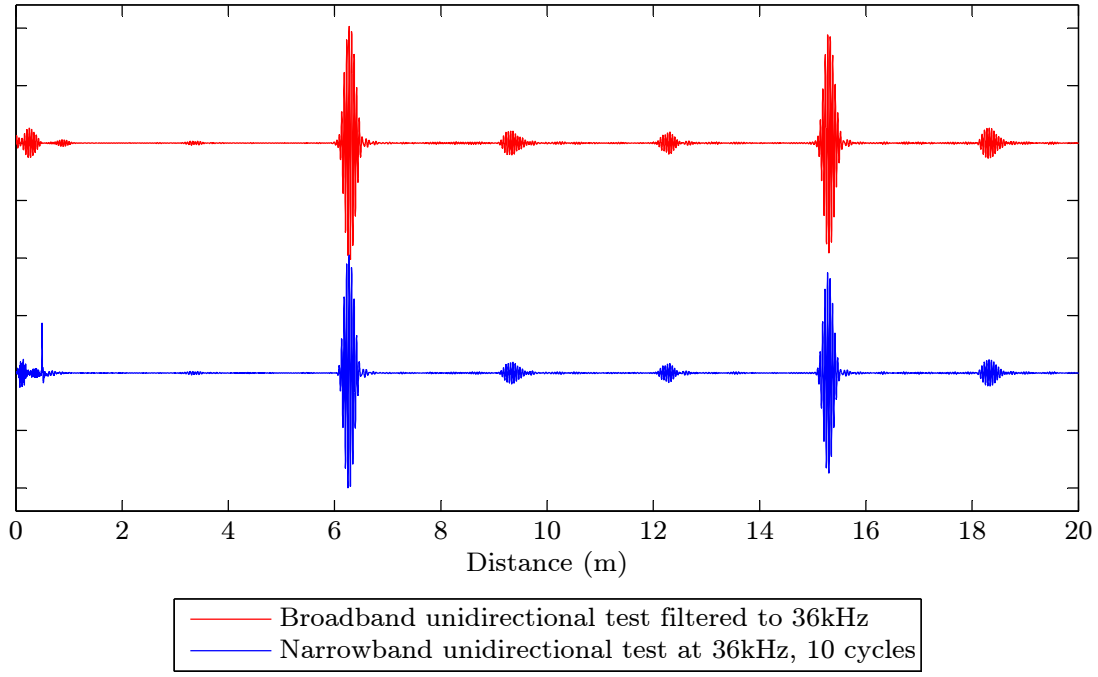

FIGURE 5.21: Three ring torsional unidirectional result at 36kHz (30mm ring spacing)

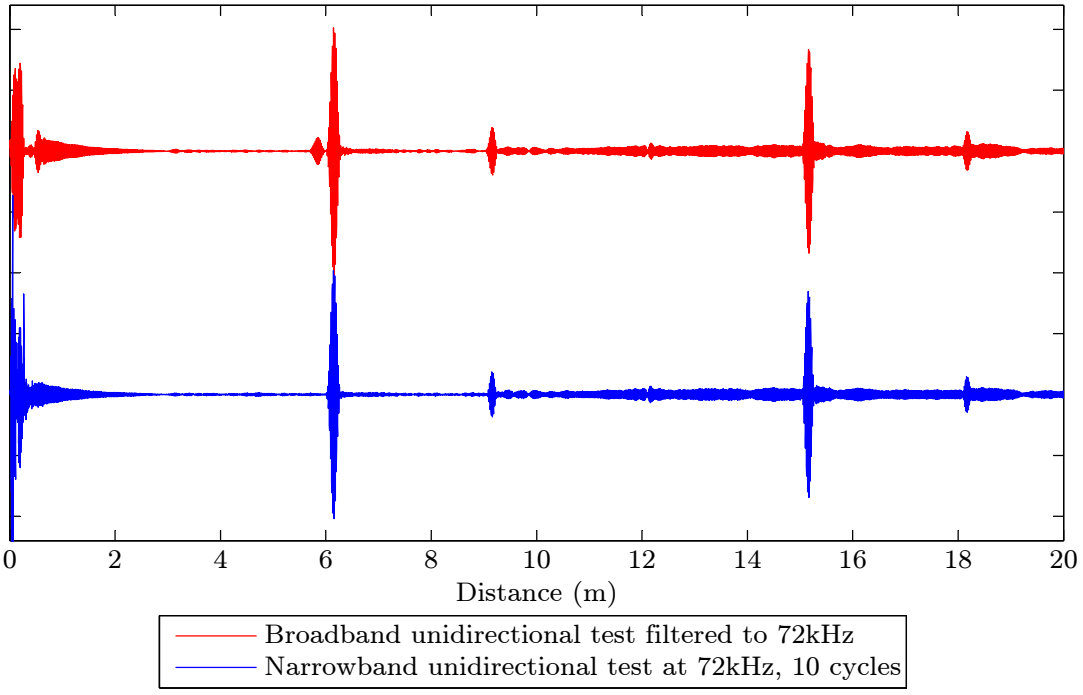

FIGURE 5.22: Three ring torsional unidirectional result at 72kHz (30mm ring spacing)

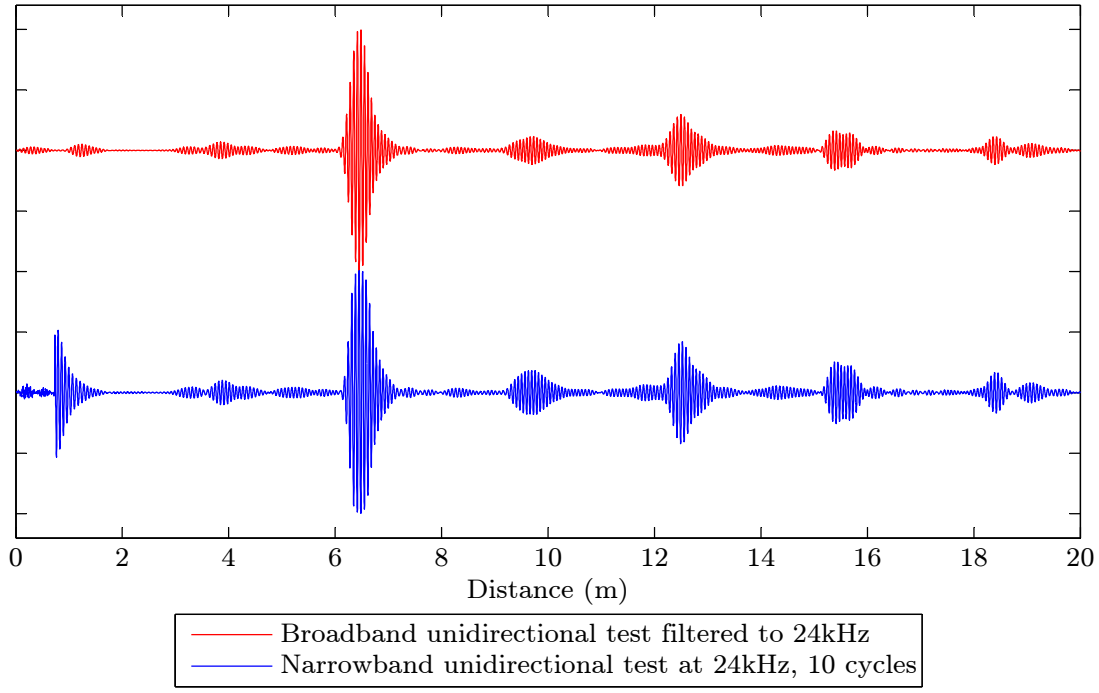

FIGURE 5.23: Three ring torsional unidirectional result at 24kHz (45mm ring spacing)

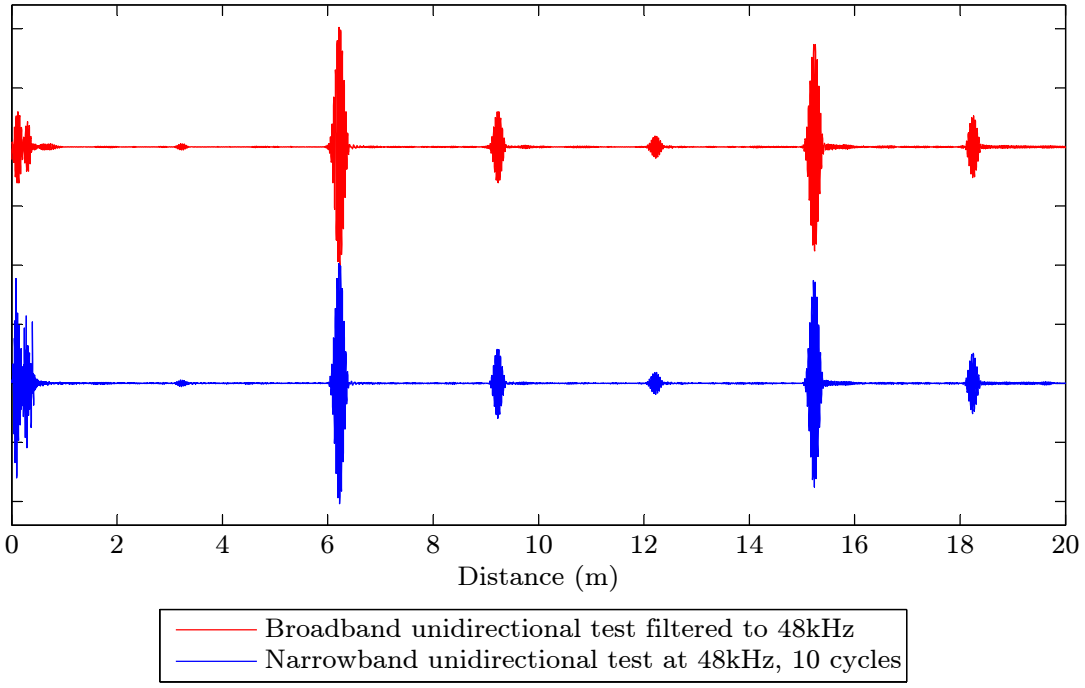

FIGURE 5.24: Three ring torsional unidirectional result at 48kHz (45mm ring spacing)

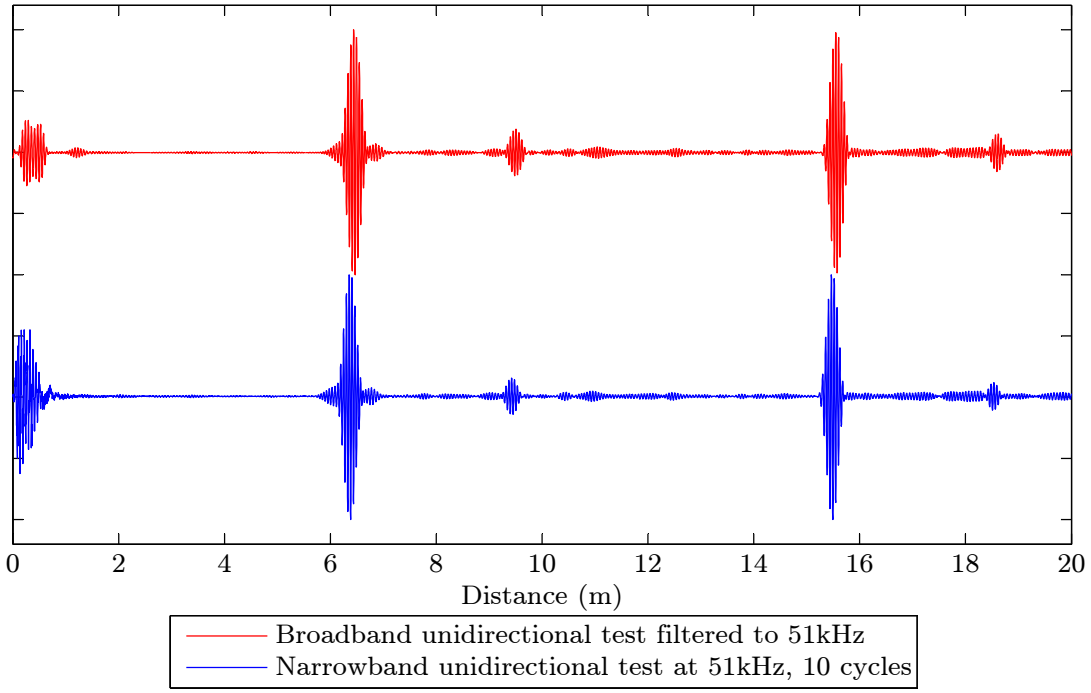

FIGURE 5.25: Three ring longitudinal unidirectional result at 51kHz (30mm ring spacing)

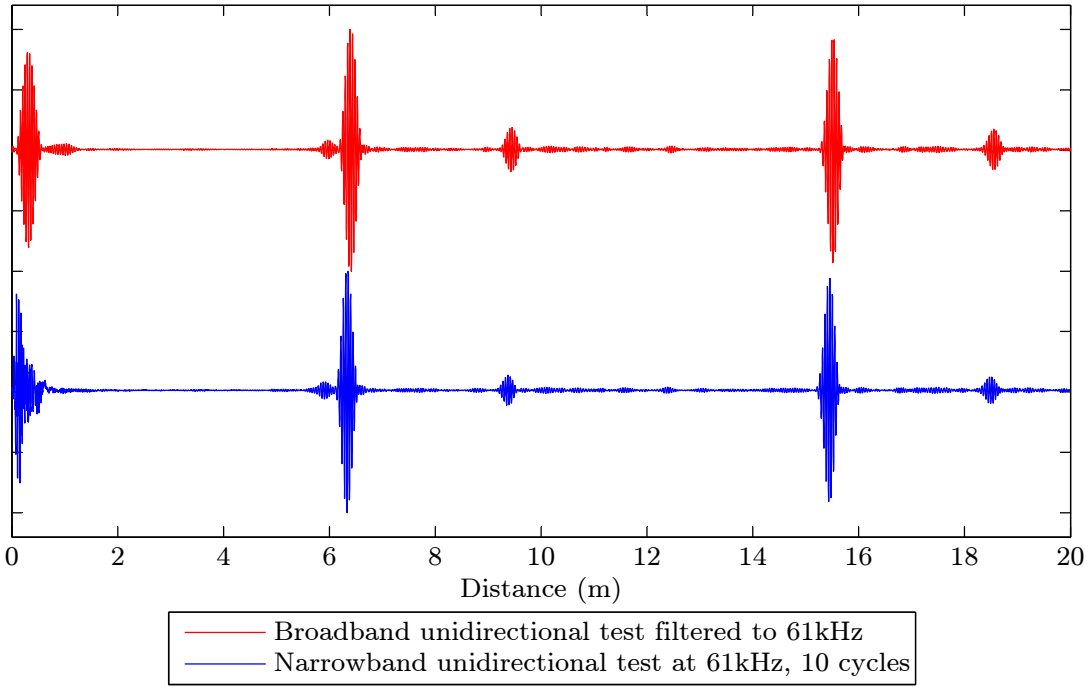

FIGURE 5.26: Three ring longitudinal unidirectional result at 61kHz (30mm ring spacing)

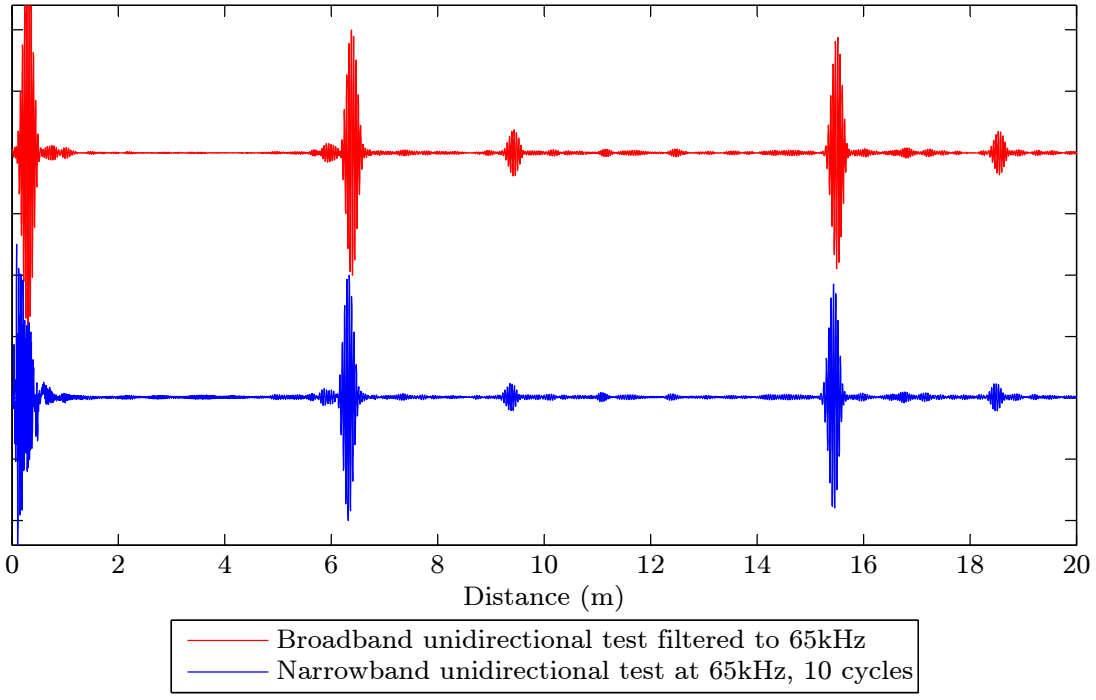

FIGURE 5.27: Three ring longitudinal unidirectional result at 65kHz (30mm ring spacing)

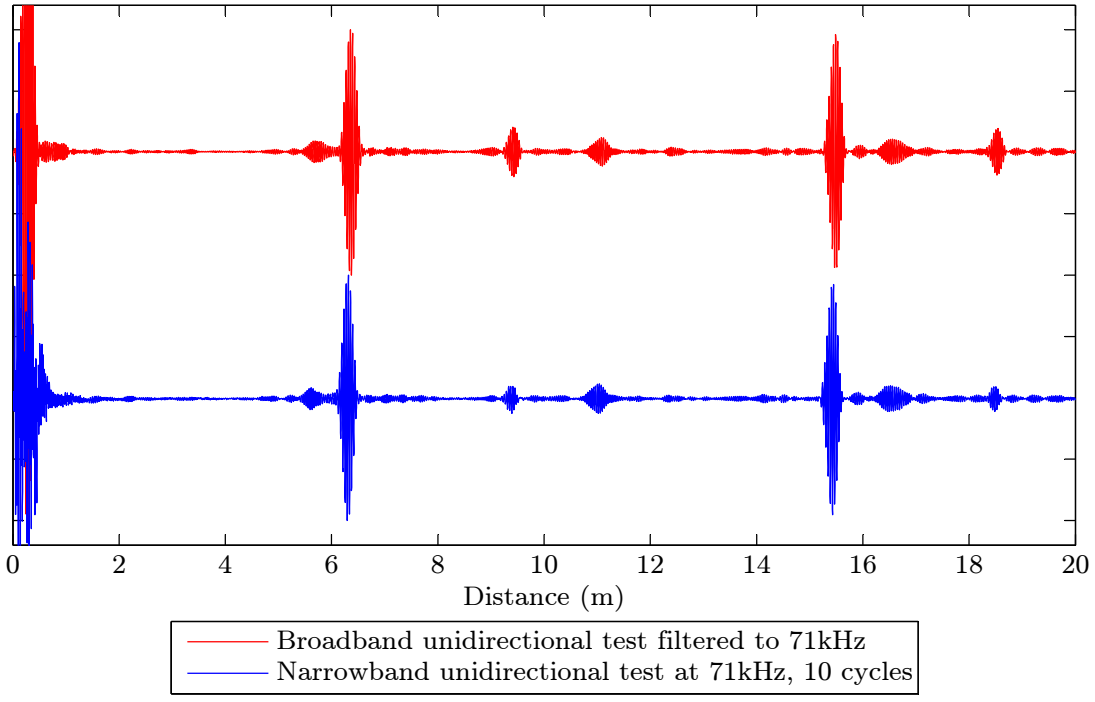

FIGURE 5.28: Three ring longitudinal unidirectional result at 71kHz (30mm ring spacing)

Chapter 6

Field Validation of Broadband Excitation for a Guided Wave Inspection Technique

6.1 Background

Chapter 5 set the scene for the application of a broadband excitation to an actual GWT field inspection. It was shown, for all configurations of the GWT pipe inspection tools produced by Plant Integrity, that the LFM chirp method proposed and optimised in Chapter 4 can produce equivalent laboratory results to the current narrowband excitation with minimal error. A key step in Chapter 5 was achieving directionality for an LFM chirp test using a propagation routine based upon all of the frequency components within the broadband transmit signal. This step combined with the custom FFT filter proposed means that equivalent narrowband results can be produced efficiently by using only one test. Due to the frequency dependence of nearly every aspect of this inspection technique, the LFM chirp is an attractive solution for determining the optimum test frequency during an inspection.

This chapter presents field inspection data collected using the commercial Teletest software via a broadband collection routine performed in the background and recommended by the author during this research. The standard narrowband responses presented will include actual damage identified by a trained GWT inspection engineer during the field

inspections. Unfortunately on this occasion no $L(0,2)$ test data were collected; this chapter will only cover a torsional tool configured in three rings. Signal pre-conditioning and data presentation will be discussed ahead of the presentation of narrowband and broadband results.

6.2 Objectives

The aim of the work within this chapter is to investigate the application of the broadband transmission signal proposed in this thesis to an actual guided wave field inspection.

As such, specific objectives are as follows:

- Define a specified broadband transmission routine to be implemented in a commercial GWT software for all configurations of available tools.
- Implement the broadband reception processing techniques proposed in Chapters 4 and 5 to present unidirectional, emulated narrowband tests from the available broadband data gathered in the field.
- Implement post-processing routines to present both broadband and narrowband data in a format which is used for damage interpretation by a GWT inspection engineer.
- Extract quantitative information from the inspection plots to assess the performance of broadband excitation within an actual GWT field inspection.

6.3 Methodology

6.3.1 Software implementation

Early on in the research covered in this thesis the author demonstrated the performance of a broadband transmission in Thornicroft and Catton (2010) and Thornicroft and Catton (2011). At the time of writing up this work, the development did not use a custom filter which managed the phase differences experienced between the narrowband and broadband case; a standard equiripple FIR filter was used which was effective enough in

reproducing a comparable amplitude but there were issues with phase delays and the so-called *group* delay associated with the transmission of an LFM chirp signal. Despite filter issues experienced during post-processing, it was decided to implement the transmission of an LFM chirp within the commercial Teletest inspection software. During this time the broadband methods developed by the author were also implemented across the ultrasonic guided wave group at TWI successfully for a range of guided wave applications including tomography of plates, transducer chracterisation, laser vibrometry and other waveguide geometries.

6.3.2 Data collection

The data collection process is controlled by the Teletest commercial software. The user defines parameters specific to the structure such as Outside Diameter (OD) of the pipe, the Wall Thickness (WT) and material. These parameters contribute to the generation of unique dispersion curves for the pipe to be inspected and therefore, a set of recommended frequency limits within the inspection should take place. The LFM chirp collection was added to the software in such a way that it was hidden from the user. The information and data on the additional collections were stored on disc within the same data file which the software creates so that the author could subsequently extract it using external methods such as MATLAB or Python routines.

6.3.3 Data analysis

For the results in this chapter the classification of individual narrowband responses from an inspection point of view are all down to the judgement of the inspection engineer. As the LFM chirp results and processing routines are not currently available in the commercial software, the performance of the emulated narrowband signals created will be determined via a quantified comparison using the responses highlighted by the inspection engineer.

6.4 Gathering of Broadband GWT Field Data

The pipeline used for the field study within this chapter is part of a large oil transmission facility in North America. In North America the governing bodies concerned with the safe processing and transmission of hazardous materials use GWT as an instrumental part of integrity assessment of this category of structures. An example of official regulatory documentation concerning this inspection technology can be found in PHMSA (2010).

6.4.1 Test schedule

The tests performed during this inspection covered a variety of sizes of pipes at several locations. There were 96 sets of data available to the author for processing. For conciseness approximately 10% of this total have been presented here. The table below shows a summary of the 10 inspections:

Test ID	Wavemode	No. Rings	Ring Spacing (mm)	Frequency (kHz)	Plot Ref.
106	Torsional	3	30	64	Figure 6.4
47	Torsional	3	30	72	Figure 6.5
83	Torsional	3	45	48	Figure 6.6
124	Torsional	3	45	48	Figure 6.7
788	Torsional	3	30	36	Figure 6.8
59	Torsional	3	45	48	Figure 6.9
72	Torsional	3	30	36	Figure 6.10
89	Torsional	3	30	72	Figure 6.11
98	Torsional	3	30	72	Figure 6.12
127	Torsional	3	45	48	Figure 6.13

TABLE 6.1: Schedule of field tests presented

6.5 Pre-processing GWT signals

6.5.1 Minimising initial signal crosstalk (XT)

As explained earlier, the pulser/receiver generates excitation signals at 300V peak to peak. Signal reception however occurs at millivolt levels. The transmit and receive channels are laid out on separate Printed Circuit Boards (PCBs) but undesired capacitive coupling generated during this process mean that there is some elctromagnetic (EM) breakthrough (also known as crosstalk or XT) into the receiver channels. Therefore during the initial part of the ultrasonic trace a large amplitude representation of the input signal can be seen. The amplitude of this breakthrough far exceeds that of the received trace and therefore skews any results displayed in the frequency domain. Figure 6.1 shows that by multiplying the corrupted signal with a smoothed heaviside step function the crosstalk can be removed in a controlled manner.

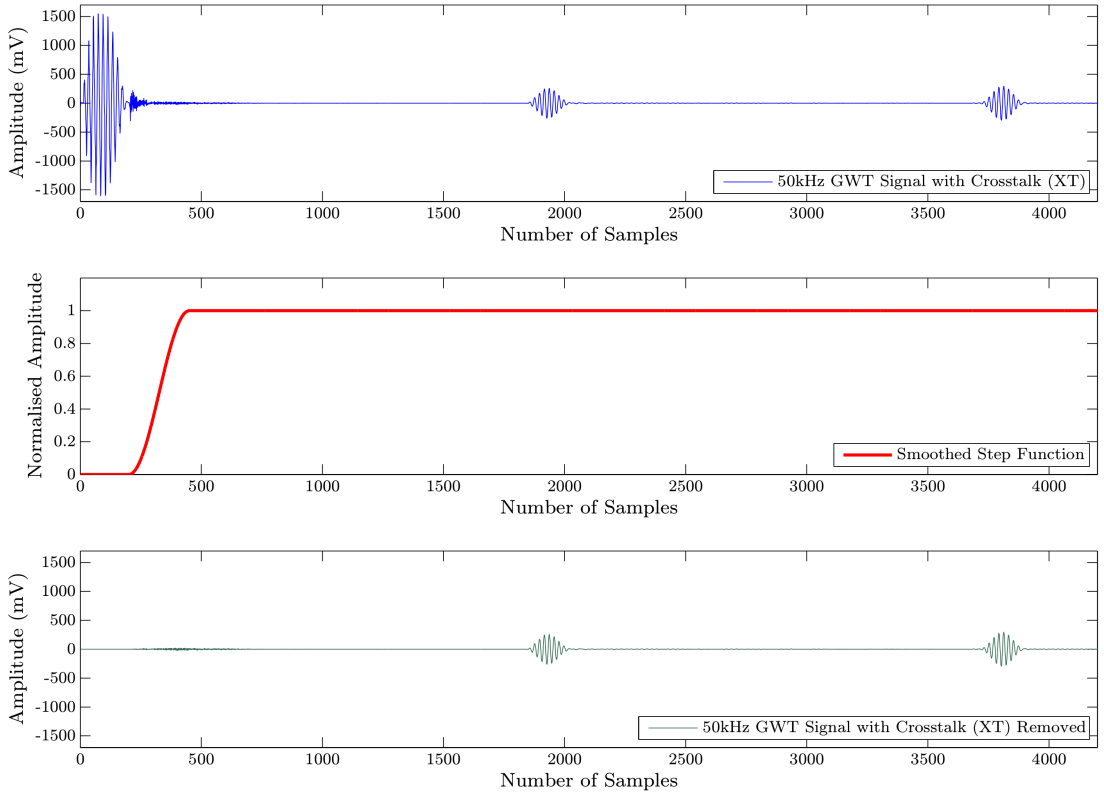

FIGURE 6.1: An example of the removal of the crosstalk from a 50kHz GWT signal (in blue) using a smoothed heaviside step function. The reception of the later signals in the green trace are unaffected

6.5.2 Enveloping the signal

The ultrasonic signals presented in this document up until this point have been in a sinusoidal form *i.e.* they are composed of sine and cosine components giving them both positive and negative values. This information is a direct representation of the mechanical waves sensed by the transducer. Presenting the signals in this way is convenient for spectral analysis but is too complex for NDT inspectors and pipeline operators to base conclusions about pipeline integrity on. In addition, a GWT inspection involves more than one wavemode that are overlaid on the same plot to make an instant judgement on integrity. A convenient method of achieving simplicity in presentation is to calculate the Hilbert transform of the sinusoidal signal.

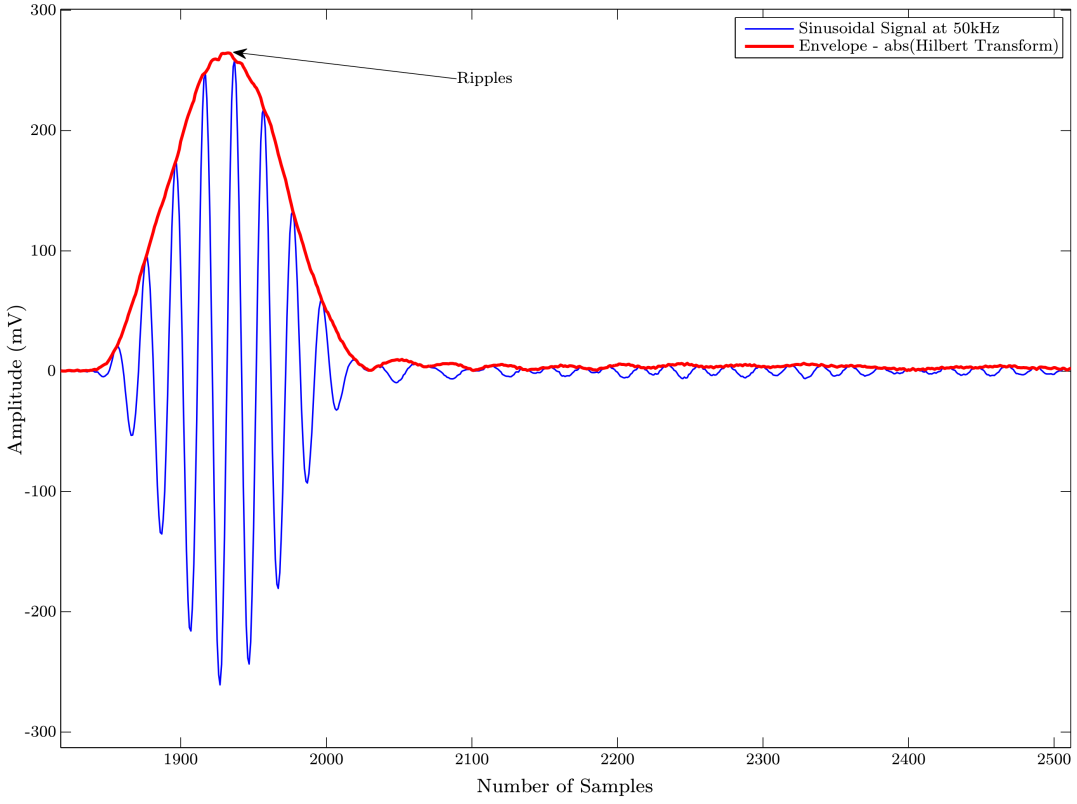

FIGURE 6.2: An example of the formation of an envelope of a 50kHz GWT signal (in blue) using the absolute values of the Hilbert transform (in red)

The absolute values of the Hilbert transform of a sinusoidal signal form an envelope. An example of this for a GWT signal is shown in Figure 6.2. The ripples highlighted in this plot are low frequency artifacts arising from the transform and do not appear once the GWT data is filtered.

6.6 Discussion of Results

The results displayed in this section are summarised in Table 6.1. The pipelines being surveyed possess a variety of Outside Diameters (ODs) and wall thicknesses. All of these results have been chosen because there is some level of damage evident in the existing narrowband scans. The emulated narrowband signals (the LFM chirp filtered version) will be compared to the existing narrowband method based upon the relative level of sound intensity (in dB) between key features appearing in each scan. If the level of damage measured is comparable then the use of the proposed broadband signal as an efficient replacement method becomes valid.

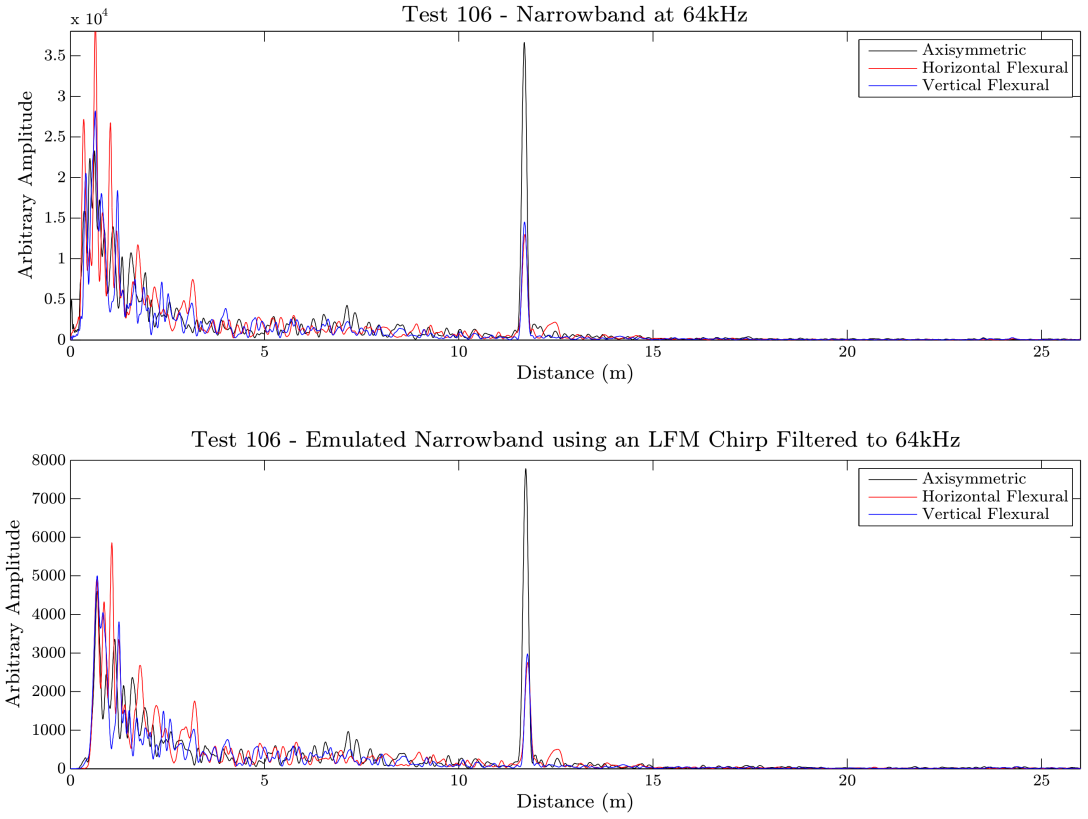

FIGURE 6.3: Comparison between narrowband and filtered broadband inspection results. Test ID 106: 64kHz, three ring torsional at 30mm ring spacing

Figure 6.3 above shows the result from Test ID 106. This pipeline has and Outside Diameter (OD) of 14inch (355.6mm) with a Wall Thickness (WT) of 9.53mm. The data displayed here are the so-called linear A-Scans which the operator uses to determine the features within the pipeline. This is done in the distance domain via judgements on range and amplitude. The black trace in both cases is the axisymmetric response (in this case

$T(0,1)$) and the red and blue traces are flexural responses (in this case $F(1,2)$). The red trace is the $F(1,2)$ which oscillates horizontally (in terms of cross-sectional displacement) with respect to the top dead centre datum of the tool. This datum can be considered as being at 0°/360°. The cross-sectional displacement for the blue trace is 90°to the red trace and is therefore termed the vertical flexural. The flexural responses highlight the cross-sectional orientation of a flaw or feature. The linear method of presenting the data here does not show up the responses beyond 15m from the transducer. This decay is due to material attenuation which has a negative exponential effect on amplitude with propagated distance for mechanical waves in elastic materials.

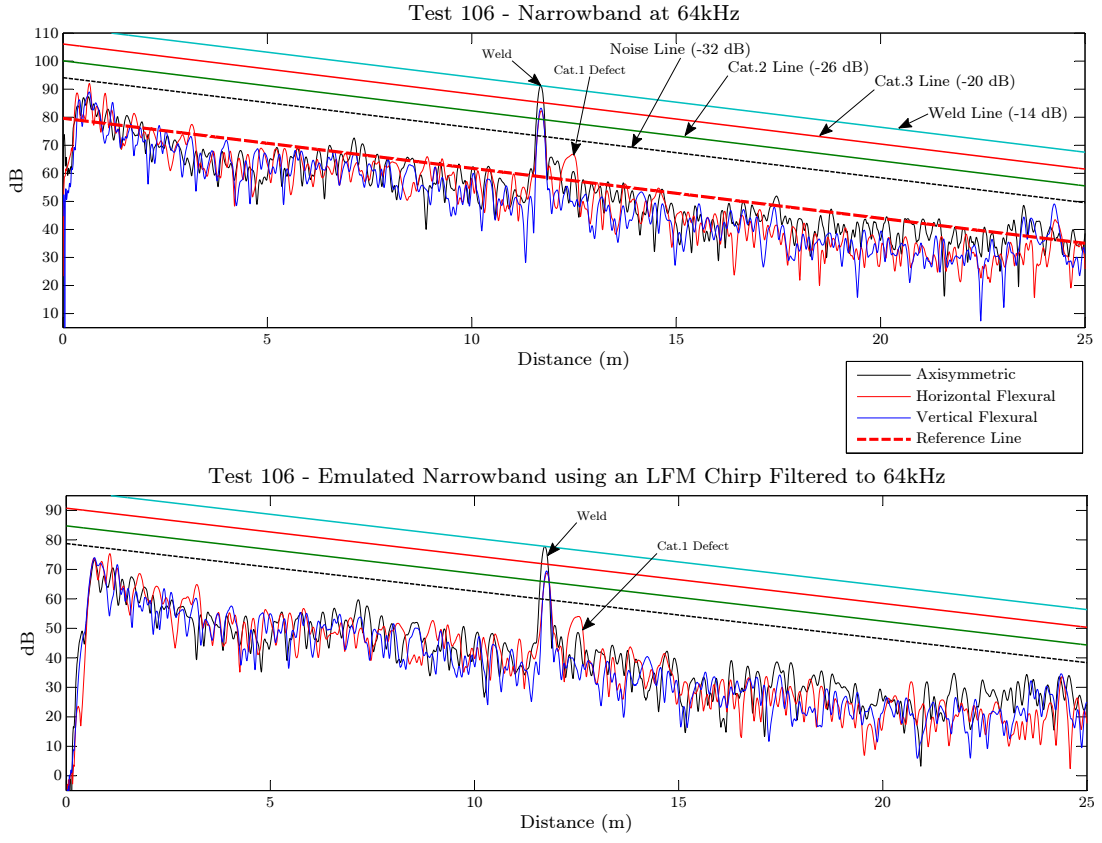

FIGURE 6.4: Comparison between narrowband and filtered broadband inspection results. Test ID 106: 64kHz, three ring torsional at 30mm ring spacing

Figure 6.3 showed that long range signals (>15m away from the transducer), if presented on a linear y scale, become too low to measure relative to the large weld signal observed at 11.5m from the GWT tool. The non-linearity of attenuation can be accounted for by using the following equation for sound intensity in decibels (dB):

$$y_{(dB)} = 20\log_{10}(y) \tag{6.1}$$

The result of adjusting the y scale in Figure 6.3 using Equation 6.1 is the response plotted in Figure 6.4. In order to set sensitivity for all measurements within the scan, one or more reference signals should be selected from which relative amplitudes and Distance Amplitude Correction (DAC) curves can be set. Currently this reference signal for pipes with a wall thickness of between 7mm and 13mm is either a girth weld or a pipe end. The increase in thickness due to girth weld reinforcement creates a response which represents approximately 20% (-14dB) of a pipe end response which is considered a perfect reflector (*i.e.* 100% of the sound propagates back to the tool and is therefore the 0dB line). Expressing the y axis in decibels also reveals a linear decay in the signal. The gradient of this general decay in the signal can be used to align the DAC curves if there is only one weld signal present in the scan. If there is more than one weld in the trace then the -14dB DAC curve is fitted to the peaks of the weld responses. Once the result is calibrated by positioning the DAC correctly, noise or damage are can then measured relative to both a 100% reflector and the known weld signal at -14dB. Noise in this case is comprised of random noise and non-random scatter caused by reflections from features or discontinuities within the tested length. This non-random scatter is also termed *coherent noise* as it exists within the same frequency bandwidth of the test and can possess a similar amplitude as actual flaws. The decay of the coherent noise floor was used to calculate an approximate rate of attenuation of the tests shown. This was achieved by implementing a peak detection routine in MATLAB which indexed the peaks within the noise up until a key feature such as the weld in Figure 6.4. A simple linear regression was then applied to fit a curve to the peaks detected within the coherent noise. This is shown as the dashed, red *reference line* in Figure 6.4. Setting this gradient up allows all of the other associated DACs to be correct to the attenuation of the trace. Responses from flaws and discontinuities are categorised as follows:

- The category 3 line is used for a severe anomaly and is set at -20dB (-6dB below the weld line)
- The category 2 line is used for a moderate anomaly and is set at -26dB (-12dB below the weld line)
- The noise line (-32dB) is used to determine the end of the test or to determine an excessive and therefore unacceptable noise level. It is also used to determine to

point at which signals from features are attenuated such that they are the same level as the noise floor. This point is known as the diagnostic length.

Note: Category 1 anomalies are identified as being responses which exceed the general noise floor by 6dB and are categorised as such up until the category 2 line

Figure 6.4 shows that the emulated narrowband which is derived from the LFM chirp has good agreement with the standard narrowband collection at 64kHz. The range of the weld and the category 1 flaw identified by the inspection engineer has been replicated satisfactorily. The parameters associated with the two scans can be summarised as follows:

Excitation Method	Feature	Range (m)	y (dB)	Relative Amplitude (dB)	Rate of Attenuation (dB/m)
Narrowband 64kHz	**Weld**	**11.65**	**91.26**	**0**	1.78
	Cat.1	12.48	66.75	24.51	
Broadband	**Weld**	**11.72**	**77.83**	**0**	1.62
	Cat.1	12.53	54.02	23.81	

TABLE 6.2: Summary of Test ID 106 measurements

Table 6.2 presents key results within the data presented in Figure 6.4. The weld highlighted in red is the feature which is considered as a reference for measurement and therefore reads as 0dB in terms of relative sound intensity. Girth welds are considered as a consistent features within each scan and therefore make excellent candidates for reference signals. There is a slight discrepancy in range of the weld which amounts to approximately 70mm between the two methods but over the stated range this amounts to 0.6% error which is negligible. The relative amplitude of the Cat.1 flaw is also agreeable. The difference in the rate of attenuation in the final column of Table 6.2 is down to errors in the linear fit method used to calculate the reference line (in dashed red).

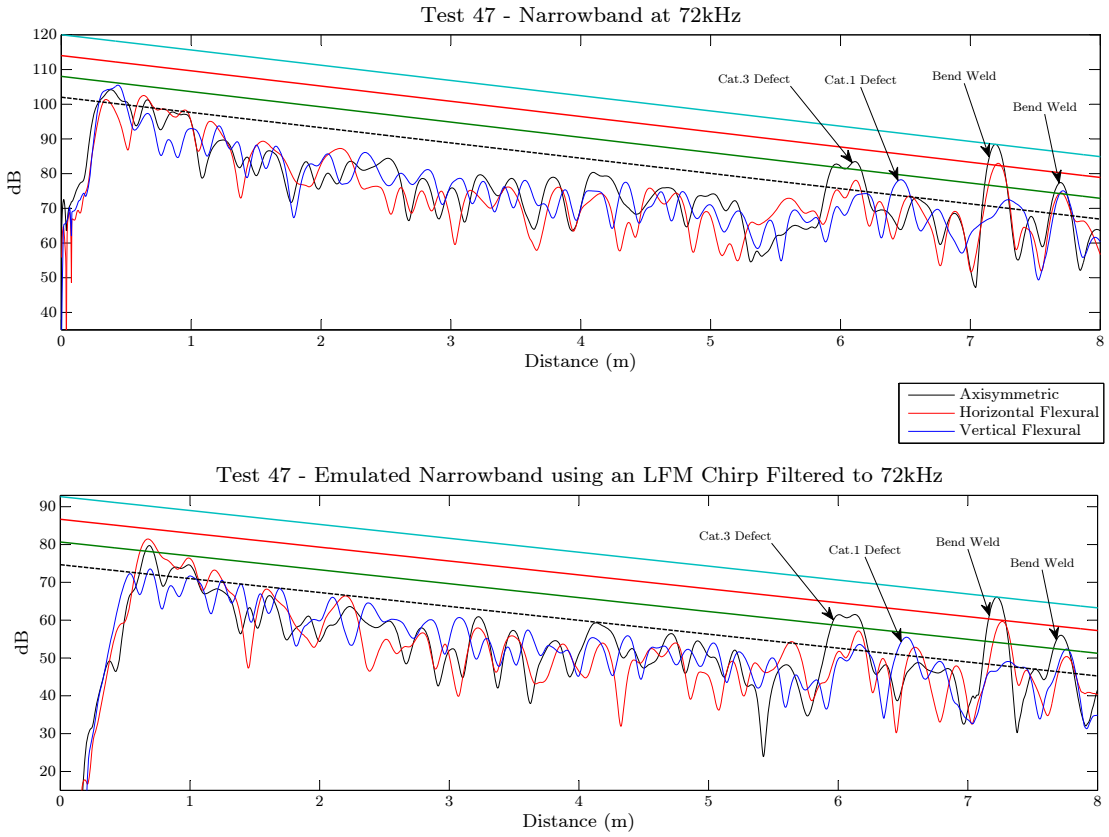

FIGURE 6.5: Comparison between narrowband and filtered broadband inspection results. Test ID 47: 72kHz, three ring torsional at 30mm ring spacing

Excitation Method	Feature	Range (m)	y (dB)	Relative Amplitude (dB)	Rate of Attenuation (dB/m)
Narrowband 72kHz	Cat.2	5.96	82.77	5.64	4.43
	Cat.1	6.46	78.22	10.19	
	Bend Weld	**7.20**	**88.41**	**0.00**	
	Bend Weld	7.69	77.43	10.98	
Broadband	Cat.2	5.99	61.22	4.86	3.67
	Cat.1	6.53	55.48	10.60	
	Bend Weld	**7.23**	**66.08**	**0.00**	
	Bend Weld	7.72	56.00	10.08	

TABLE 6.3: Summary of Test ID 47 measurements

Test ID 47 shown in Figure 6.5 contains four features identified by the inspection engineer. Before the bend weld there are two highlighted flaws. The flaw features show good comparable range, envelope and relative intensity between the two methods of excitation. There is a slight difference in rate of attenuation measured between the narrowband and broadband data. This is due to a small variation early in the signal. This early portion of the signal was used to form the reference line via a simple linear regression and this difference has amounted to an error between the gradients of the narrowband and broadband reference lines.

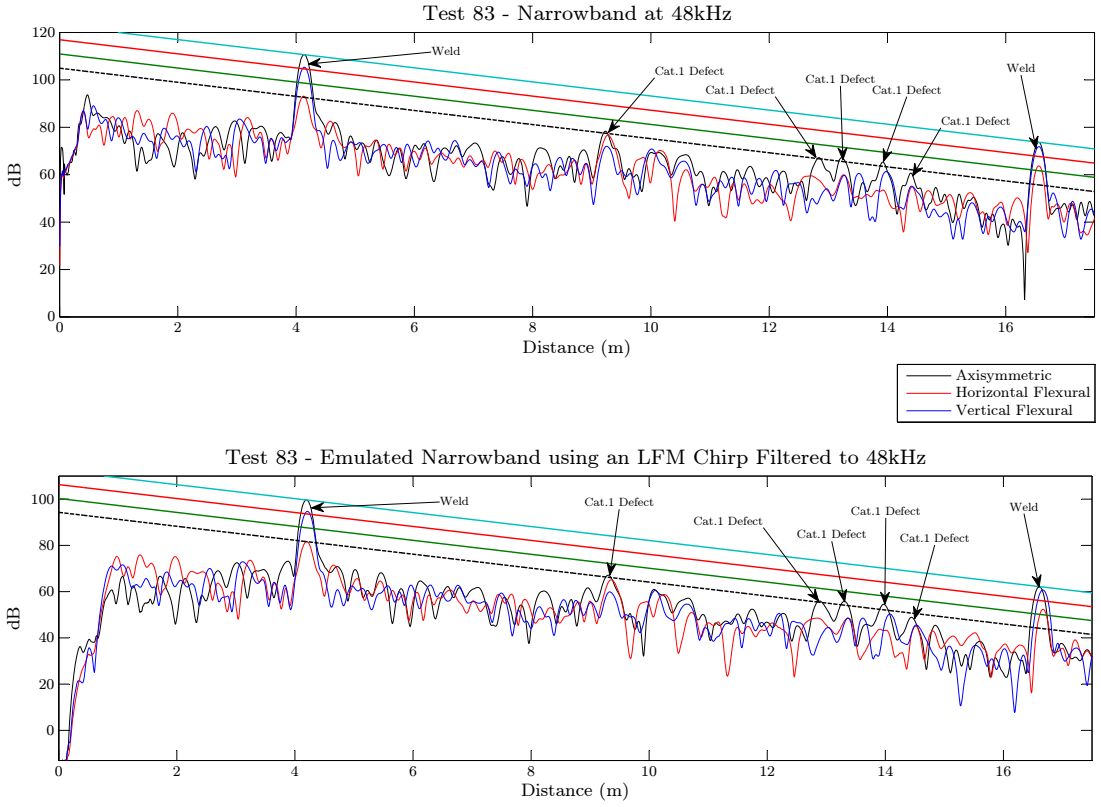

FIGURE 6.6: Comparison between narrowband and filtered broadband inspection results. Test ID 83: 48kHz (10 cycles), three ring torsional at 45mm ring spacing

Excitation Method	Feature	Range (m)	y (dB)	Relative Amplitude (dB)	Rate of Attenuation (dB/m)
Narrowband 48kHz	**Weld**	**4.14**	**110.60**	**0.00**	2.96
	Cat.1	9.24	78.22	32.38	
	Cat.1	12.84	67.15	43.45	
	Cat.1	13.24	67.11	43.49	
	Cat.1	13.92	65.33	45.27	
	Cat.1	14.39	60.65	49.95	
	Weld	16.56	73.64	36.96	
Broadband	**Weld**	**4.19**	**99.66**	**0.00**	3.02
	Cat.1	9.30	67.13	32.53	
	Cat.1	12.88	55.90	43.76	
	Cat.1	13.30	55.77	43.89	
	Cat.1	13.96	54.52	45.14	
	Cat.1	14.44	48.91	50.75	
	Weld	16.62	62.13	37.53	

TABLE 6.4: Summary of Test ID 83 measurements

The results for Test ID 83 (above in Figure 6.6) show that two girth welds were identified within the tested length. As mentioned earlier, the weld signal is used as a reference for this technique and by using the weld peak value for fitting a DAC curve and not the noise, the rate of attenuation error between the two excitation methods is minimised. Range and relative amplitudes measured between the two methods are agreeable and lie within normal variation of the GWT technique.

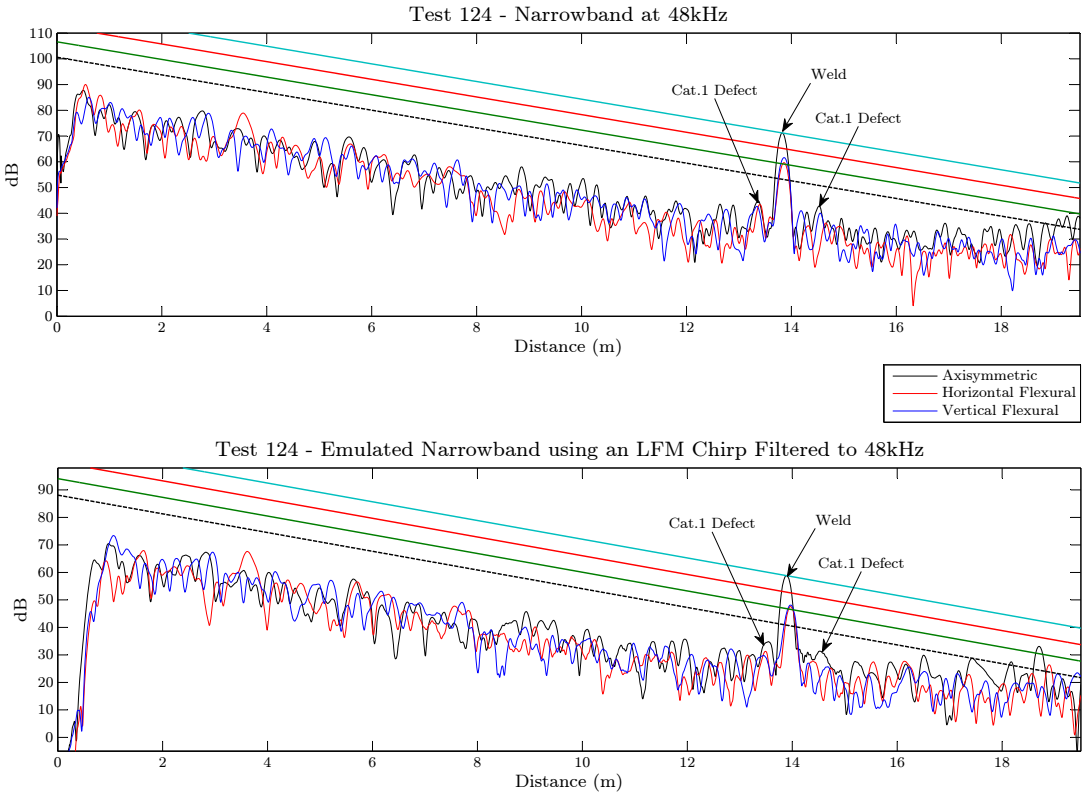

FIGURE 6.7: Comparison between narrowband and filtered broadband inspection results. Test ID 124: 48kHz (10 cycles), three ring torsional at 45mm ring spacing

Excitation Method	Feature	Range (m)	y (dB)	Relative Amplitude (dB)	Rate of Attenuation (dB/m)
Narrowband 48kHz	Cat.1	13.36	44.87	26.33	3.43
	Weld	**13.83**	**71.20**	**0.00**	
	Cat.1	14.53	42.83	28.37	
Broadband	Cat.1	13.54	34.75	24.08	3.40
	Weld	**13.88**	**58.83**	**0.00**	
	Cat.1	14.52	31.37	27.46	

TABLE 6.5: Summary of Test ID 124 measurements

Test ID 124 contains only one weld but the signature of the noise floor is a lot less variable than other scans reported here so the linear fit method used to calculate the reference line has yielded a more accurate value for rate of attenuation. There is some error associated with the range of the first Cat.1 defect at 13.36m. The emulated narrowband method shows a range of 13.54, this leaves an error of 180mm.

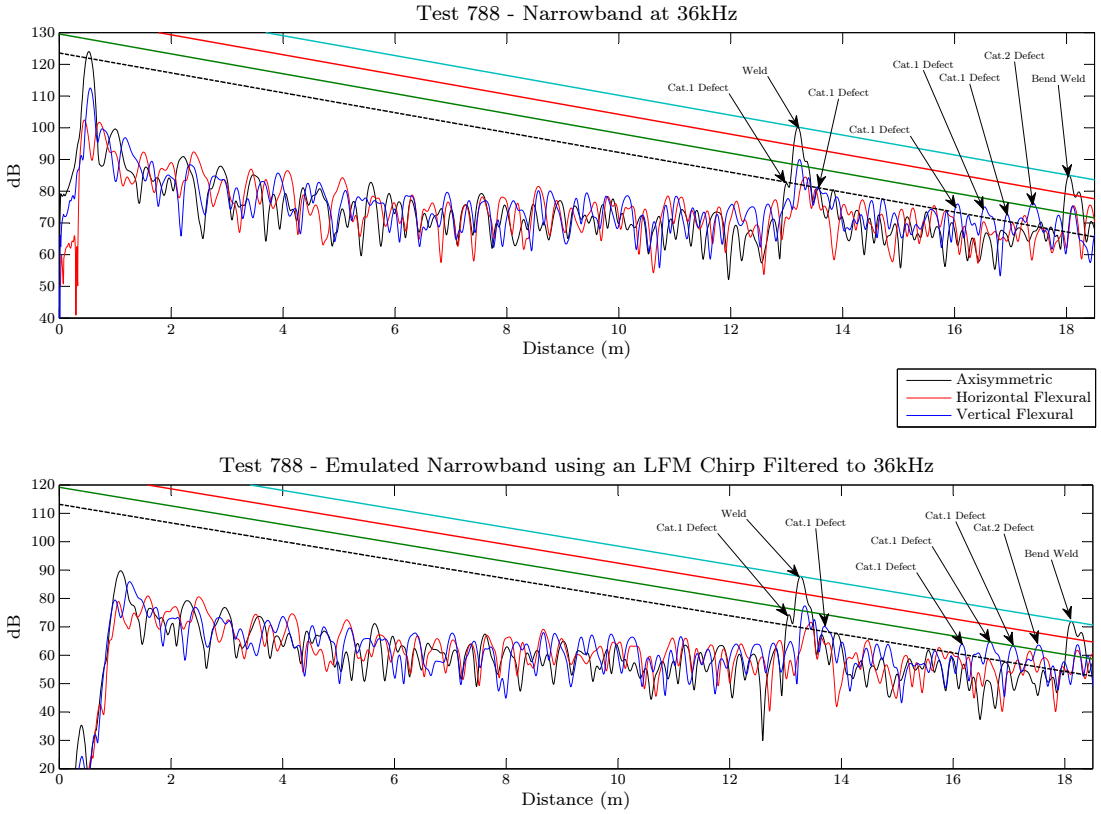

FIGURE 6.8: Comparison between narrowband and filtered broadband inspection results. Test ID 788: 36kHz (7 cycles), three ring torsional at 30mm ring spacing

Excitation Method	Feature	Range (m)	y (dB)	Relative Amplitude (dB)	Rate of Attenuation (dB/m)
Narrowband 36kHz	Cat.1	13.01	82.80	17.40	3.13
	Weld	**13.20**	**100.20**	**0.00**	
	Cat.1	13.40	84.13	16.07	
	Cat.1	16.06	75.97	24.23	
	Cat.1	16.54	75.05	25.15	
	Cat.1	16.94	72.80	27.40	
	Cat.2	17.41	76.34	23.86	
	Weld	18.04	85.03	15.17	
Broadband	Cat.1	13.06	74.23	13.54	3.27
	Weld	**13.27**	**87.77**	**0.00**	
	Cat.1	13.52	72.58	15.19	
	Cat.1	16.15	63.86	23.91	
	Cat.1	16.65	64.72	23.05	
	Cat.1	17.07	63.24	24.53	
	Cat.2	17.52	63.58	24.19	
	Weld	18.11	71.91	15.86	

TABLE 6.6: Summary of Test ID 788 measurements

Test ID 788 was carried out using 36kHz and 7 cycles. 36kHz is an optimum frequency for the tool configuration (3 ring torsional with 30mm ring spacing) but since there has been damage identified within (or very near to) the first girth weld at 13.27m the inspection engineer has reduced the pulse width to increase the temporal/spatial resolution. The filter proposed in Chapter 4 has the ability to take any narrowband configuration of

input signal as a template and so therefore emulating the configuration used here in test ID 788 is not an issue. Despite a number of flaw reflectors appearing in the area of concern beyond the first girth weld, the two excitation methods have good agreement.

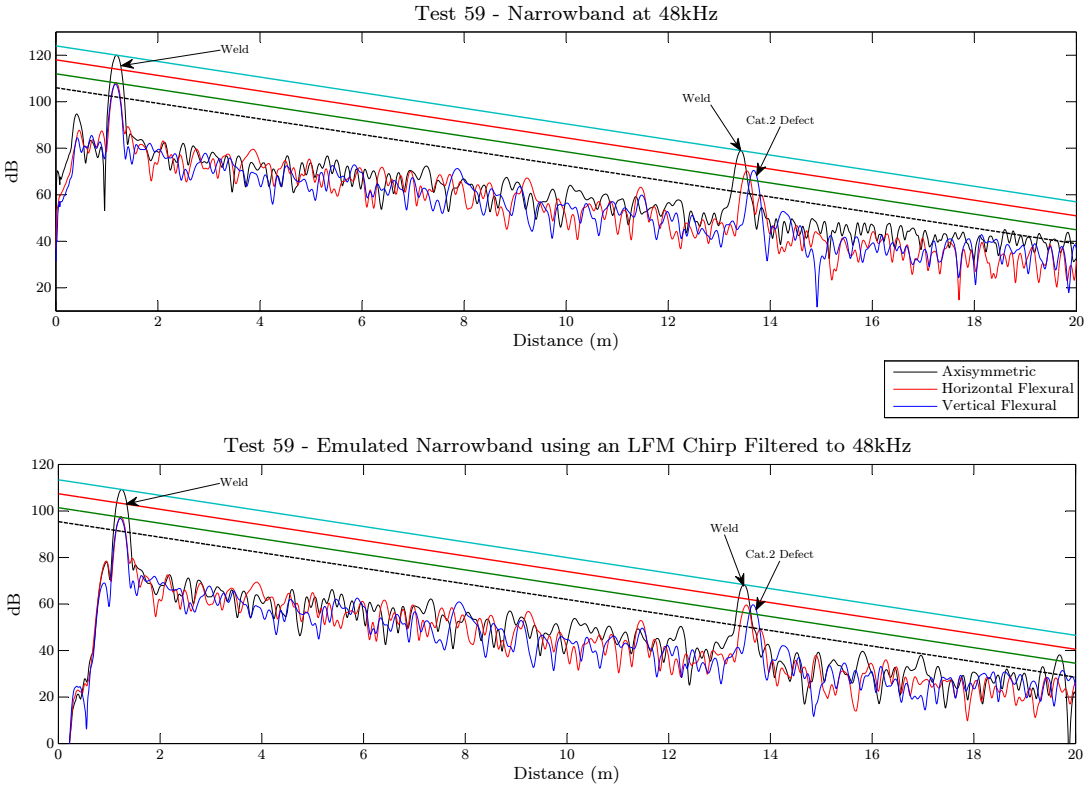

FIGURE 6.9: Comparison between narrowband and filtered broadband inspection results. Test ID 59: 48kHz (10 cycles), three ring torsional at 45mm ring spacing

Excitation Method	Feature	Range (m)	y (dB)	Relative Amplitude (dB)	Rate of Attenuation (dB/m)
Narrowband 48kHz	**Weld**	**1.18**	**120.00**	**0.00**	
	Weld	13.42	78.98	41.02	3.35
	Cat.1	13.67	70.46	49.54	
Broadband	**Weld**	**1.24**	**109.20**	**0.00**	
	Weld	13.49	68.29	40.91	3.34
	Cat.1	13.68	59.50	49.70	

TABLE 6.7: Summary of Test ID 59 measurements

Figure 6.9 shows that the quality of the data collected at this location is very good. This is an example of a very quiet GWT scan *i.e.* low noise. The relative measurements between the two excitation methods here show good agreement. The Cat.2 flaw appears within the weld response. This suggests that the root of the weld has suffered from gross corrosion. The rate of attenuation measurement between the two scans show minimum error.

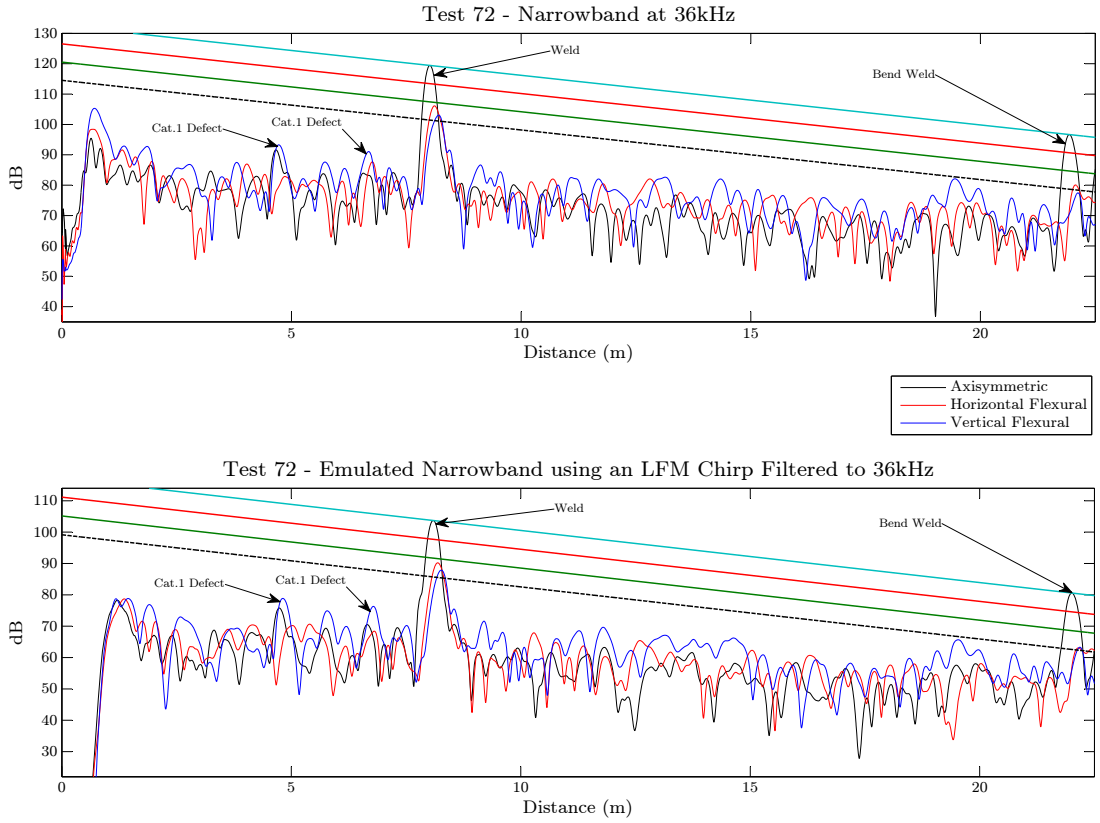

FIGURE 6.10: Comparison between narrowband and filtered broadband inspection results. Test ID 72: 36kHz (10 cycles), three ring torsional at 30mm ring spacing

Excitation Method	Feature	Range (m)	y (dB)	Relative Amplitude (dB)	Rate of Attenuation (dB/m)
Narrowband 48kHz	Cat.1	4.73	93.26	26.14	1.64
	Cat.1	6.68	91.08	28.32	
	Weld	**8.02**	**119.40**	**0.00**	
	Bend Weld	21.93	96.67	22.73	
Broadband	Cat.1	4.82	78.86	24.84	1.66
	Cat.1	6.79	76.32	27.38	
	Weld	**8.10**	**103.70**	**0.00**	
	Bend Weld	22.01	80.58	23.12	

TABLE 6.8: Summary of Test ID 72 measurements

Data from test ID 72 shows two Cat.1 flaws measured before the first girth weld. Both of these responses exist below the noise line at -32dB with respect to a 100% reflector but the inspection engineer has highlighted these features for a follow up inspection using UT. Again, the results shown for both excitation methods have good agreement.

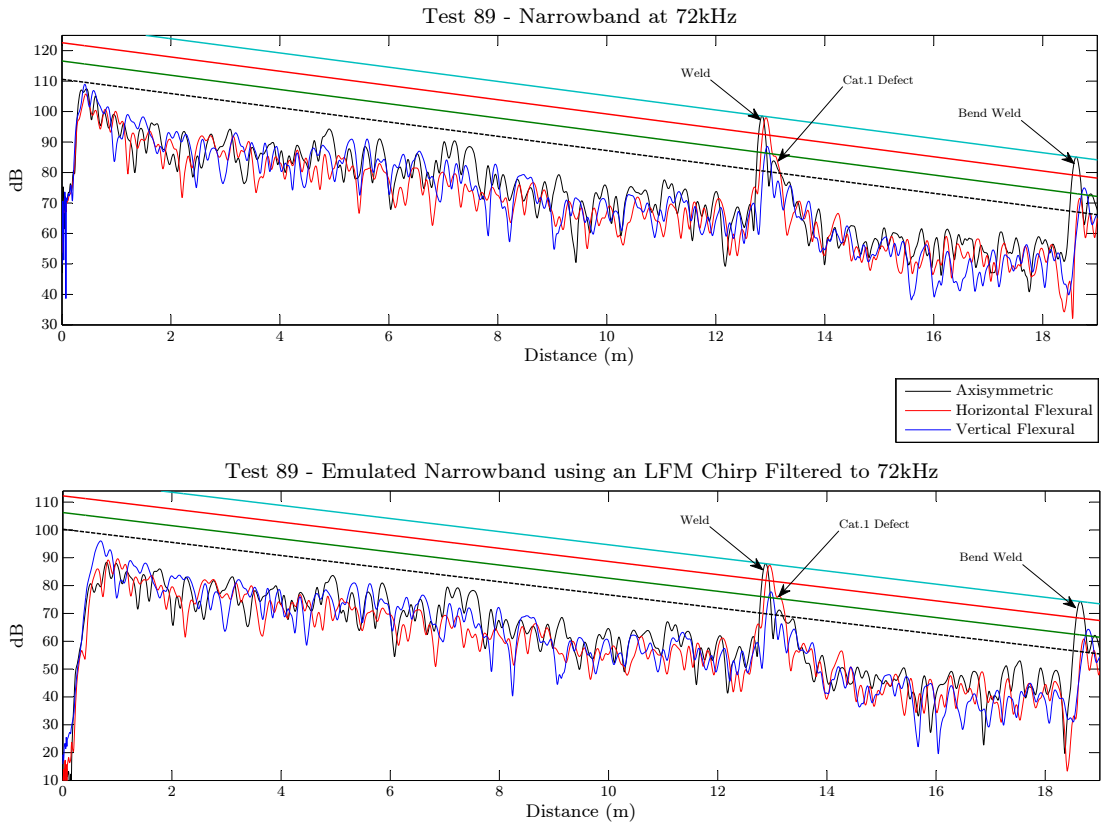

FIGURE 6.11: Comparison between narrowband and filtered broadband inspection results. Test ID 89: 72kHz (10 cycles), three ring torsional at 30mm ring spacing

Excitation Method	Feature	Range (m)	y (dB)	Relative Amplitude (dB)	Rate of Attenuation (dB/m)
Narrowband 72kHz	**Weld**	**12.85**	**98.51**	**0.00**	2.34
	Cat.1	13.11	84.75	13.76	
	Bend Weld	18.61	85.07	13.44	
Broadband	**Weld**	**12.88**	**87.88**	**0.00**	2.36
	Cat.1	13.15	75.95	11.93	
	Bend Weld	18.65	74.23	13.65	

TABLE 6.9: Summary of Test ID 89 measurements

Figure 6.11 shows a three ring torsional inspection at 72kHz. The inspection engineer has indicated damage within the weld response. The fact that there is a high horizontal flexural signal (the red trace) present within the weld response indicates that there is localised corrosion present. Both excitation methods highlight the horizontal flexural response but there is some error in the small shoulder at the trailing edge of the pulse. The rate of attenuation here is agreeable between the two methods.

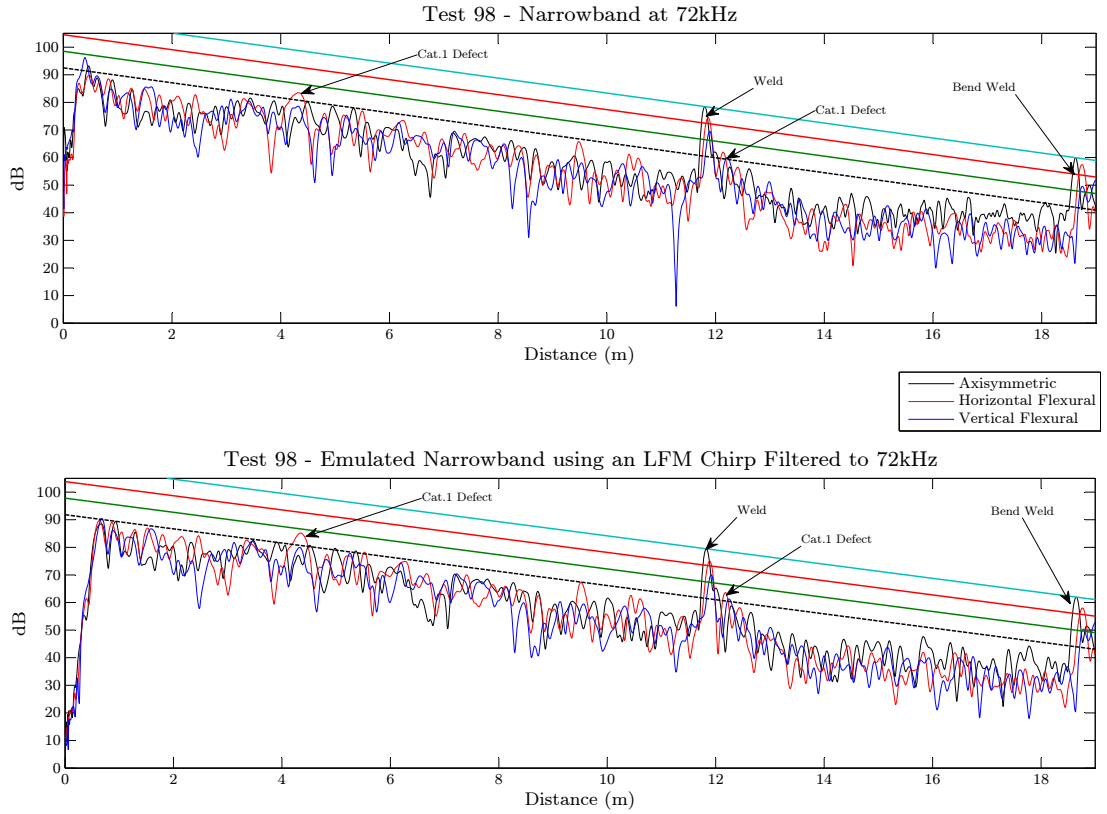

FIGURE 6.12: Comparison between narrowband and filtered broadband inspection results. Test ID 98: 72kHz (10 cycles), three ring torsional at 30mm ring spacing

Excitation Method	Feature	Range (m)	y (dB)	Relative Amplitude (dB)	Rate of Attenuation (dB/m)
Narrowband 72kHz	Cat.1	4.34	83.45	-4.97	2.71
	Weld	**11.80**	**78.48**	**0.00**	
	Cat.1	12.15	61.85	16.63	
	Bend Weld	18.62	59.95	18.53	
Broadband	Cat.1	4.36	85.14	-5.69	2.56
	Weld	**11.83**	**79.45**	**0.00**	
	Cat.1	12.18	63.57	15.88	
	Bend Weld	18.65	61.95	17.50	

TABLE 6.10: Summary of Test ID 98 measurements

The data collected for Test ID 98 contains two responses which have been classified as Cat.1 flaws. The red peak at 4.34m is a horizontal flexural signal which has been flagged due to the amplitude relative to the noise floor. The second Cat.1 indication is just beyond the first girth weld and appears within both scans with a similar signature. There is good range correlation between the two excitation methods for this test.

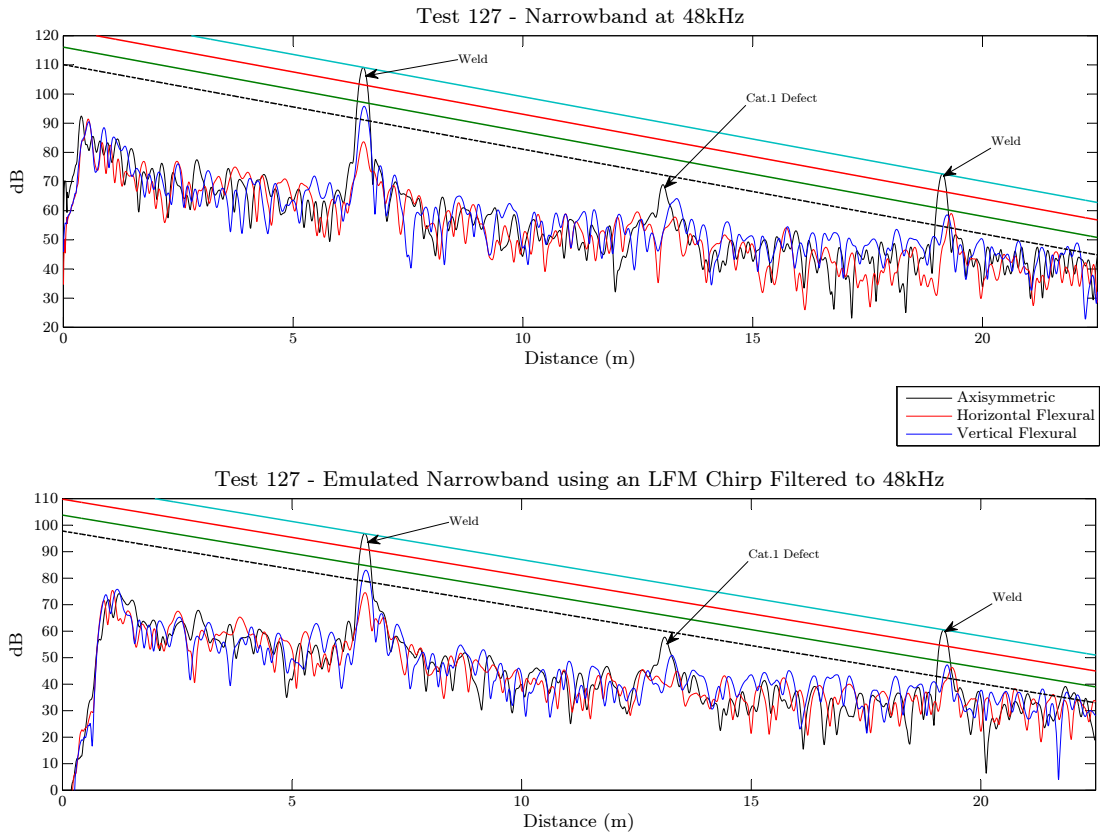

FIGURE 6.13: Comparison between narrowband and filtered broadband inspection results. Test ID 127: 48kHz (10 cycles), three ring torsional at 45mm ring spacing

Excitation Method	Feature	Range (m)	y (dB)	Relative Amplitude (dB)	Rate of Attenuation (dB/m)
Narrowband 48kHz	**Weld**	**6.27**	**109.10**	**0.00**	
	Cat.1	13.05	68.92	40.18	3.35
	Weld	19.14	72.56	36.54	
Broadband	**Weld**	**6.59**	**96.79**	**0.00**	
	Cat.1	13.11	57.74	39.05	3.34
	Weld	19.19	60.51	36.28	

TABLE 6.11: Summary of Test ID 127 measurements

Test ID 127 contains two girth welds and a single Cat.1 flaw between the two weld responses. The signature of both scans are similar and the range and relative amplitude values within Table 6.11 also indicate this.

6.7 Conclusions

This chapter presented GWT inspection data containing LFM chirp signals. The developments within Chapters 4 and 5 culminated in a set of excitation, transmission and reception criteria and allowed the author to make recommendations for the inclusion of LFM chirp signals into the commercial Teletest software as a hidden collection process.

The post-processing and comparison of these GWT field inspection data has shown that there is minimal error between the narrowband and emulated narrowband results presented. The filter was able to emulate the narrowband result in Figure 6.8 which further confirms the hypothesis that if the equivalent frequency content exists within the broadband pulse then emulation of the narrowband signal is possible. Presenting the results on a logarithmic y axis however, has exacerbated small errors which exist between the two excitation methods but this error has not exceeded normal variation which exists within this NDT technique.

Chapter 7

Conclusions and Further Work

7.1 Thesis Review

The frequency dependence of the majority of parameters associated with Guided Wave Testing reveals the need for a method by which several test frequencies can be examined in an efficient manner. Currently the narrowband excitation method is limited as large frequency sweeps are collected to determine an optimum frequency. If a response measured in the field needs to be further resolved in time/distance, *e.g.* the corrosion observed at the weld in Figure 6.8 then an additional test is carried out and examined. By using a broadband pulse such as the LFM chirp this operation is cut down significantly and will only take the milliseconds required to apply the filter and plot. The main objective of this thesis has been to refine and apply this technique to a guided wave inspection system.

Chapter 1 opened the document and introduced the subject, industrial need and main contributions. A summary of the research carried out is given here.

Chapter 2 introduced the reader to some of the main points of guided wave theory and the application of guided waves to pipe inspection and some of the technology used. Chapter 3 presented a review of the literature related to guided wave inspection. This activity served two purposes: the first being to find possible weaknesses in the technology and therefore possible improvements and the second element being an educational journey as the subject of ultrasonic testing using guided waves is specialised and required background work during the early stage of the research to enable a contribution.

The main hypothesis of the thesis was tested in Chapter 4. The idea that a narrowband signal of any configuration can be extracted from a broadband guided wave test was tested. An excitation signal was developed and tested. An FFT filter which was based upon the desired spectrum of the desired narrowband excitation was developed. The experiment set up only considered a single ring of transducers thus reducing potential experimental error. The T(0,1) wavemode was chosen as the simplest case to replicate due to its non-dispersive behaviour again reducing the chance of experimental error. The results showed that it is possible to extract any desired signal providing the frequency components exist within the excited bandwidth. One frequency dependent aspect to the GWT system used was the received transfer function. This output parameter produced a biased frequency spectrum which would prevent any effective, global time-frequency analysis to be carried out.

Once the idea of broadband excitation progressed from an idea to the positive results of Chapter 4 the technique was then considered for application in the commercial GWT tools designed and manufactured by Plant Integrity in Chapter 5. Each configuration demands a different excitation routine in order to successfully produce sound in one direction. This is termed here as unidirectional propagation. A propagation routine was developed for each case based upon a propagation equation which considers each frequency component in the bandwidth and not just the centre frequency. The power output curves for the ideal and broadband cases were shown for each tool configuration with good agreement. Results for a selection of frequencies showed that unidirectional propagation for a broadband excitation signal (the LFM chirp selected in Chapter 4) was indeed successful.

The development of a unidirectional broadband signal for GWT opened up the possibility for this technology to be applied in the field during actual site inspections. The excitation parameters were recommended by the author and the idea was applied to the commercial Teletest as a background data collection process. The results presented in Chapter 6 have been extracted from raw data collected on location at a oil transmission facility in North America. The post-processing techniques stated in Chapters 4 and 5 were applied to the data and the emulated narrowband signals showed good correlation with the standard narrowband results.

7.2 Brief summary of the main contributions

The main findings and contributions brought by this thesis can be summarised briefly as follows:

- Contrary to recommendations in published literature, including standards governing the ultrasonic testing of pipelines using guided waves, it was demonstrated that a broadband excitation can be used to produce information comparable to equivalent narrowband tests about the structure being inspected.

- An adaptable FFT filter was developed to extract any configuration of narrowband GWT result required from a broadband test. This filter could allow an inspection engineer to investigate a flaw in more detail in terms of spatial resolution and gives an option to toggle through emulated A-Scans to select an optimum frequency efficiently.

- An excitation routine was developed for broadband excitation which considered each frequency component and ensured optimum cancellation of sound in the opposite direction to the test. This ensured that the broadband signal was amplified in one direction.

- The unidirectional excitation routine was expanded to include the dispersive longitudinal mode $L(0,2)$. A frequency dependent phase velocity prevents the use of a fixed group delay when deriving the transmission signals for each transducer ring. During propagation to the next ring the $L(0,2)$ becomes distorted meaning that when the multiple rings are combined a transmission error will result and sound will leak in the opposite direction to the test. The routine applied in this thesis considers the phase velocity from the $L(0,2)$ dispersion curve for the given pipe and ensures that the process maximises the broadband $L(0,2)$ in the test direction.

- It was shown that the broadband transmission developed can be applied with minimum error in the field. The relative amplitude levels and range of the features within the pipelines including flaws were in good agreement with those measured using standard GWT methodology.

The potential for broadband excitation in terms of test efficiency and the flexibility the technique brings in terms of additional information available within one received test has been recognised. As such, the developments shown in this document are being written into the next generation of GWT software produced by Plant Integrity.

7.3 Further Work

7.3.1 Using a non-linear FM to correct a biased transfer function in an ultrasonic guided wave system

One area which has been identified in this thesis as being problematic is the biased transfer function observed in the GWT system. It is thought that this bias is related to mechanical resonance occurring during transduction. Broadband excitation was able to highlight this phenomenon. During the experiments set up in Chapter 4 the FFT of the pipe end reflection was examined yielding the result shown in Figure 4.8. The strong and narrow peak here possesses the hallmark traits of a mechanical resonance. For this system it reduces the capability for time-frequency analysis as the dominant peak at resonance would mask results at other frequencies. In order to improve or open up this as an option when analysing GWT signals the biased transfer function observed would have to be compensated for or designed out through mechanical changes. One option to be explored further would be to alter the signature of the Frequency Modulation (FM) of the chirp signal transmitted. It was noticed during this research that exponential chirp signals possess a skewed frequency response. This idea may be expanded to use as a correction factor for the resonance of the GWT system. A convenient starting point would be to adjust the chirp rate (k) so that a non-linear FM was produced to oppose the bias generated by the GWT system. Revision of chirp theory gives an angle from which to consider an approximate non-linear FM solution:

The phase shift in time of an LFM chirp:

$$\phi_{LFM}(t) = \int \left(\omega_1 + \left(\frac{\omega_2 - \omega_1}{\tau} \right) t \right) dt \tag{7.1}$$

$$\phi_{LFM}(t) = \omega_1 t + \frac{1}{2} \left(\frac{\omega_2 - \omega_1}{\tau} \right) t^2 \tag{7.2}$$

Where ω is angular frequency the lower and upper corner frequencies are ω_1 and ω_2 respectively, τ is the chirp pulse duration, ϕ_{LFM} is the associated phase angle with t being time.

The phase can be adjusted to create a non-linear chirp rate:

$$\phi_{NLFM}(t) = \int \left(\omega_1 + (\omega_2 - \omega_1) \left(\frac{t}{\tau} \right)^b \right) dt \tag{7.3}$$

$$\phi_{NLFM}(t) = \omega_1 t + (\omega_2 - \omega_1) \left(\frac{t^{(b+1)}}{(b+1)\tau^b} \right) \tag{7.4}$$

Where $\phi_{NLFM}(t)$ is non-linear FM phase as a function of time and b is the so-called bias factor. When b is between 0 and 1 the frequency spectrum will be biased to high frequencies, when $b = 1$ the chirp rate is linear and when b exceeds 1 then a low frequency bias results.

Applying Equation 7.4 to the chirp originally derived in Equation 4.7 alters the chirp rate.

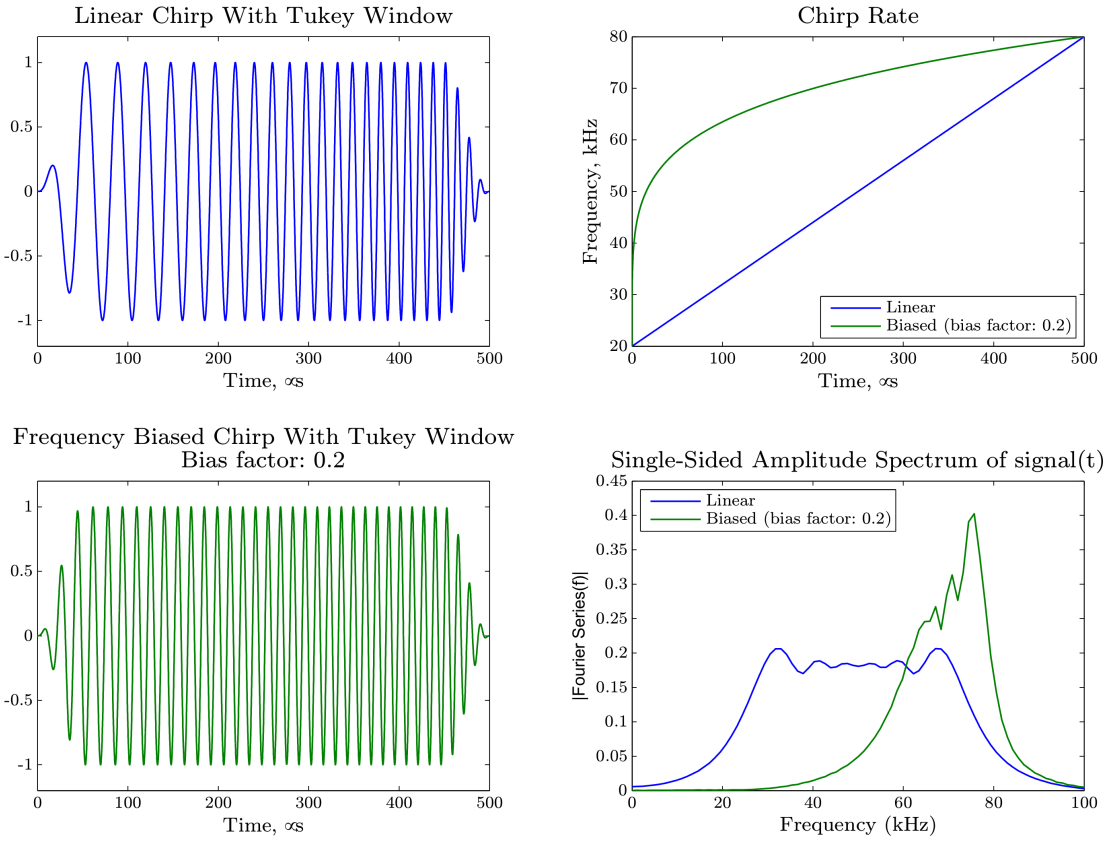

FIGURE 7.1: An example of the effect chirp rate bias has on the frequency content of the signal. The bias applied here is 0.2 (the data in green)

Figure 7.1 shows the principle of the adjustment of the chirp rate by applying a non-linear phase shift across the chirp function.

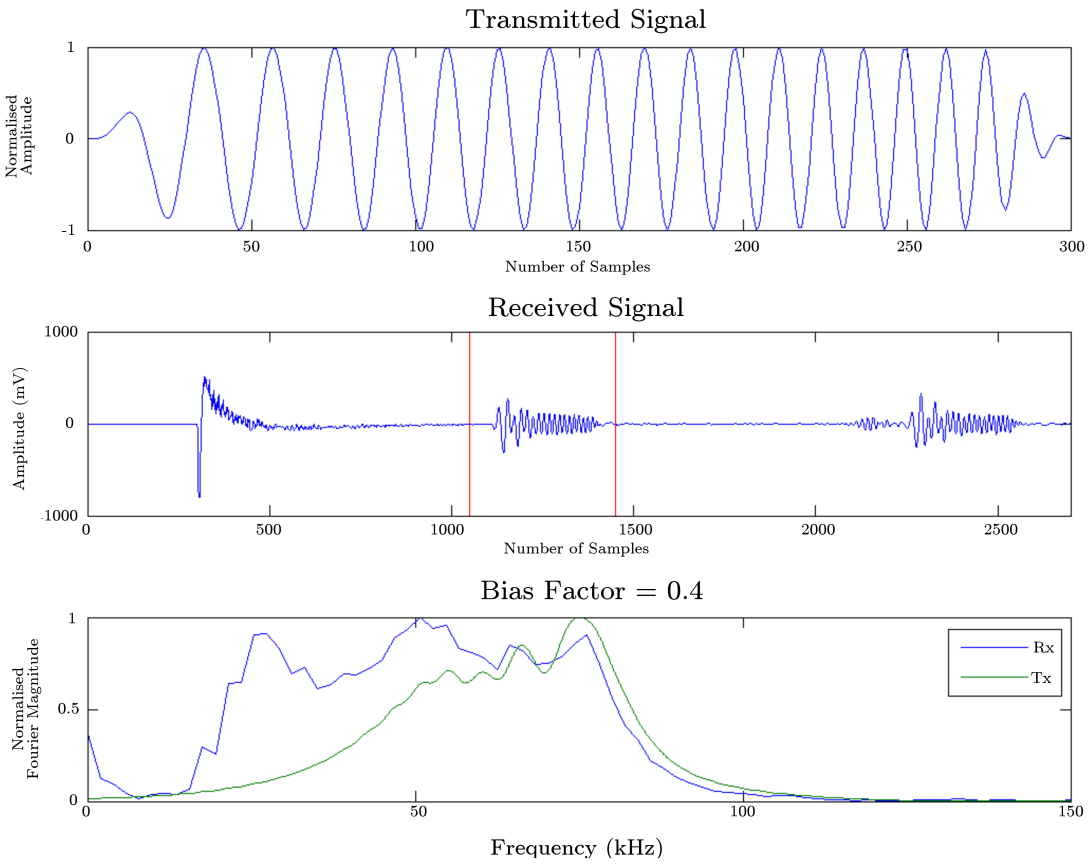

FIGURE 7.2: Initial promising results which show that in principle the received spectrum can be corrected. The bias here was set to 0.4.

Figure 7.2 above shows initial results using a NLFM chirp on an 8inch schedule 40 pipe. The top axes show the biased transmission signal using $b = 0.4$ on a normalised scale. The centre axes show the time domain received signal. Upon initial inspection the response gated between approximately 1000 and 1500 samples appears to have a flatter frequency response than the results shown in Figure 4.7, *i.e.* the higher frequencies towards the latter part of the pulse appear to be represented better. The bottom axes shows the frequency response of the transmit and receive signals. The receive signal (in blue) has an almost rectangular frequency response whilst the transmit frequency response is skewed to favour the higher frequencies during excitation. This correction approach could open up the possibility of representing pipeline data in the time-frequency domain to aid the selection of the optimum frequency. Currently the magnitude of the resonant frequency is too dominant for TFRs to work effectively for this technology. This work is currently ongoing but initial results look promising.

7.3.2 Adapting transducer ring spacing to provide a wider range of test frequencies

Chapter 5 introduced a method of obtaining a unidirectional broadband signal for a GWT system. A set of ring excitation signals were demonstrated for current tool configurations of the Teletest GWT system. For each configuration the output curves are cyclic because there is a fixed ring spacing and a range of available excitation frequencies exist. Each frequency will produce a pulse with a different fraction of wavelength with respect to the ring spacing. Superposition when the ring signals are comnbined to generate the unidirectional test signal across the excitation bandwidth results in this cyclic effect. The problem is fully defined. However, adjusting the ring spacing results in a different output curve. With some optimisation a better frequency distribution may be available.

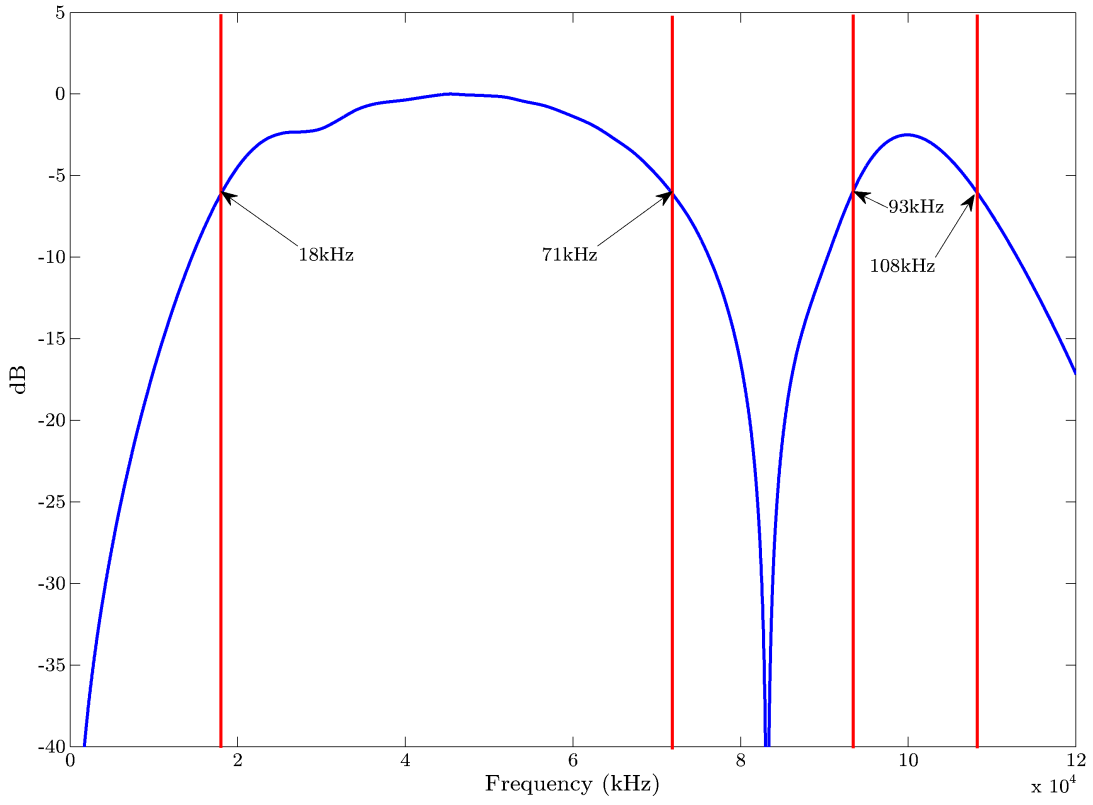

FIGURE 7.3: An example of the increase in available bandwidth as a result of changing the ring spacing to 15mm.

Figure 7.3 shows the output curves for a three ring torsional tool with a 15mm ring spacing. The vertical red lines represent the -6dB points on the curve. This dB limit

is often used in GWT and UT because it represents the point at which half of the amplitude of the signal is lost. The curve shows that the majority of the GWT excitation bandwidth (20kHz to 100kHz) is confined within these -6dB limits. There is a trough between 71kHz and 91kHz however, this bandwidth is often problematic because circumferential Lamb waves are strengthened within the tool at these frequencies due to an optimum circumferential transducer spacing for this type of propagation. 15mm ring spacing provides a very open bandwidth information within which is lost using a 30mm ring spacing. The broadband excitation would benefit from the proposed narrow spacing as the full reception spectrum could be presented as a time-frequency image without any troughs in the data. This proposed hardware configuration is currently under investigation by the author.

References

D. N. Alleyne. *The nondestructive testing of plates using ultrasonic Lamb waves*. PhD thesis, Imperial College of Science, Technology and Medicine, 1991.

D. N. Alleyne and P. Cawley. A two-dimensional Fourier transform method for the measurement of propagating multimode signals. *The Journal of the Acoustical Society of America*, 89(3):1159–1168, March 1991.

D. N. Alleyne and P. Cawley. Optimization of Lamb wave inspection techniques. *NDT & E International*, 25(1):11–22, May 1992.

D. N. Alleyne and P. Cawley. The practical excitation and measurement of Lamb waves using piezoelectric transducers. *Review of Progress in Quantitative Nondestructive Evaluation*, 13:181–188, May 1994.

D. N. Alleyne and P. Cawley. The long range detection of corrosion in pipes using lamb waves. In D. O. Thompson and D. E. Chimenti, editors, *Review of Progress in Quantitative Nondestructive Evaluation*, pages 2073–2080. Springer US, 1995.

D. N. Alleyne and P. Cawley. The excitation of Lamb waves in pipes using dry-coupled piezoelectric transducers. *Journal of Nondestructive Evaluation*, 15(1):11–20, 1996a.

D. N. Alleyne and P. Cawley. The effect of discontinuities on the long-range propagation of Lamb waves in pipes. *Proceedings of the Institution of Mechanical Engineers, Part E: Journal of Process Mechanical Engineering*, 210:217–226, 1996b.

D. N. Alleyne and P. Cawley. Long range propagation of Lamb waves in chemical plant pipework. *Materials Evaluation*, pages 504–508, 1997.

D. N. Alleyne, T. P. Pialucha, and P. Cawley. A signal regeneration technique for long-range dispersion of dispersive Lamb waves. *Ultrasonics*, 34(1):201–204, 1993.

D. N. Alleyne, B. Pavlakovic, M. Lowe, and P. Cawley. Rapid, long range inspection of chemical plant pipework using guided waves. *AIP Conference Proceedings*, 557(1): 180–187, 2001.

D. N. Alleyne, T. Vogt, and P. Cawley. The choice of torsional or longitudinal excitation in guided wave pipe inspection. *Insight*, 51(7):373–377, July 2009.

A. Armenàkas, D. Gazis, and G. Herrmann. *Free vibrations of circular cylindrical shells.* Pergamon Press, 1969.

R. Blackman and J. Tukey. *The Measurement Of Power Spectra From The Point Of View Of Communications Engineering.* Dover, 1959.

B. Boashash and V. Sucic. A resolution performance measure for quadratic time-frequency distributions. *Proceedings of the Tenth IEEE Workshop on Statistical Signal and Array Processing*, pages 584–588, 2000.

B. Boashash and V. Sucic. High performance time-frequency distributions for practical applications. In L. Debnath, editor, *Wavelets and signal processing*, chapter 6. Birkhäuser Boston, 2003.

W. Böttger, H. Schneider, and W. Weingarten. Prototype EMAT system for tube inspection with guided ultrasonic waves. *Nuclear Engineering and Design*, 102:369–376, 1987.

R. Bracewell. *The Fourier transform and its applications.* McGraw-Hill, 2 edition, 1986.

BS 9690-1:2011. Non-destructive testing – Guided wave testing Part 1: General guidance and principles, 2011.

R. A. Carmona, W. L. Hwang, and B. Torrésani. Characterization of signals by the ridges of their wavelet transforms. *IEEE Transactions on Signal Processing*, 45(10): 2586–2590, October 1997.

P. Catton. *Long range ultrasonic guided waves for the quantitative inspection of pipelines (EngD thesis).* Brunel University, 2008.

P. Cawley and D. N. Alleyne. Inspection of pipes, 1996. International Patent WO 96/12951.

L. Cohen. *Time-Frequency Analysis: Theory and Applications.* Prentice Hall, 1994.

C. E. Cook. Pulse compression - key to more efficient radar transmission. *Proceedings of the IRE*, 48(3):310–316, 1960.

J. W. Cooley and J. W. Tukey. An algorithm for the machine computation of the complex Fourier series. *Mathematics of Computation*, 19:297–301, 1965.

G. P. DeVault and C. W. Curtis. Problem of elastic bar with mixed time-dependent end conditions of general form. *The Journal of the Acoustical Society of America*, 31:635, 1959.

J. J. Ditri and J. L. Rose. Excitation of guided elastic wave modes in hollow cylinders by applied surface tractions. *Journal of Applied Physics*, 72(7):2589–2597, 1992.

B. Engineer. *The mechanical and resonant behaviour of a dry coupled thickness-shear PZT transducer used for guided wave testing in pipe line.* PhD thesis, Brunel University, 2013. (in press).

P. Flandrin. *Time-Frequency / Time-Scale Analysis.* Academic Press, 1999.

E. N. Fowle, D. R. Carey, R. E. V. Schuur, and R. C. Yost. A pulse compression system employing a linear fm gaussian signal. *Proceedings of the IEEE*, 51(2):304–312, 1963.

T. H. Gan, D. A. Hutchins, D. R. Billson, and D. W. Schindel. The use of broadband acoustic transducers and pulse-compression techniques for air-coupled ultrasonic imaging. *Ultrasonics*, 39:181–194, 2001.

D. C. Gazis. Three-dimensional investigation of the propagation of waves in hollow circular cylinders. I. analytical foundation. *The Journal of the Acoustical Society of America*, 31(5):568–573, May 1959a.

D. C. Gazis. Three-dimensional investigation of the propagation of waves in hollow circular cylinders. II. numerical results. *The Journal of the Acoustical Society of America*, 31(5):573–578, May 1959b.

J. W. Gibbs. Fourier's series. *Nature*, 59(1539):606, 1899.

K. F. Graff. *Wave Motion in Elastic Solids.* New York: Dover, 1991.

R. W. Hamming. *Digital Filters.* Prentice Hall, 1977.

T. Ikeda and T. Hayashi. High S/N ratio guided wave inspection of pipe using chirp pulse compression. *ASME/JSME 2004 Pressure Vessels and Piping Conference*, 484: 41–45, July 2004.

G. Konstantinidis, B. Drinkwatera, and P. Wilcox. The temperature stability of guided wave structural health monitoring systems. *Journal of Smart Materials and Structures*, 15(4):967–976, 2006.

M. Kowatsch and H. R. Stocker. Effect of Fresnel ripples on sidelobe suppression in low time-bandwidth product linear FM pulse compression. *IEE Proceedings-F: Communications, Radar and Signal Proceedings*, 129(1):41–44, February 1982.

M. Kulesh, M. Holschneider, M. S. Diallo, Q. Xie, and F. Scherbaum. modeling of wave dispersion using continuous wavelet transforms. *Pure and Applied Geophysics*, 162: 843–855, 2005.

M. Kulesh, M. Holschneider, M. Ohrnberger, and E. Lück. Modeling of wave dispersion using continuous wavelet transforms II: wavelet-based frequency-velocity analysis. *Pure and Applied Geophysics*, 165:255–270, 2008.

H. Kwun and A. E. Holt. Feasibility of under-lagging corrosion detection in steel pipe using the magnetostrictive sensor technique. *NDT & E International*, 28(4):211–214, 1995.

H. Lamb. On waves in an elastic plate. *Proceedings of the Royal Society of London*, 93 (648):114–128, 1917.

A. Lank. The principle of 4 ring excitation and its application to the testing of thick walled pipes. Technical report, Plant Integrity Ltd., 2001.

A. Lank. The principle of 3 ring excitation. Technical report, Plant Integrity Ltd., 2002.

B. M. Lempriere. *Ultrasound and Elastic Waves - Frequently Asked Questions*. Academic Press, 2002.

J. Li and J. L. Rose. Angular-profile tuning of guided waves in hollow cylinders using a circumferential phased array. *IEEE Transactions on Ultrasonics, Ferroelectrics and Frequency Control*, 49(12):1720–1729, 2002.

A. E. H. Love. *Some Problems of Geodynamics*. Cambridge University Press, 1911.

M. Lowe, D. N. Alleyne, and P. Cawley. Defect detection in pipes using guided waves. *Ultrasonics*, 36:147–154, 1998.

B. R. Mahafza. *Radar systems analysis and design using MATLAB*, chapter 5. Chapman & Hall, 2000.

A. H. Meitzler. Mode coupling occurring in the propagation of elastic pulses in wires. *The Journal of the Acoustical Society of America*, 33(4):435–445, April 1961.

T. E. Michaels, J. E. Michaels, S. J. Lee, and X. Chen. Chirp generated acoustic wavefield images. *Health Monitoring of Structural and Biological Systems*, 7984(79840J):1–11, 2011.

Y. Mizutani and S. Inokawa. A fundamental study of an inspection method for thin-walled structures using Lamb waves induced by chirp signals. *The 3rd International Conference on Experimental Mechanics*, 2004.

W. Mohr and P. Höller. On inspection of thin-walled tubes for transverse and longitudinal flaws by guided ultrasonic waves. *IEEE Transactions on Sonics and Ultrasonics*, 23(5):369–374, September 1976.

P. Mudge. Field application of the teletest long range ultrasonic testing technique. *Insight*, 43:74–77, 2001.

M. Niethammer, L. J. Jacobs, J. Qu, and J. Jarzynski. Time-frequency representation of Lamb waves using the reassigned spectrogram. *The Journal of the Acoustical Society of America*, 107(5):L19–L24, May 2000.

M. Niethammer, L. J. Jacobs, J. Qu, and J. Jarzynski. Time-frequency representations of Lamb waves. *The Journal of the Acoustical Society of America*, 109(5):1841–1847, May 2001.

A. V. Oppenheim and R. W. Schafer. *Digital Signal Processing*. Prentice Hall, 1975.

P. Pallav, T. H. Gan, and D. A. Hutchins. Elliptical-Tukey chirp signal for high-resolution, air-coupled ultrasonic imaging. *IEEE Transactions on Ultrasonics, Ferroelectrics and Frequency Control*, 54(8):1530–1540, August 2007.

B. Pavlakovic, M. Lowe, D. N. Alleyne, and P. Cawley. *Disperse: A general purpose program for creating dispersion curves*, volume 16 of *Review of Progress in Quantitative Nondestructive Evaluation*. Plenum Press, New York, 1997.

PHMSA. *Guidelines for integrity assessment of cased pipe for gas transmission pipelines in HCAs*. Pipeline and Hazardous Materials Safety Administration (PHMSA), 2010.

M. Pollakowski and H. Ermert. Chirp signal matching and signal power optimization in pulse-echo mode ultrasonic nondestructive testing. *IEEE Transactions on Ultrasonics, Ferroelectrics and Frequency Control*, 41(5):655–659, September 1994.

M. Pollakowski, H. Ermert, L. von Bernus, and T. Schmeidl. The optimum bandwidth of chirp signals in ultrasonic applications. *Ultrasonics*, 31(6):417–420, 1993.

W. H. Prosser, M. D. Seale, and B. T. Smith. Time-frequency analysis of the dispersion of Lamb modes. *The Journal of the Acoustical Society of America*, 105(5):2669–2676, May 1999.

J. L. Rose. *Ultrasonic Waves in Solid Media*. Cambridge University Press, 1999.

J. L. Rose. A baseline and vision of ultrasonic guided wave inspection potential. *Journal of Pressure Vessel Technology*, 124:273–282, 2002.

J. L. Rose, S. P. Pelts, and M. J. Quarry. A comb transducer model for guided wave nde. *Ultrasonics*, 36:163–169, 1998.

H. Schneider. The nondestructive testing of tubes and pipes for nuclear application. *Nuclear Engineering and Design*, 81:69–76, 1984.

M. G. Silk and K. F. Bainton. The propagation in metal tubing of ultrasonic wave modes equivalent to Lamb waves. *Ultrasonics*, 17:11–19, January 1979.

D. Sjöberg. *Electromagnetic Wave Propagation, Lecture 7: Pulse propagation in dispersive media*. Lund University, 2010. University Lecture.

S. W. Smith. *The Scientist and Engineer's Guide to Digital Signal Processing*, chapter 18: FFT Convolution. California Technical Publishing, 2011.

J. W. Strutt. *The Theory of Sound*. The Macmillan Company, 1896.

Z. Su and L. Ye. *Identification of damage using Lamb waves*. Springer, 2009.

K. Thornicroft and P. Catton. LRUT using chirp and broadband excitation methods. Technical report, The Welding Institute: Exploratory Research Project (Internal Report), July 2010.

K. Thornicroft and P. Catton. Long range ultrasonic testing using a broadband excitation method. Technical report, The Welding Institute: Industrial Member Report, September 2011.

K. Toiyama and T. Hayashi. Pulse compression technique considering velocity dispersion of guided wave. *Review of Quantitative Nondestructive Evaluation*, 27:587–593, 2008.

J. W. Tukey. An introduction to the calculations of numerical spectrum analysis. In B. Harris, editor, *Advanced Seminar on Spectral Analysis of Time Series*, pages 25–46. Wiley, New York, 1967.

I. A. Viktorov. *Rayleigh and Lamb Waves - Physical Theory and Applications*. Plenum Press: New York, 1967.

H. Wilbraham. On a certain periodic function. *The Cambridge and Dublin Mathematical Journal*, 3:198–201, 1848.

P. D. Wilcox. A rapid signal processing technique to remove the effect of dispersion from guided wave signals. *IEEE Transactions on Ultrasonics, Ferroelectrics and Frequency Control*, 50(4):582–588, April 2003.

K. Xu, D. Ta, and W. Wang. Multiridge-based analysis for separating individual modes from multimodal guided wave signals in long bones. *IEEE Transactions on Ultrasonics, Ferroelectrics and Frequency Control*, 57(11):2480–2490, November 2010.

J. Zemanek. An experimental and theoretical investigation of elastic wave propagation in a cylinder. *The Journal of the Acoustical Society of America*, 51(1B):265–283, January 1972.